

PREFACE

Individuals who have contributed to the Phase II effort include Dr. Robert P. Wei, Principal Investigator (fracture mechanics and materials science); Dr. D. Gary Harlow (probability modeling); Dr. Ming Gao (materials science); Dr. Kuang-Chung Wan (Ph.D. 1996, Applied Mechanics); Dr. Chi-Min Liao (Ph.D., 1997, Materials Science and Engineering); Dr. Evan J. Dolley, Jr. (Ph.D., 1999, Mechanical Engineering and Mechanics); Mr. Baekho Lee (M.S., 1999, Mechanical Engineering and Mechanics); Ms. Svetlana Oshkai (M.S. candidate in Mechanical Engineering and Mechanics); Ms. Julie DeMoyer and Mr. Jeffrey Zoleta (undergraduates in Mechanical Engineering and Mechanics), and Ms. L. D. Domanowski (undergraduate from Bucknell University). Ms. Domanowski was supported by a summer internship provided by the P.C. Rossin College of Engineering and Applied Science at Lehigh University.

Acknowledgements

This research was supported by the Federal Aviation Administration under Grant 92-G-0006 with complementary support by the Air Force Office of Scientific Research under Grants F49620-98-1-0198 and F49620-96-1-0245. The authors wish to acknowledge the Air Vehicles Directorate of the US Air Force Research Laboratory for providing sections of the wing panels from the CZ-184 aircraft used in this investigation; the Boeing Company, Information, Space & Defense Systems for making the data available to us; and Joe Luzar of Boeing-Wichita for his technical assistance and helpful discussions. L.D. Domanowski was supported by a summer internship provided by the P.C. Rossin College of Engineering and Applied Science at Lehigh University.

TABLE OF CONTENTS

	Page
PREFACE	ii
ACKNOWLEDGMENT	iii
TABLE OF CONTENTS	iv
LIST OF FIGURES	vi
LIST OF TABLES	xi
EXECUTIVE SUMMARY	xii
1. BACKGROUND AND OBJECTIVES	1-1
2. TECHNICAL APPROACH	2-1
3. LOCALIZED (PITTING) CORROSION	3-1
3.1 Constituent Particles	3-1
3.2 Pitting Corrosion	3-2
3.3 Electrochemical Measurements	3-8
3.4 Mechanistic Models	3-13
4. TRANSITION FROM PITTING TO FATIGUE CRACK GROWTH	4-1
5. FATIGUE CRACK GROWTH	5-1
5.1 Chemically Short-Crack Behavior	5-1
5.1.1 2024-T3 Aluminum Alloy	5-1
5.1.2 7075-T651 Aluminum Alloy	5-1
5.2 Impact of Chemically Short-Crack Behavior on Fatigue Life	5-4
5.2.1 7075-T651 Aluminum Alloy	5-4
5.2.2 2024-T3 Aluminum Alloy	5-7
6. MODELING AND INSIGHT	6-1
6.1 Effect of Pitting Corrosion on Fatigue Life	6-1
6.1.1 Modeling and Initial Comparison	6-1
6.1.2 Further Verifications	6-2
6.1.3 Probabilistic Analysis	6-3
6.2 A Mechanistically Based Probability Approach: Probabilities of Occurrence and Detection	6-3

	Page
7. PROBABILITY MODELING AND ANALYSIS OF J-STARS TEARDOWN DATA FROM TWO B707 AIRCRAFT	7-1
7.1 Modification of the Mechanistically Based Probability Model	7-1
7.2 PoO and Statistical Analysis of J-Stars Teardown Data	7-3
7.3 Estimation of Multisite Damage (MSD)	7-7
7.4 Metallographic Examinations of Damage and Implications	7-9
7.5 Statistical Analyses of the Lower Left Wing Skin of CZ-184 Aircraft	7-12
8. SUMMARY	8-1
9. REFERENCES	9-1
APPENDIX A – Presentations and Publications From the Program	A-1

LIST OF FIGURES

Figure		Page
2-1	Schematic Diagram of the Development of Corrosion and Corrosion Fatigue Crack Growth	2-1
2-2	Flow Diagram Showing the Overall Processes for Corrosion and Fatigue Damage	2-2
3-1	SEM Micrograph Showing Pitting Induced by Constituent Particles in a 2024-T3 Aluminum Alloy	3-2
3-2	SEM Micrograph of the Crosssection of Severe Corrosion Pits in a 2024-T3 Aluminum Alloy (TS) Surface Along With an Inset Showing the Appearance of the Corresponding Pits on the LS Surface	3-3
3-3	SEM Microfractographs of Fatigue Fracture Surface of a 2024-T3 Alloy Showing a Severe Corrosion Pit as the Crack Nucleus	3-4
3-4	SEM Micrographs Showing Severe Pitting in a 2024-T3 Aluminum Alloy After 500 Hours in 0.5M NaCl Solution at Room Temperature	3-4
3-5	SEM Micrographs of the Epoxy Replica of a Severe Corrosion Pit in 2024-T3 Aluminum Alloy	3-5
3-6	TEM Micrograph of 7075-T651 Aluminum Alloy Showing Oxide Left Behind by Particle-Induced Corrosion	3-6
3-7	Low- and High-Magnification TEM Micrographs Showing an Al ₂ Cu Particle and Its Environs in a 2024-T3 Aluminum Alloy (a) Before and (b) After 180-min. (Cumulative) Immersion in 0.5M NaCl Solution at Room Temperature	3-7
3-8	TEM Micrographs Showing an Al ₂ CuMg Particle and Its Environs in a 2024-T3 Aluminum Alloy (a) Before and (b) After 15-min. Immersion in 0.5M NaCl Solution at Room Temperature	3-8
3-9	Relationship Between Cathode-to-Anode Area Ratio and Current Densities of Alloy A-Al Couple in Neutral 0.5M NaCl Solution	3-9
3-10	Relationship Between Cathode-to-Anode Area Ratio and Current Densities of Alloy B-Al Couple in Neutral 0.5M NaCl Solution	3-10

Figure		Page
3-11	Relationship Between Cathode-to-Anode Area Ratio and Current Densities of Alloy A-Al Couple in 0.5M NaCl + 0.07M AlCl ₃ Solution (pH \cong 3.5)	3-10
3-12	Relationship Between Cathode-to-Anode Area Ratio and Current Densities of Alloy B-Al Couple in 0.5M NaCl + 0.07M AlCl ₃ Solution (pH \cong 3.5)	3-11
3-13	Conceptual Models of Particle-Matrix Interactions (Local Corrosion) for (a) a Cathodic and (b) an Anodic Particle	3-14
3-14	Schematic Diagram of a Conceptual Model for Pitting in the Transverse Orientation Involving Matrix Dissolution Around Clusters of Cathodic (Type C) Constituent Particles	3-15
4-1	Schematic of a Proposed Corrosion/Fatigue Map Showing the Relationship Between Stress-Intensity Factor Range and Frequency With the Applied Cyclic Stress Range as a Parameter	4-2
4-2	The Relationship Between the Stress-Intensity Factor Range of Equivalent Cracks at Fatigue Crack Nucleation and the Frequency of the Applied Cyclic Stress	4-2
5-1	Chemically Short-Crack Behavior in the 2024-T3 Aluminum Alloy in a Deaerated and Aerated Solution With [O ₂] = 7 ppm	5-2
5-2	Chemically Short-Crack Behavior in the 2024-T3 Aluminum Alloy in the Aerated Solution With [O ₂] = 30 ppm	5-2
5-3	Chemically Short-Crack Behavior in the 7075-T6 Aluminum Alloy	5-3
5-4	Effect of Frequency on the Chemically Short-Crack Behavior in a 7075-T6 Aluminum Alloy at a ΔK of 5 MPa m ^{1/2}	5-3
5-5	Effect of Frequency on the Chemically Short-Crack Behavior in a 7075-T6 Aluminum Alloy at a ΔK of 10 MPa m ^{1/2}	5-4
5-6	Power-Law Relationship for the Chemically Long and Short-Crack Regimes for a 7075-T6 Aluminum Alloy in a 0.5M NaCl Solution	5-6

Figure		Page
5-7	Reduction in Fatigue Life From a Crack Length of 0.03 mm to 1 mm Caused by Chemically Short-Crack Behavior in the 7075-T6 Aluminum Alloy	5-7
5-8	The Reduction in the 2024-T3 Fatigue Life From a Crack Length of 0.03 mm to 1 mm When Considering Chemically Short-Crack Behavior at a Frequency of 10 Hz	5-7
6-1	Influence of Stress, Initial Pit Size, and Frequency on Fatigue (Crack Growth) Life	6-2
6-2	Observed Reduction in Fatigue Life for the 2024-T4 Aluminum Alloy as a Function of the Initial Pit Size	6-3
6-3	Estimated Fatigue Life is in Good Agreement With the Actual Fatigue Life for the 2024-T4 Aluminum	6-3
6-4	Observed Reduction in Fatigue Life for the 2024-T3 Aluminum Alloy as a Function of Pre-corrosion Time in a 0.5M NaCl Solution	6-4
6-5	Fractograph Showing a Corrosion Pit That Nucleated the Dominant Crack in the 2024-T3 Aluminum Alloy After 384 Hours of Pre-corrosion	6-4
6-6	Observed Reduction in Fatigue Life for the 2024-T3 Aluminum Alloy as a Function of Initial Pit Size	6-5
6-7	Estimated Fatigue Life is in Good Agreement With the Actual Fatigue Life for the 2024-T3 Aluminum Alloy	6-6
6-8	Pit Depth Distribution Following 384 Hours of Corrosion in an Aqueous 0.5M NaCl Solution on the 2024-T3 Aluminum Alloy	6-7
6-9	Estimated and Actual Distributions of Fatigue Life Showing That the Distribution of Pit Depth Dictates the Distribution of Fatigue Life for the 2024-T3 Aluminum Alloy	6-7
6-10	Evolution of Average Damage Size With and Without Corrosion	6-9
6-11	Probability Distribution of Damage at a Given Time at 293 K and 10 Cyc/Day	6-10
7-1	Schematic Diagram of the Processes for Airworthiness, Structural Integrity, and Durability Assessments	7-2

Figure		Page
7-2	A Comparison Between the Predicted and Observed PoO for Hole-Wall Damage in the Left-Hand Lower Wing Skins (2024-T3 Aluminum Alloy) of the CZ-180 Aircraft	7-5
7-3	A Comparison Between the Predicted and Observed PoO for Hole-Wall Damage in the Left-Hand Lower Wing Skins (2024-T3 Aluminum Alloy) of the CZ-184 Aircraft	7-5
7-4	A Comparison Between the Predicted and Observed PoO for Hole-Wall Damage in the Left-Hand Lower Wing Stiffeners (7075-T6 Aluminum Alloy) of the CZ-180 Aircraft	7-6
7-5	A Comparison Between the Predicted and Observed PoO for Hole-Wall Damage in the Left-Hand Lower Wing Stiffeners (7075-T6 Aluminum Alloy) of the CZ-184 Aircraft	7-6
7-6	A Comparison Between the Predicted and Observed PoO, With Estimated Error Bars for the Data for Hole-Wall Damage in the Left-Hand Lower Wing Stiffeners of the CZ-184 Aircraft	7-7
7-7	Variations in the Simulated Damage Distributions for 100 Fastener Holes Based on the PoO for the Skin of the CZ-184 Aircraft	7-8
7-8	Simulated Damage Distribution for 1,000 Fastener Holes Based on the PoO for the Skin of the CZ-184 Aircraft	7-8
7-9	SEM Micrograph of Corrosion-Related Distributed Damage at Hole 54 in Panel B2-2-2 of the CZ-184 Aircraft	7-10
7-10	SEM Micrograph of a Section Through an Elongated Damage at Hole 77 in Wing Panel B3-2-5 of the CZ-184 Aircraft Showing Corrosion Attack of the Fatigue Crack	7-10
7-11	SEM Micrograph of a Through Section of a Shallow Damage at Hole 77 in Wing Panel B3-2-5 of the CZ-184 Aircraft Suggesting That the Crack Was Dissolved by Corrosion	7-11
7-12	Optical Micrograph of a Highly Stressed Region of Hole 107 in Wing Panel B3-2-2 of the CZ-184 Aircraft Showing Extensive Corrosion Fatigue Cracking	7-11
7-13	Optical Micrograph of a Highly Stressed Region of Hole 103 in Wing Panel B3-2-2 of the CZ-184 Aircraft Showing Extensive Corrosion Fatigue Cracking	7-12

Figure		Page
7-14	Comparison of the PoO for the Maximum MHWC Lengths Reported by J-STARS, Measured Using Video Imaging Microscopy, and Effective Length Estimated From the Overall Extent of the Field of Damage for Selected Holes From the CZ-184 Aircraft	7-13
7-15	A Portion of Section 2 Along Stiffener 4 From the CZ-184 Aircraft for Which Microscopy and Statistical Analyses are Made	7-13
7-16	Comparison of the PoO for All MHWC Lengths Reported by J-STARS and All of Those Measured Using Video Imaging Microscopy for 110 Holes From Section 2 Along Stiffener 4 From the CZ-184 Aircraft	7-14
7-17	Density of Measured Cracks Per Fastener Hole for Section 2, Stiffener 4 From the CZ-184 Aircraft	7-15
7-18	Damage Distribution of Maximum Crack Lengths for 110 Fastener Holes From Section 2 Along Stiffener 4 From the CZ-184 Aircraft	7-15

LIST OF TABLES

Table		Page
3-1	Open Circuit Potentials (OCP) of Pure Al and Alloys A and B in Neutral 0.5M NaCl Solution	3-9
3-2	Limiting Current Densities and Transition Area Ratio of Various Galvanic Couples in Various Solutions	3-12
5-1	Crack Growth Rate Coefficients and Exponents for the 7075-T6 Alloy at 10 and 0.5 Hz	5-5
5-2	Estimated Fatigue Life for the 7075-T6 Chemically Short-and Long-Crack Regimes at 10 Hz	5-6

EXECUTIVE SUMMARY

In support of the National Aging Aircraft Research Program (NAARP) of the Federal Aviation Administration (FAA), Lehigh University undertook a multidisciplinary program of research to study corrosion and corrosion fatigue of airframe materials. The program was initiated on 15 June 1992 for a 3-year period as Phase I and was extended from 15 June 1995 to 30 September 1999 as Phase II. It was complemented by a companion program under the sponsorship of the Air Force Office of Scientific Research (AFOSR). The objectives of these programs are (1) the development of a basic understanding of the processes of localized corrosion and corrosion fatigue crack nucleation and growth in high-strength aluminum alloys used in airframe construction, (2) the formulation of kinetic models for these elemental processes, and (3) the integration of these models into probabilistic models that can provide guidance in formulating methodologies for service-life prediction and airworthiness assessment. Experimental efforts under the FAA-sponsored program were directed at the 2024-T3 aluminum alloy, while those under the AFOSR-sponsored program were concentrated on the 7075-T651 alloy. This report summarizes research performed under the Phase II program from 15 June 1995 to 30 September 1999 and includes modeling efforts in which shared FAA and AFOSR sponsorship necessarily occurred.

Research under these programs has demonstrated the efficacy and value of using a multidisciplinary, mechanically based probability approach to address the issues of aging of civil and military aircraft. Localized corrosion and corrosion fatigue (acting in competition) have been shown to be a principal material aging mechanism in structural aluminum alloys used in aircraft construction. The operation of this mechanism in service is confirmed by teardown inspection data from the lower wing panels and stiffeners from two transport aircraft that had been in commercial service for about 24 and 30 years. It is supported by preliminary metallographic information from the lower wing panels of one of the aircraft. Localized corrosion nucleated at constituent particles in highly stressed areas of aluminum alloys through particle-induced galvanic attack of the matrix and grew from particle to particle in a cluster or contiguous clusters of particles to form severe corrosion pits. These severe pits (on the order of 50 to 200 μm in depth) served as nuclei for fatigue cracking and can reduce the fatigue (crack growth) life by a factor of 10. Localized corrosion, therefore, is deemed to be the principal contributor to the early onset of multisite (fatigue) damage (MSD), and its impact on structural integrity and flight safety needs to be assessed.

Based on the understanding developed under these programs, a simplified, mechanistically based probability model (incorporating localized corrosion and fatigue crack nucleation and growth) was formulated. Using laboratory data on localized corrosion and fatigue crack growth rates and by considering only the primary (typical) loading from ground-air-ground cycles, the evolution of corrosion and fatigue damage in the fuselage and lower wing skins of a commercial transport aircraft was estimated. The predicted probability of occurrence (PoO) of damage is compared against the probability of detection (PoD) through the use of state-of-the-art nondestructive inspection (NDI) techniques. The comparisons suggest that the present level of PoD (for example, at 50% for a 1.27-mm deep crack using the ultrasonic technique) is inadequate. The fact that sizing of damage is not a required part of NDI is troubling. For airworthiness assessment and fleet life management, quantitative characterization of damage size should be an

integral part of an effective airworthiness assurance methodology. An appropriate nondestructive inspection target for damage sizes, at one-tenth the current level of sensitivity, should be set to recognize the role of corrosion in fostering the early onset of MSD.

The estimated distributions in corrosion and corrosion fatigue damage were compared against teardown inspection data from the lower wing panels and stiffeners from two transport aircraft that had been in commercial service for about 24 and 30 years. These aircraft had been examined as a part of the Air Force Joint Surveillance Target and Attack Radar System (J-STARS) program. The good agreement between the estimated and observed damage distributions demonstrated the efficacy of the approach and the feasibility of using short-term laboratory data to predict long-term performance. The utility of the model in estimating stress-life (S-N) response and the distribution of damage for structural integrity assessment that involves MSD is also shown. Results from this research are ready to be transitioned and can serve as the basis for developing methodologies for design and sustainment management of civil and military aircraft.

1. BACKGROUND AND OBJECTIVES.

Localized corrosion (in the form of pitting and exfoliation) and corrosion fatigue crack nucleation and growth are clearly recognized as degradation mechanisms that affect the structural reliability, durability, and integrity (safety) of commercial transport aircraft. The Aloha incident, as well as studies by the airframe manufacturers (for example, the Aging Aircraft Evaluation Program by Boeing), indicate that corrosion is far more widespread than anticipated [1]. A quantitative methodology for defining suitable inspection intervals and mandating repairs is needed for effectively managing the nation's fleet of commercial and military transport aircraft. The development of such a methodology requires a quantitative understanding, characterization, and modeling of the elemental processes of damage evolution and the integration of the various models into a probabilistic framework for estimating service lives or the probability of occurrence (PoO) or distribution of damage over time. The methodology can also be integrated into the design process to effect life-cycle design optimization and sustainment planning for new aircraft and into the development of suitable fixes for the current fleet.

Lehigh University proposed to undertake a 3-year program of research to study corrosion and corrosion fatigue of airframe materials in support of the Federal Aviation Administration Aging Aircraft Program. The proposed program was accepted by the FAA and research was initiated on 15 June 1992 (Phase I). It was extended as Phase II, effective 15 June 1995, and covered the period to 30 September 1999 through no-cost extensions. The program was complemented by programs sponsored by the Air Force Office of Scientific Research (AFOSR) from 1 July 1993 to 31 January 2001.

The objectives of these programs are (1) the development of a basic understanding of the processes of localized corrosion and corrosion fatigue crack nucleation and growth in high-strength aluminum alloys used in airframe construction, (2) the formulation of kinetic models for these elemental processes, and (3) the integration of these models into probabilistic models that can provide guidance in formulating methodologies for service-life prediction and airworthiness assessment. Experimental efforts under the FAA-sponsored program were directed at the 2024-T3 aluminum alloy, while those under the AFOSR-sponsored program were concentrated on the 7075-T651 alloy.

2. TECHNICAL APPROACH.

The technical approach involves the development of mechanistic understanding of the processes of localized corrosion and corrosion fatigue crack growth in terms of electrochemistry, microstructure and fracture mechanics, as well as the identification of sources of variability and characterization of their distribution. Based on this information, mechanistically based probability models are formulated to serve as the basis for developing methodologies for the sustainment and management of aging commercial and military aircraft.

The development of damage is illustrated schematically in figure 2-1 and is shown in a flow diagram in figure 2-2. The early stage is dominated by corrosion in the form of pitting (or other localized corrosion) and the later stage by corrosion fatigue crack growth. Within the context of these mechanisms, an upper bound of damage is to be defined in terms of structural reliability and damage tolerance considerations for mandating repairs. The research is focused, therefore, on the quantitative understanding and characterization and kinetic modeling of the following elemental processes:

- Onset of localized corrosion damage (particularly mechanisms and kinetics of pit nucleation and growth).
- Transition from pitting to fatigue crack growth.
- Early stages of corrosion fatigue crack growth (short-crack regime).
- Corrosion fatigue crack growth.

Crack Nucleation and Growth

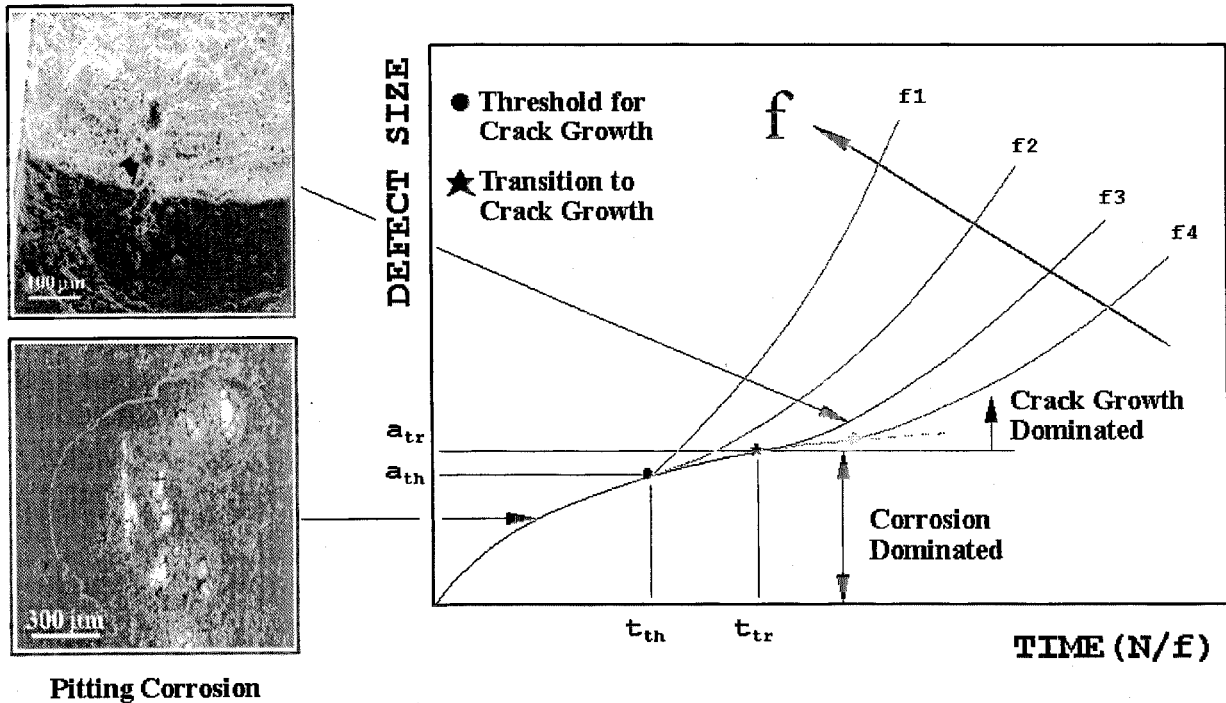


FIGURE 2-1. SCHEMATIC DIAGRAM OF THE DEVELOPMENT OF CORROSION AND CORROSION FATIGUE CRACK GROWTH

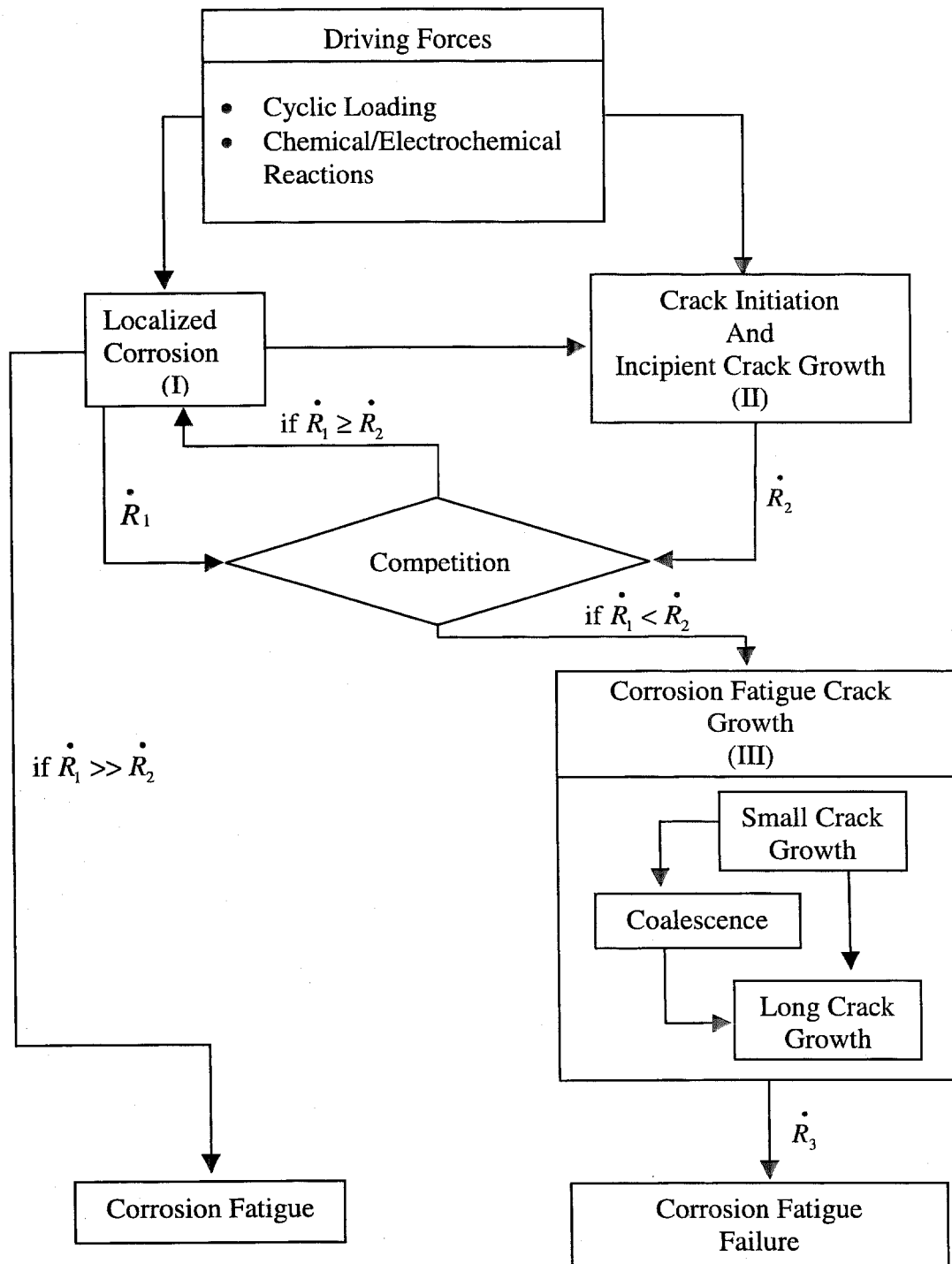


FIGURE 2-2. FLOW DIAGRAM SHOWING THE OVERALL PROCESSES FOR CORROSION AND FATIGUE DAMAGE

Formulation of a predictive model must include the probabilistic contributions from material properties and key variables on the rate of corrosion (particularly pit nucleation and growth), the transition from corrosion to cracking (i.e., crack nucleation) and corrosion fatigue crack growth.

The principal issues being addressed are as follows:

- Identification and verification of key internal and external variables that control each of the aforementioned unit processes for corrosion and corrosion fatigue cracking and determination of the stochastic nature of each process.
- Quantification of the probability distribution function (including time variance) of each of the key variables.
- Development of a quantitative understanding of the rate controlling step and mechanism for each damage process and formulation of a mechanistic (deterministic) model for each that describes the functional dependence on the key variables.
- Integration of mechanistic models and probability distribution functions and formulation of mechanistically based probability models for life prediction and reliability assessment.
- Validation of the approach and models through comparisons with available in-service or teardown inspection data on aging or retired aircraft.

The concept of a competition between localized (pitting) corrosion and corrosion fatigue crack growth in high-strength aluminum alloys was confirmed by experimental observations early in the program [1,2]. In addition, the early experiments showed localized (pitting) corrosion to be associated with constituent particles, and pit growth appeared to result from the coalescence of pits formed in a particle cluster or clusters. The particle density can be high (i.e., about 3,000 particles/mm² for those with projected surface area >1 μm² in a 1960s vintage 2024-T3 alloy) [1,2]. Clustering and banding were evident and appeared to depend on orientation. The research emphasis in Phase I, therefore, was placed on the role of constituent particles on pitting corrosion and the transition to fatigue crack growth. During Phase II, emphasis was placed on the development of a more detailed understanding and modeling of pitting corrosion and fatigue crack growth (in the short-crack regime). A simplified probabilistic model of corrosion and corrosion fatigue was formulated and was used to estimate the probability of occurrence (PoO) and distribution of damage. The estimates were used to assess the probability of detection (PoD) by nondestructive inspection (NDI) techniques and for validation through comparisons with data on aircraft that have been in long-term service.

In this report, principal findings from Phase II are summarized in the following sections. Information from the companion AFOSR sponsored program is included. A cumulative list of presentations and publications from these programs is appended to this report.

3. LOCALIZED (PITTING) CORROSION.

Studies of localized corrosion were focused upon pitting corrosion as a precursor to corrosion fatigue cracking in the 2024-T3 and 7075-T651 (bare) alloys and were carried out principally at room temperature in 0.5M NaCl solutions. Initial results showed that localized corrosion (pitting) resulted from galvanic coupling of the matrix with constituent particles in the alloys [1,2]. Pitting was found to depend strongly on temperature and solution pH. The pitting rate increased with increasing temperature (corresponding to an activation energy of about 40 kJ/mol), and was higher at more basic pH levels. The process appeared to be very complex, involving 3D interactions with the constituent particles. Corrosion sensitivity appeared to be orientation dependent; being more severe in the thickness orientation (the orientation that is more representative of the surface of a rivet or fastener hole) because of local segregation of the constituent particles.

To better understand particle-induced localized (pitting) corrosion, more detailed studies of pitting were carried out on the transverse sections of these alloys at room temperature by *in situ* monitoring and by post corrosion examinations using optical and SEM. A replication technique was developed to facilitate examinations of the morphology of corrosion pits in three dimensions and measurements of pitting kinetics. Identification of the constituent particles and observations of particle-induced galvanic corrosion were carried out by TEM along with measurements of galvanic current between pure aluminum and model compounds that are representative of the composition of certain constituent particles. In addition, initial statistical models for particle and pit distribution and pit growth were developed. Principal results from these studies are briefly summarized.

3.1 CONSTITUENT PARTICLES.

Two types of constituent particles were identified initially by energy dispersive x-ray spectroscopy (EDS) in the SEM [1,2]: Type A particles that are anodic and Type C particles that are cathodic with respect to the matrix. In the 2024-T3 alloy, Type A particles are those that contain Al and Cu or Al, Cu, and Mg. Type C particles represent a complex group with varying amounts of Al, Cu, Fe, and Mn (and sometimes Si). Types A and C particles in 7075-T651 alloy, on the other hand, contain Al, Cu, Mg, and Zn and Al, Cu, Fe, Cr, Mn, and Zn, respectively. The density of these particles (with projected surface area greater than $1 \mu\text{m}^2$) was about 3,000 particles/ mm^2 in the 2024-T3 alloy¹ versus about 1,500 particles/ mm^2 in the newer 7075-T651 alloy. The distributions in particle sizes for the two alloys are similar. Elemental maps showed that nearly 75% of the constituent particles in the 2024-T3 alloy were Type A, whereas Type C constituted over 80% of the particles in the 7075-T651 alloy. More detailed characterizations by analytical electron microscopy (AEM) and x-ray microprobe analysis [3] showed Type A particles in the 2024-T3 alloy to be principally Al_2Cu and Al_2CuMg . They tended to be small and were nearly equiaxed. Type C particles, on the other hand, were identified with complex intermetallics. Typical particles that were examined showed them to be of the type $(\text{Fe,Mn})_x\text{Si}(\text{CuAl})_y$ and appeared to be modified forms of $\text{Al}_8\text{Fe}_2\text{Si}$ or $\text{Al}_{10}\text{Mn}_3\text{Si}$. They tended to be larger, often elongated and aligned along the rolling direction. In the 7075-T651 alloy, Type C particles were identified as orthorhombic $\text{Al}_{23}\text{CuFe}_4$ that contained small amounts of Cr, Mn, and Zn. The remaining particles in this alloy

¹ The 2024-T3 sheet was of 1960s vintage, and the 7075-T6 sheet was of 1980s vintage.

are principally amorphous SiO₂, which are inert. The compositions of these particles are consistent with the results of x-ray microprobe analyses.

3.2 PITTING CORROSION.

Pitting in these alloys, in a 0.5M NaCl solution, showed that localized corrosion (pitting) was associated with constituent particles. Based on electrochemical considerations, a distinction should have been drawn between anodic (Type A) and cathodic (Type C) particles; with anodic particles tending to dissolve themselves, while cathodic particles promoting dissolution of the adjacent matrix. Evidence from this research showed, however, that the anodic particles tended to take on a cathodic character as a result of deposition of Cu onto the particles during corrosion or through preferential dissolution of Al or Mg [4,5].

The pitting process is very complex and involves 3D interactions with constituent particles. Two modes of pitting corrosion were clearly identified: namely, (1) general pitting over the specimen surface and (2) severe localized pitting at selected sites. General pitting occurs almost immediately upon specimen immersion and leads to the formation of small, shallow pits over the entire specimen surface, figure 3-1. Each pit was clearly identified with a constituent particle on the specimen surface and corresponded with particle or matrix dissolution. Severe localized pitting at selected sites is attributed to the interactions of the matrix with a cluster or clusters of constituent particles. The particle clusters form local galvanic cells to sustain continued matrix dissolution and result in larger and deeper pits.

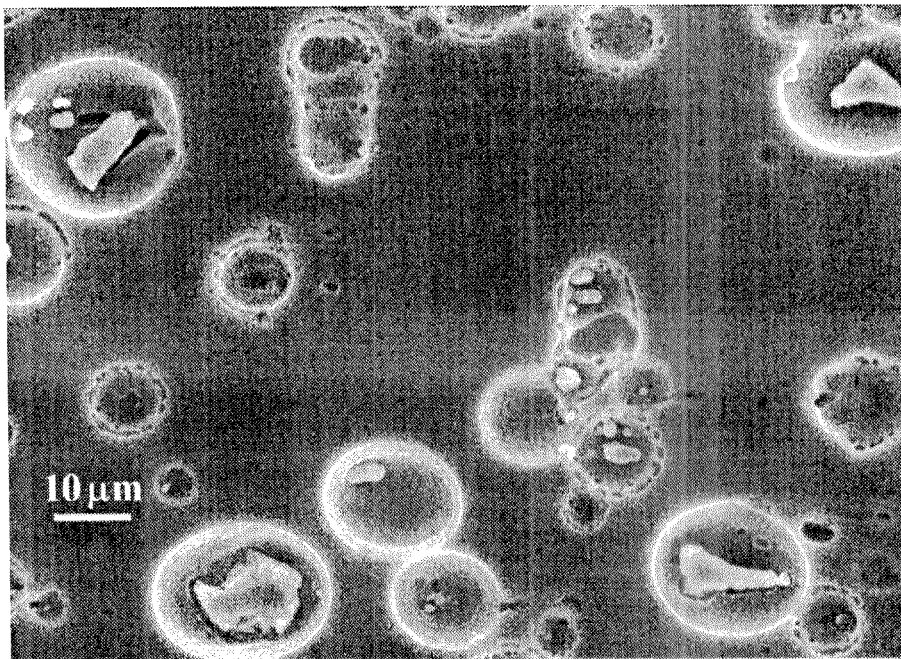


FIGURE 3-1. SEM MICROGRAPH SHOWING PITTING INDUCED BY CONSTITUENT PARTICLES IN A 2024-T3 ALUMINUM ALLOY

Figure 3-2 shows SEM micrographs of the cross section of pits formed from such clusters of constituent particles and an inset of the pits at the specimen surface [5,6]. The larger of the two pits is approximately 500 μm long and 70 μm wide at the surface and approximately 300 μm deep at this section. The overall shape of the pit reflects the planar distribution of constituent particles in this alloy. A comparison of the deeper severe pit in figure 3-2 with the SEM microfractograph of a fatigue crack origin (a corrosion pit represented by the dark region at the center of the microfractograph) in figure 3-3 shows that their overall features are nearly identical. The associated surface features of the fatigue origin (not shown) are also identical to those shown in the inset in figure 3-2. Similar comparisons clearly identify severe localized pits as nuclei for corrosion fatigue cracking.

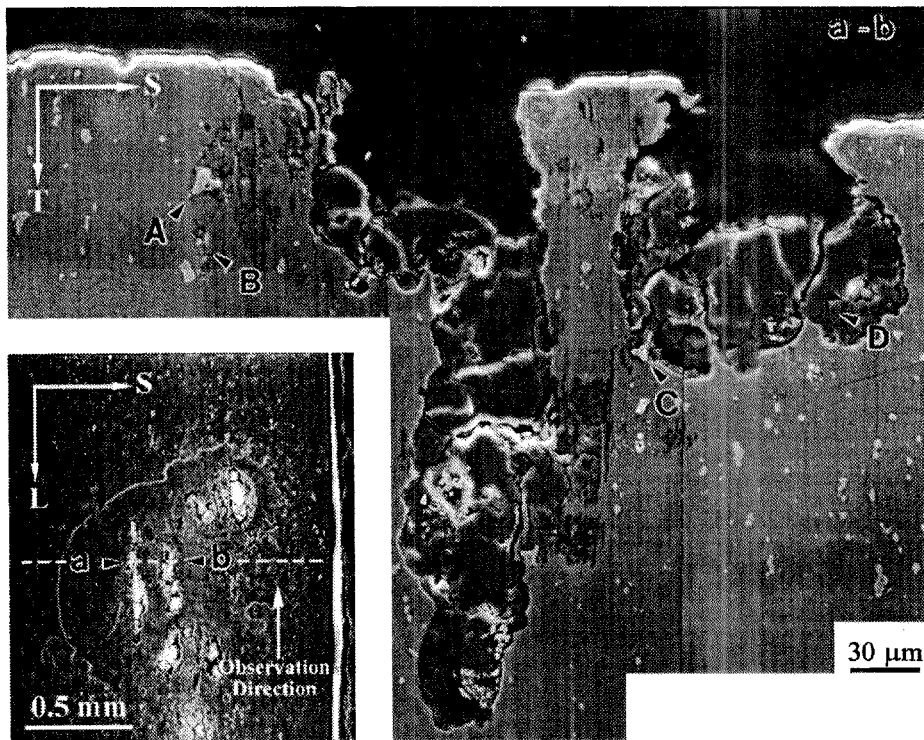


FIGURE 3-2. SEM MICROGRAPH OF THE CROSSSECTION OF SEVERE CORROSION PITS IN A 2024-T3 ALUMINUM ALLOY (TS) SURFACE ALONG WITH AN INSET SHOWING THE APPEARANCE OF THE CORRESPONDING PITS ON THE LS SURFACE

The 3D nature of the severe pits is captured by the comparison of the corroded LS (longitudinal-thickness) surface of a 1.6-mm-thick 2024-T3 aluminum alloy sheet after 500 hours of exposure to 0.5M NaCl solution, with the corresponding epoxy replica in figure 3-4 [5,6]. Each severe pit seen on the corroded surface is clearly associated with one on the replica (designated from 1 to 17 in figures 3-4(a) and (b)). Many detailed features of the corroded surface may be seen on the surface of the replica; compare, for example, the lightly corroded (cathodically protected) region surrounding each pit and the many small pits on the surface (figures 3-4(a) and 3-5(b)). The severe pits tend to be concentrated (>50%) along the midthickness region of the sheet and are narrow and long and substantially larger than the surface opening. For example, the surface length and width of pit 4 are 230 and 80 μm , respectively, as compared to an overall length and width of over 430 by

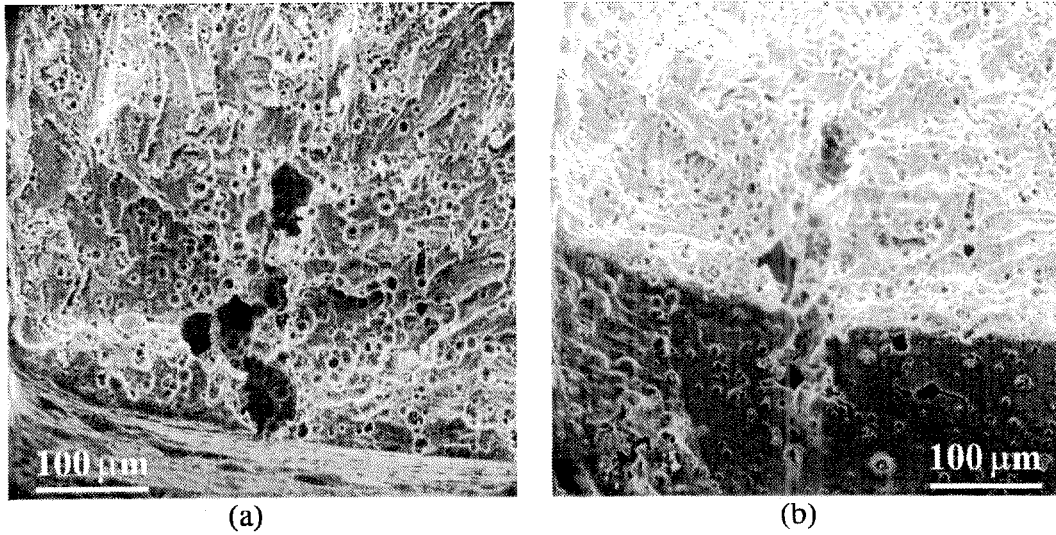


FIGURE 3-3. SEM MICROFRACTOGRAPHS OF FATIGUE FRACTURE SURFACE OF A 2024-T3 ALLOY SHOWING A SEVERE CORROSION PIT AS THE CRACK NUCLEUS: VIEWED (a) NORMAL AND (b) AT 45° TO THE FRACTURE SURFACE

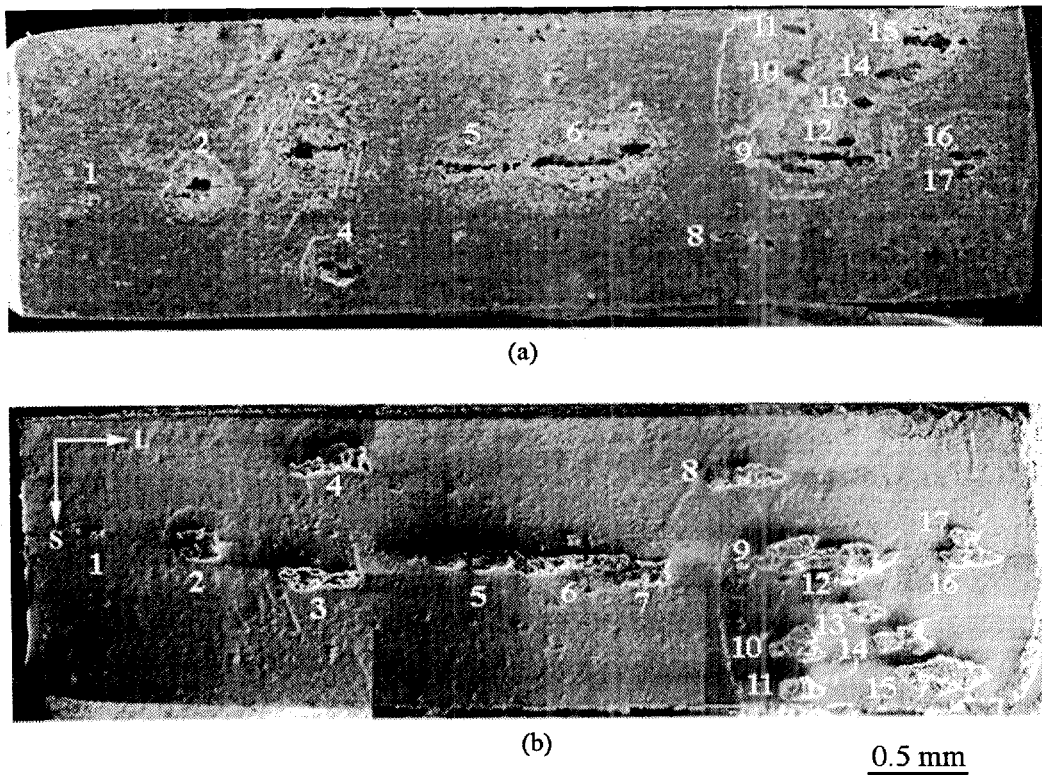


FIGURE 3-4. SEM MICROGRAPHS SHOWING SEVERE PITTING IN A 2024-T3 ALUMINUM ALLOY AFTER 500 HOURS IN 0.5M NaCl SOLUTION AT ROOM TEMPERATURE: (a) THE LS SURFACE AFTER CHEMICAL CLEANING AND (b) THE CORRESPONDING 3D REPLICA [6]

130 μm shown by the replica. The height (or depth of penetration) of the pits ranged from about 100 to over 300 μm . The replicas show substantial corrosion attack beneath the specimen surface and potential linkup of several pits into a single large pit of a complex shape (see, for example, pits 5, 6, and 7). They confirm that surface measurements alone would underestimate the extent and kinetics of pitting attack.

SEM micrographs of the replica of pit 2, in plan and side views, are shown at a higher magnification in figure 3-5. Figure 3-5 shows the typically complex form of a severe corrosion pit. The appearance of the replica is consistent with the postulated role of constituent particles in promoting pitting corrosion in the high-strength aluminum alloys. The individual rounded features are believed to correspond to galvanic corrosion of the matrix by the cathodic constituent particles in the alloy, and the overall planar appearance is attributed to the planar array of these particles in the rolled sheet. The open space seen in figure 3-5(b) suggests the role corrosion played around a particle (or a cluster of particles) at the surface in allowing the electrolyte to penetrate into the alloy and effect substantial corrosion beneath the surface. The 3D nature of these pits is best seen through the use of stereo imaging techniques (not shown here). The shape of the replica for pit 2 might be likened to that of one-half of a pecan or walnut with the center representing the small pit opening at the surface and the rest the cavernous pit below the surface.

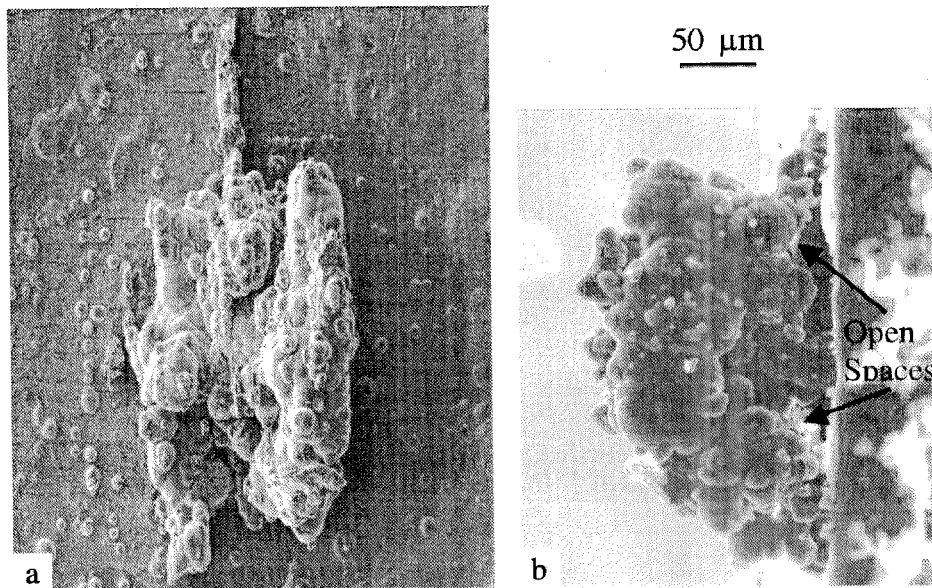


FIGURE 3-5. SEM MICROGRAPHS OF THE EPOXY REPLICA OF A SEVERE CORROSION PIT IN 2024-T3 ALUMINUM ALLOY: (a) PLAN (BOTTOM) AND (b) ELEVATION (SIDE) VIEW RELATIVE TO THE ORIGINAL PIT

To provide unambiguous confirmation for the role of constituent particles in promoting pitting, a series of experiments were carried out with the aid of TEM on the 2024-T3 and 7075-T651 aluminum alloys [4]. The constituent particles were first identified and the TEM (thin foil) samples were then repeatedly immersed in 0.5M NaCl solution and re-examined for galvanic corrosion attack. Figure 3-6 shows a pair of TEM micrographs to illustrate the typical galvanic corrosion of the matrix that results from the coupling with a cathodic constituent particle in the 7075-T651 alloy.

The larger semicircular region in figure 3-6(a) represents oxides that had been left behind by the corrosion. The smaller semicircular depression represents the original position of the particle in the

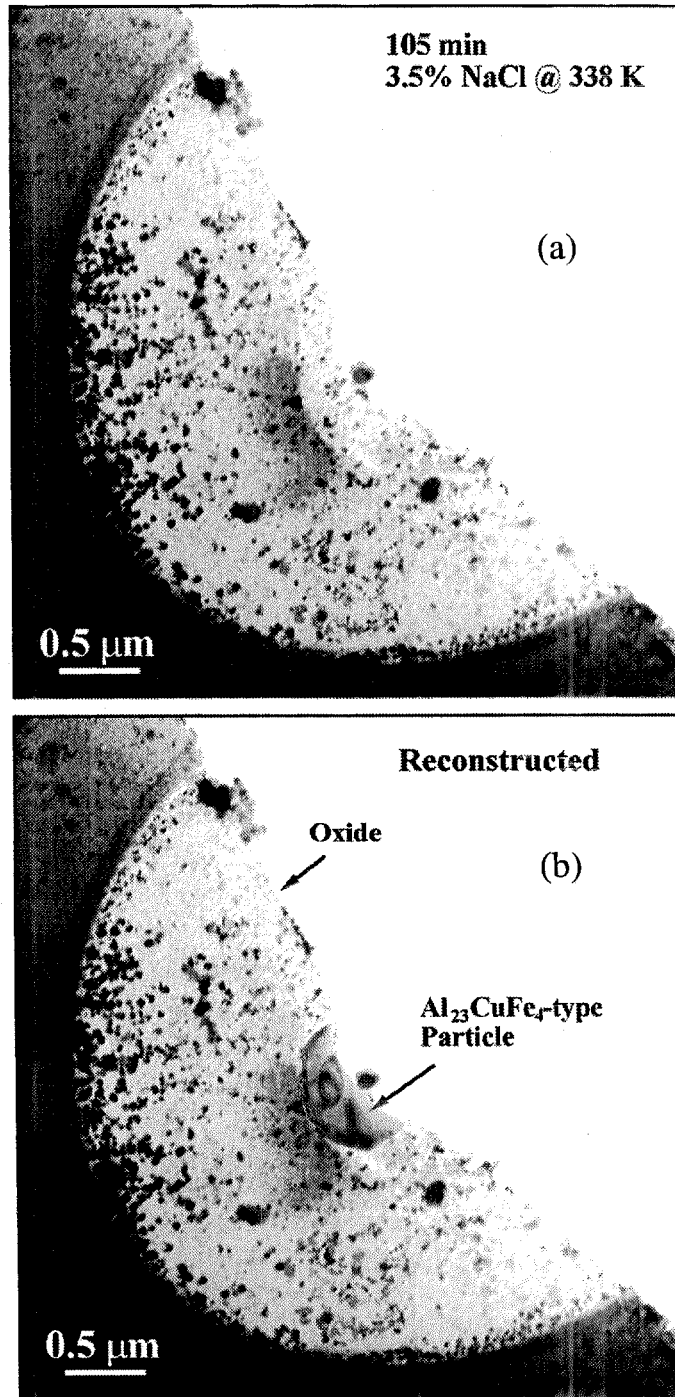


FIGURE 3-6. TEM MICROGRAPH OF 7075-T651 ALUMINUM ALLOY SHOWING OXIDE LEFT BEHIND BY PARTICLE-INDUCED CORROSION: (a) RESIDUAL OXIDE AND (b) RECONSTRUCTED IMAGE SHOWING POSITION OF ORIGINAL PARTICLE

thin foil which had fallen out during corrosion. The relative positions of the particle and the corroded region are shown in figure 3-6(b), with the particle photographically superimposed back into its original position. The size of the corroded region (about five times the particle radius) attests to the effective range of the potential field surrounding the particle.

For the 2024-T3 alloy, Al_2CuMg and Al_2Cu are anodic with respect to the matrix; Al_2Cu , however, is cathodic relative to pure aluminum. The (Fe,Mn) containing particles are cathodic relative to the alloy and pure aluminum. The TEM studies showed matrix dissolution around the (Fe,Mn) containing particles as a result of galvanic coupling between the particle and the matrix. Extensive matrix dissolution was also observed around the nominally anodic Al_2Cu particles as a result of plating of Cu back onto the particles during corrosion, figure 3-7. Although the Al_2CuMg particles dissolved rapidly as a result of galvanic coupling to the matrix, some matrix dissolution was also noted as a result of Cu deposition or Cu enrichment through preferential dissolution of Al and Mg from these particles, figure 3-8.

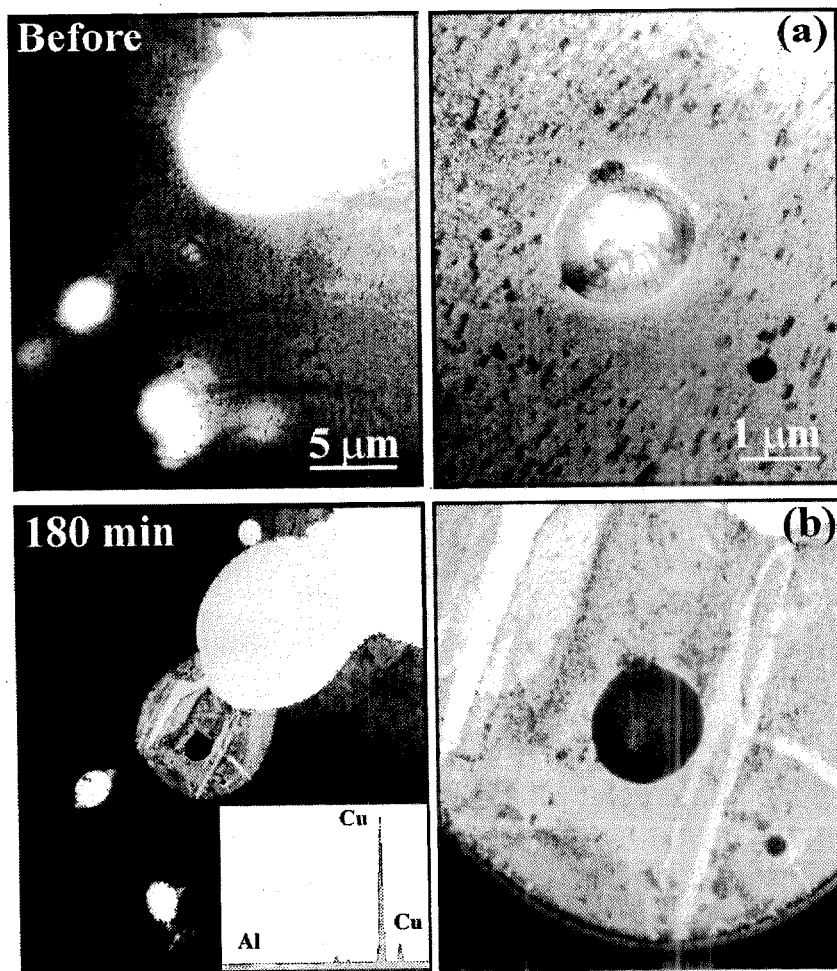


FIGURE 3-7. LOW- AND HIGH-MAGNIFICATION TEM MICROGRAPHS SHOWING A Al_2Cu PARTICLE AND ITS ENVIRONS IN A 2024-T3 ALUMINUM ALLOY: (a) BEFORE AND (b) AFTER 180-MIN. (CUMULATIVE) IMMERSION IN 0.5M NaCl SOLUTION AT ROOM TEMPERATURE. INSET IN (b) IS AN EDS SPECTRUM THAT SHOWS Cu TO BE THE PRINCIPAL COMPONENT IN THE CORROSION PRODUCT FILM

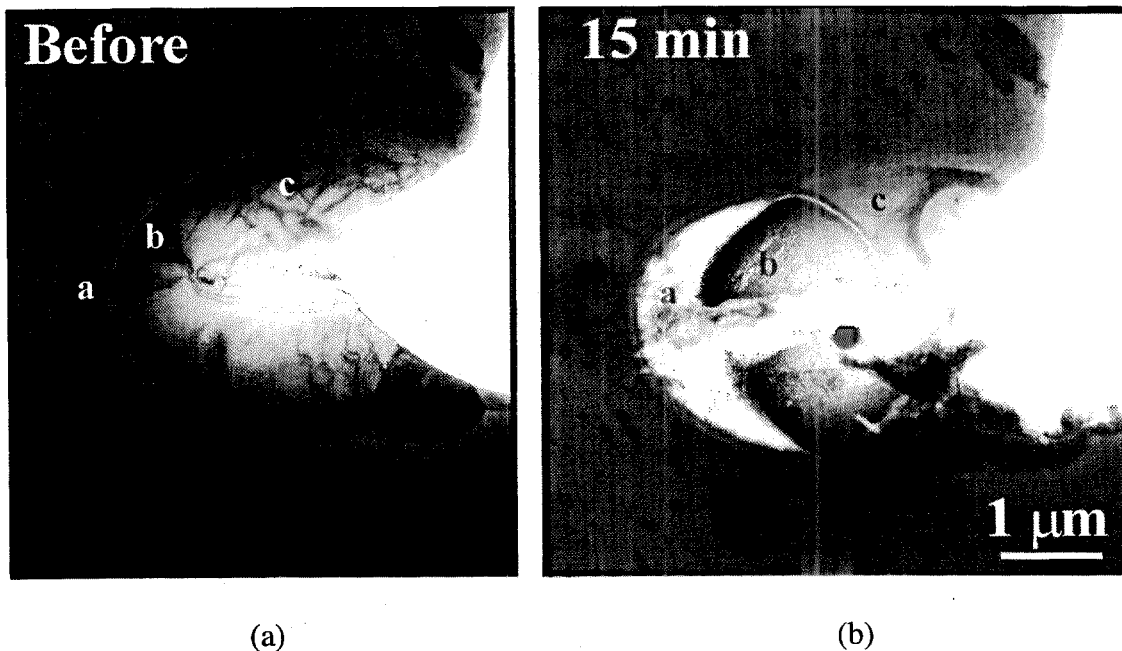


FIGURE 3-8. TEM MICROGRAPHS SHOWING AN Al_2CuMg PARTICLE AND ITS ENVIRONS IN A 2024-T3 ALUMINUM ALLOY: (a) BEFORE AND (b) AFTER 15-MIN. IMMERSION IN 0.5M NaCl SOLUTION AT ROOM TEMPERATURE

The extent of dissolution around Al_2Cu and the (Fe,Mn) containing particles were comparable to that around the Al_7CuFe_4 particles in 7075-T651. Matrix dissolution was less around the Al_2CuMg particles. The fact that it can take place around all or most of the constituent particles provides an important bridge for the development of the larger severe pits.

Dissolution current densities were estimated based on the estimated amounts of material removed by galvanic corrosion and reflected anodic or cathodic control by the particles [4]. For the anodic (Al_2CuMg) particles, the estimated current density was about 0.18 mA/cm^2 at room temperature. The estimated values were about 0.2 mA/cm^2 and 0.04 mA/cm^2 , respectively, for Al_2Cu and the (Fe,Mn) containing particles.

3.3 ELECTROCHEMICAL MEASUREMENTS.

To aid in the understanding of particle-induced pitting in 2024-T3 and 7075-T651 aluminum alloys, two model alloys, with compositions of 75%Al-25%Fe (Alloy A) and 70%Al-22%Fe-6%Cu-2%Mn (Alloy B) in atomic percent, were prepared to emulate constituent particles in these alloys [5,7]. Alloy A reflects the composition of the simplest cathodic particle in the 7075-T651 alloy and Alloy B reflects that of a typical cathodic particle in the 2024-T3 alloy. The model alloys were used to provide basic electrochemical information and for studying their galvanic interactions with pure aluminum.

TABLE 3-1. OPEN CIRCUIT POTENTIALS (OCP) OF PURE Al AND ALLOYS A AND B IN NEUTRAL 0.5M NaCl SOLUTION

Solution	Pure Al	Alloy A (Al ₃ Fe)	Alloy B (70Al-22Fe-6Cu2Mn)
0.5M NaCl, pH = 6.5	-730	-485	-620
0.5M NaCl, pH = 3.5	-1150	-600	-590
0.7M NaCl, pH = 3.5	-1150	-610	-600
0.5M NaCl + 0.07M AlCl ₃ , pH = 3.5	-1125	-660	-635

- Notes: 1. All the potentials are based on the saturated calomel electrode (SCE).
 2. Solutions were opened to the air and the [O₂] ≈ 7 ppm.
 3. All the potentials were double-checked.

The open circuit potentials (OCP) of these model alloys and pure aluminum in 0.5M and 0.7M NaCl and 0.5M NaCl + 0.07M AlCl₃ solutions are given in table 3-1. The measured anodic and cathodic current densities for the alloys A-Al and B-Al couples in the 0.5M NaCl and 0.5M NaCl + 0.07M AlCl₃ solution (at pH = 3.5 and 6.5) are shown as solid points in figures 3-9 to 3-12 as a function of the cathode-to-anode area ratio (A_c/A_a). In each case, the anodic current density (i_a) increased with area ratio at low area ratios, while the cathodic current density (i_c) remained essentially constant. At high area ratios, on the other hand, the cathodic current density decreased but the anodic current density remained constant. These results reflected the limiting cathodic or anodic current density that could be supported over the available surface area of the electrodes.

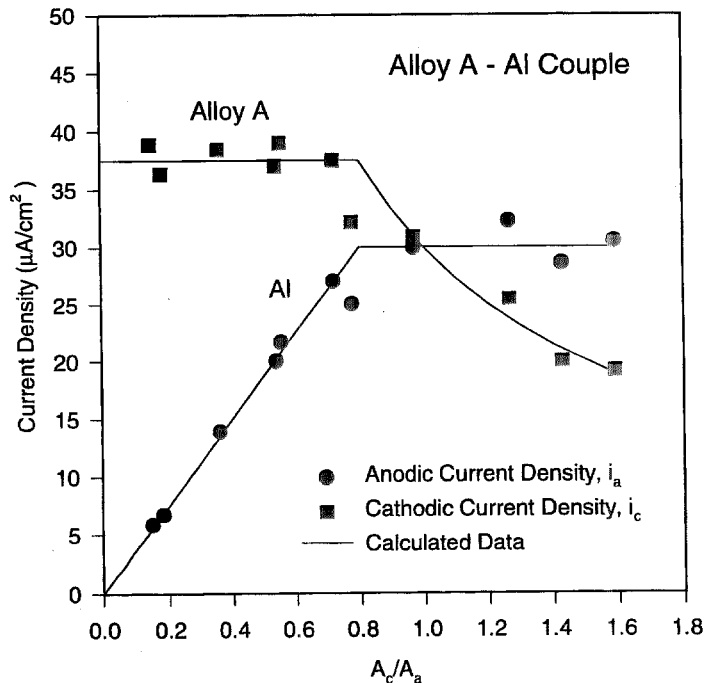


FIGURE 3-9. RELATIONSHIP BETWEEN CATHODE-TO-ANODE AREA RATIO AND CURRENT DENSITIES OF ALLOY A-AL COUPLE IN NEUTRAL 0.5M NaCl SOLUTION

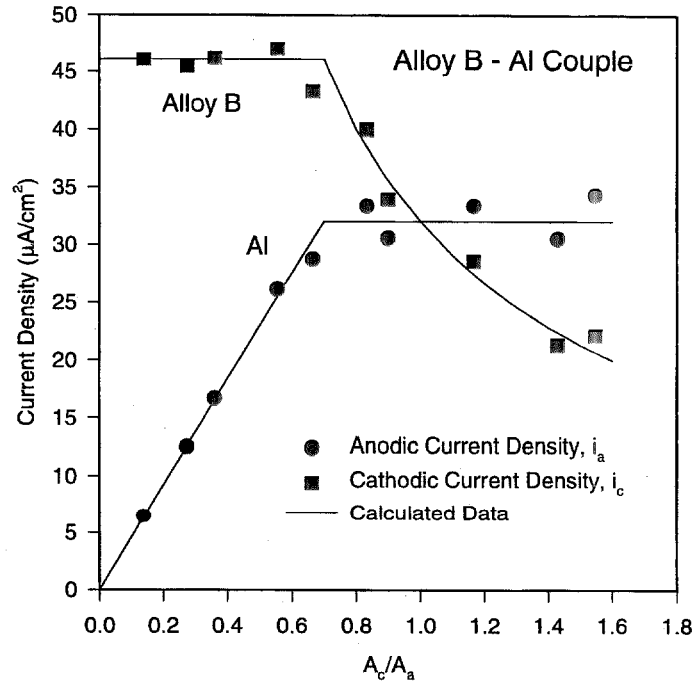


FIGURE 3-10. RELATIONSHIP BETWEEN CATHODE-TO-ANODE AREA RATIO AND CURRENT DENSITIES OF ALLOY B-AL COUPLE IN NEUTRAL 0.5M NaCl SOLUTION

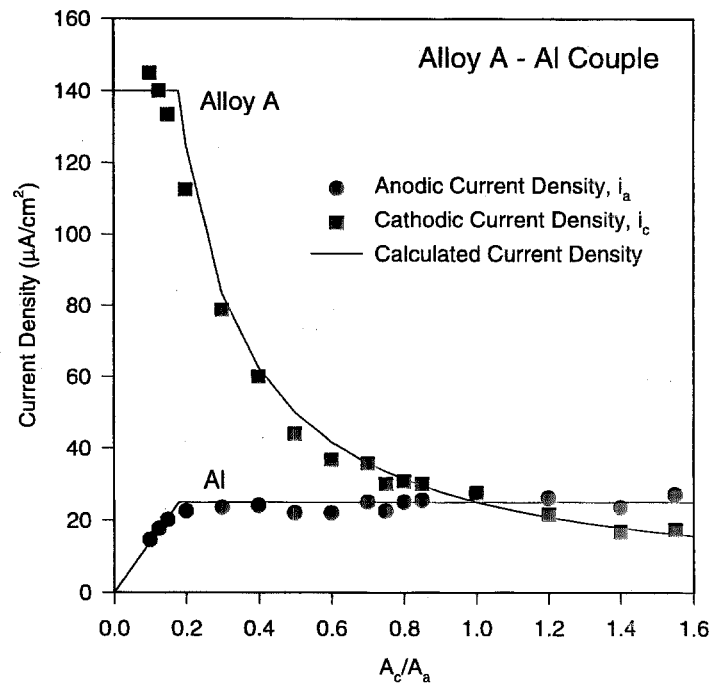


FIGURE 3-11. RELATIONSHIP BETWEEN CATHODE-TO-ANODE AREA RATIO AND CURRENT DENSITIES OF ALLOY A-AL COUPLE IN 0.5M NaCl + 0.07M AlCl_3 SOLUTION ($\text{pH} \approx 3.5$)

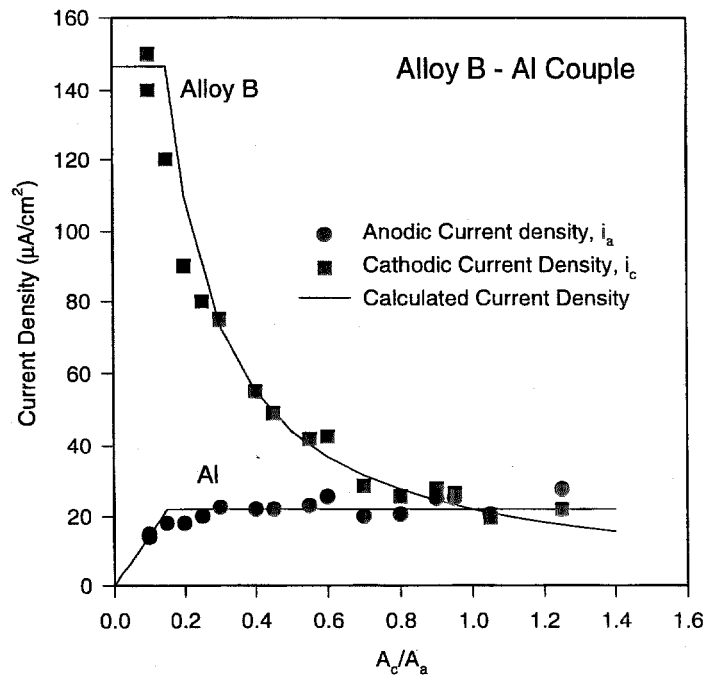


FIGURE 3-12. RELATIONSHIP BETWEEN CATHODE-TO-ANODE AREA RATIO AND CURRENT DENSITIES OF ALLOY B-AL COUPLE IN 0.5M NaCl + 0.07M AlCl₃ SOLUTION (pH \approx 3.5)

At low area ratios (or for a small cathodic surface), the galvanic current is limited by the limiting cathodic current density (i_{c0}), i.e., $i_c = i_{c0}$. The total current (I) is given by the product of i_{c0} and the cathodic area (A_c), i.e.,

$$I = i_{c0} \cdot A_c \quad (3.1)$$

The corresponding anodic current density (i_a) is then calculated by dividing the total current by the anodic area (A_a) as follows:

$$i_a = I/A_a = i_{c0} \cdot (A_c/A_a) \quad (3.2)$$

Equation 3.2 shows that, under cathodic control, i_a would decrease linearly as the area ratio (A_c/A_a) decreases. Similarly, at high area ratio, the total current is determined by the limiting anodic current density (i_{a0}), i.e., $i_a = i_{a0}$, and is proportional to the anodic area A_a :

$$I = i_{a0} \cdot A_a \quad (3.3)$$

The cathodic current density is then expressed as

$$i_c = I/A_c = i_{a0} \cdot (A_a/A_c) = i_{a0} \cdot (A_c/A_a)^{-1} \quad (3.4)$$

Under anodic control, i_c would then decrease linearly with the inverse of cathode/anode area ratio. At the transition from cathodic to anodic control, the limiting current over the cathodic and anodic surfaces would be equal to

$$I = i_{co} \cdot A_c = i_{ao} \cdot A_a \quad (3.5)$$

As such, the cathode-to-anode area ratio at the transfer of control, or the transition area ratio, $(A_c/A_a)_t$, is equal to the ratio of the limiting anodic and cathodic current densities:

$$(A_c/A_a)_t = i_{ao} / i_{co} \quad (3.6)$$

Using the average value of current densities over the estimated domains of anodic and cathodic control as the appropriate limiting current densities, the dependence of i_c and i_a on A_c/A_a was calculated using Equations 3.1 to 3.6, and are shown as solid curves in figures 3-9 to 3-12. The calculated curves fit the measured data well and support the postulate of cathodic and anodic control at low and high area ratios, respectively.

Comparisons of the limiting anodic and cathodic current densities and the transition area ratio of these two couples in 0.5M NaCl and 0.5M NaCl + 0.07M AlCl₃ solutions are listed in table 3-2. The transition area ratio for the A-Al and B-Al couples in 0.5M NaCl solution is about 0.8 and 0.75, respectively. The i_{ao} of both of the A-Al and B-Al couples in this solution is about 30 $\mu\text{A}/\text{cm}^2$, and the corresponding i_{co} is about 38 $\mu\text{A}/\text{cm}^2$ and 46 $\mu\text{A}/\text{cm}^2$, respectively. These values are consistent with current densities of 36 and 50 $\mu\text{A}/\text{cm}^2$ estimated by Wei et al. [4] from a TEM study of particle-induced corrosion for a Al₂₃Fe₄Cu particle in 7075-T6 alloy and a Fe-Mn-Cu-Si-Al particle in 2024-T3 alloy, respectively. The agreement suggested that the current densities obtained are reasonable and it is suitable to use the model alloys to characterize the electrochemical properties of constituent particles.

TABLE 3-2. LIMITING CURRENT DENSITIES AND TRANSITION AREA RATIO OF VARIOUS GALVANIC COUPLES IN VARIOUS SOLUTIONS

<i>Couples and Solution</i>	i_{ao} ($\mu\text{A}/\text{cm}^2$)	i_{co} ($\mu\text{A}/\text{cm}^2$)	$(A_c/A_a)_t$
A-Al Couple 0.5M NaCl Solution	30	38	0.8
B-Al Couple 0.5M NaCl Solution	32	46	0.75
A-Al Couple 0.5M NaCl + 0.07M AlCl ₃ Solution	26	140	0.18
B-Al Couple 0.5M NaCl + 0.07M AlCl ₃ Solution	22	147	0.15

The transition points of these two couples in 0.5M NaCl + 0.07M AlCl₃ solution (0.18 for A-Al and 0.15 for B-Al coupling) are much smaller than those in 0.5M NaCl solution (0.8 for A-Al and 0.75 for B-Al coupling). The values of i_{co} in this solution (140 $\mu\text{A}/\text{cm}^2$ for A-Al and 147

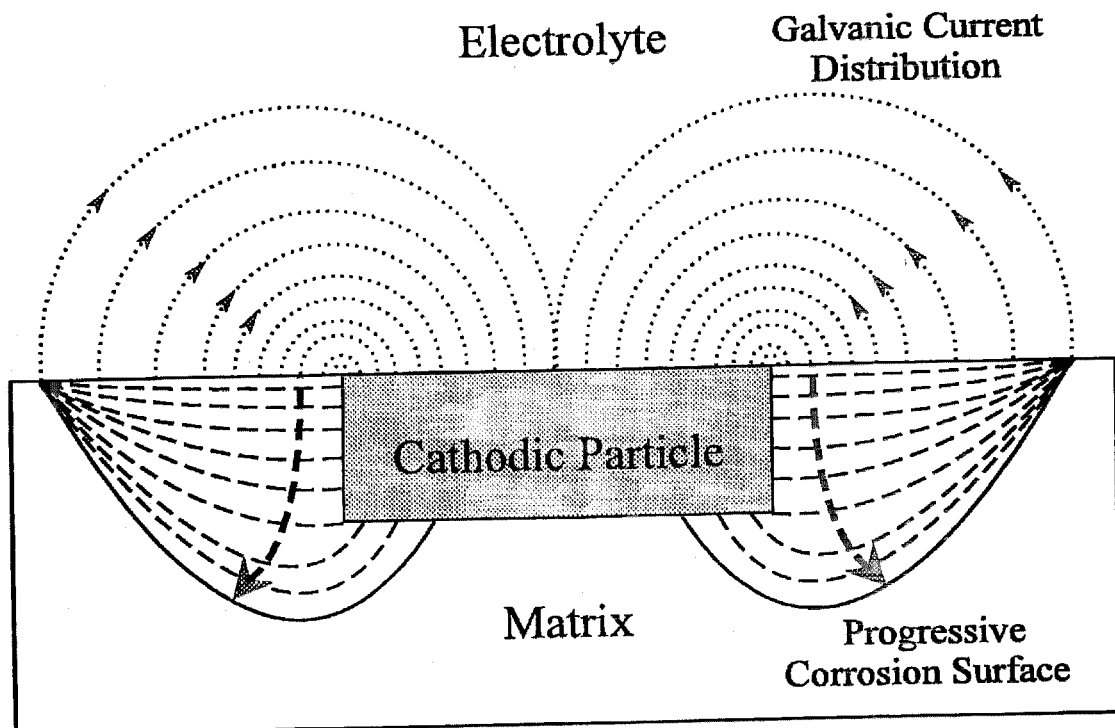
$\mu\text{A}/\text{cm}^2$ for B-Al coupling) are much higher than those in the 0.5M NaCl solution ($38 \mu\text{A}/\text{cm}^2$ for A-Al and $46 \mu\text{A}/\text{cm}^2$ for B-Al coupling) and reflect differences in pH and chloride ion concentration. The higher i_{co} suggests that a more rapid pitting attack would occur in the acidic solutions.

The observed relationship between current density and cathode-to-anode surface area ratio is important for the understanding of the kinetics of pitting corrosion. Since the surface area of a constituent particle is small relative to the matrix, the rate of particle-induced pitting in the aluminum alloys would be determined by the limiting cathodic current density over the particle(s) and the effective particle surface area. The effective surface area ratio may be estimated from the observations of Wei et al. [4]. They reported that particle-induced matrix dissolution extended over a region that is about five times the radius of the particle. The effective cathode-to-anode area ratio is, therefore, about 1/25 or 0.04. This is much smaller than the transition ratio of 0.8 and 0.75 for the A-Al and B-Al couples in the 0.5M NaCl solution and 0.18 and 0.15 in the 0.5M NaCl + 0.07M AlCl_3 solution. In the alloys, therefore, the rate of pit growth would be determined by the cathodic reactions over the particle surfaces.

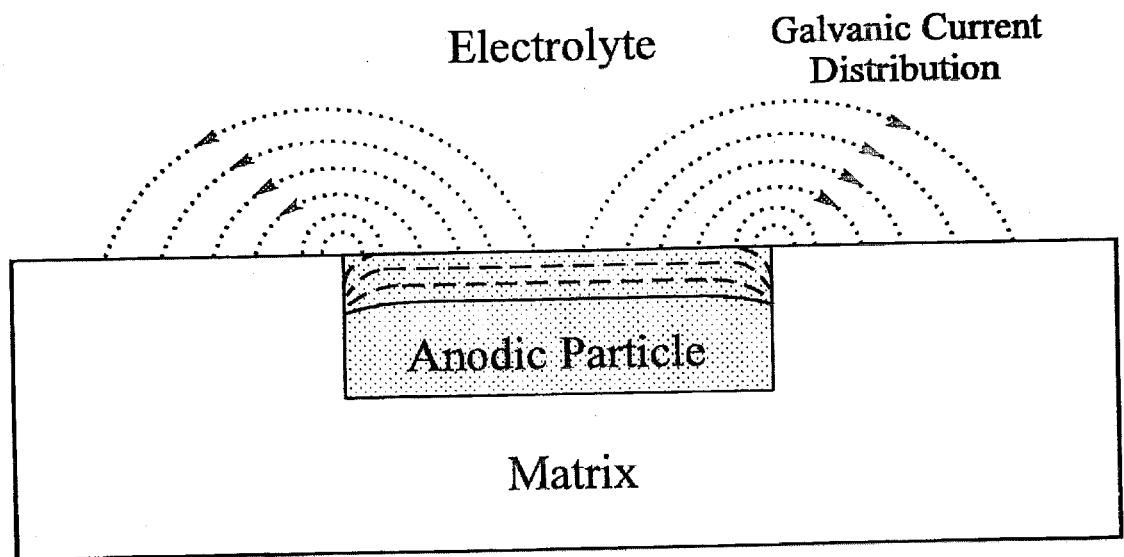
These observations have provided a clearer understanding of the phenomenon and mechanism of particle-induced pitting corrosion in commercial aluminum alloys. The galvanic coupling between constituent particles and the alloy matrix is responsible not only for the nucleation but also the growth of pits. Because the surface areas of constituent particles are always much smaller than the matrix, the particle-to-matrix area ratio would be smaller than the transition point of area ratios. The rate of particle-induced matrix dissolution (or pitting corrosion) would be cathodically controlled, with the pitting corrosion rate increasing with the particle size and the limiting cathodic current density. Higher limiting cathodic current in acidic solutions suggests that the particle-matrix couples would be more efficacious in promoting pit growth versus pit nucleation.

3.4 MECHANISTIC MODELS.

The findings confirm the original postulate for particle-induced pitting in these aluminum alloys. Based on these, and the previous SEM observations, a conceptual model for corrosion induced by a single particle is proposed, figure 3-13 [5]. A conceptual model for pit growth associated with a cluster of particles is depicted in figure 3-14 [5]. The multiparticle interactions within a pit (or occluded region surrounding the pit), however, make the problem much more challenging. Because this severe localized pitting is clearly linked to corrosion fatigue crack nucleation, emphasis will be placed on the development of mechanistic understanding and modeling of this process during the remainder of the current AFOSR program and in the proposed continuation of research. The quantitative, mechanistic model will need to incorporate the potential distribution around the particle and then be integrated into a model for severe pitting that involves clusters of constituent particles.



(a)



(b)

FIGURE 3-13. CONCEPTUAL MODELS OF PARTICLE-MATRIX INTERACTIONS (LOCAL CORROSION) FOR (a) A CATHODIC AND (b) AN ANODIC PARTICLE

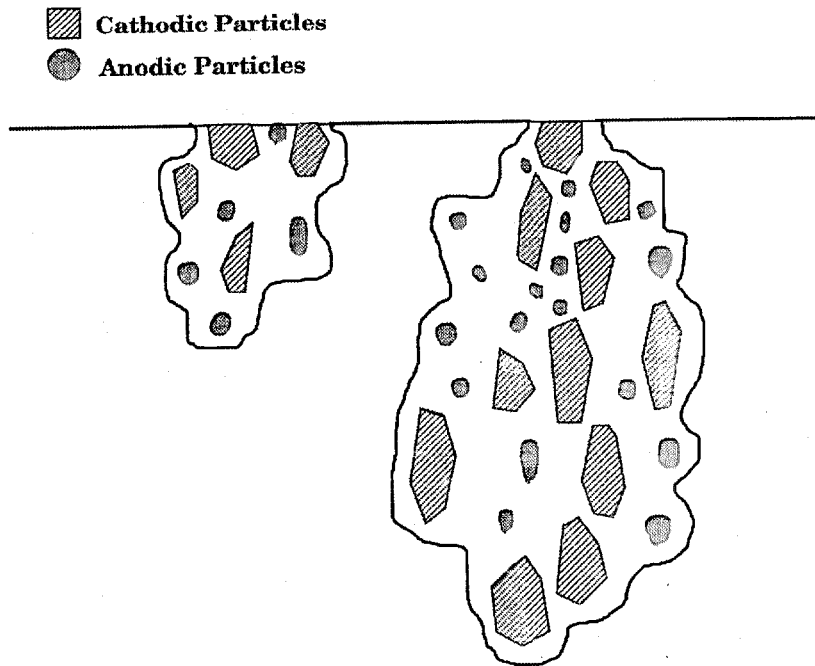


FIGURE 3-14. SCHEMATIC DIAGRAM OF A CONCEPTUAL MODEL FOR PITTING IN THE TRANSVERSE ORIENTATION INVOLVING MATRIX DISSOLUTION AROUND CLUSTERS OF CATHODIC (TYPE C) CONSTITUENT PARTICLES

4. TRANSITION FROM PITTING TO FATIGUE CRACK GROWTH.

Studies of the 2024-T3 and 7075-T651 alloys showed that fatigue failure, by-and-large, resulted from a single nucleation site [8]. Hence, a dominant flaw model for corrosion and corrosion fatigue would appear appropriate. The pit-to-crack transition size (or crack nucleation size), however, was found to depend on the cyclic-load frequency (being larger at lower frequencies). This frequency dependence reflected competition between pitting corrosion and fatigue. Corrosion fatigue crack nucleation, therefore, must be understood in terms of the competition between pitting and fatigue crack growth and is characterized by the transition to fatigue crack growth from a growing pit. Two criteria for this transition have been proposed and validated. They are (1) the cyclic stress intensity factor range (ΔK) for an equivalent crack must exceed the fatigue crack growth threshold ΔK_{th} , and (2) the time-based fatigue crack growth rate must exceed the pit growth rate; i.e.,

$$\Delta K \geq \Delta K_{th} \text{ and } \left(\frac{dc}{dt} \right)_{crack} \geq \left(\frac{dc}{dt} \right)_{pit} \quad (4.1)$$

The use of 'c' in the growth rate criterion gives recognition to the fact that the aspect ratios of most of the pits (or equivalent cracks) would lead to a higher ΔK at the surface.

To provide a graphical view of these criteria, a corrosion/fatigue map is proposed which delineates the transition ΔK (ΔK_{tr}) in relation to the cyclic-load frequency f , with the applied cyclic stress range as a parameter. The map is constructed by assuming a constant volumetric rate law for pit growth and a power-law for fatigue crack growth, with an exponent n , and is shown schematically in figure 4-1. The transition ΔK or ΔK_{tr} is given by one of the following relationships; the two relationships divide the ΔK versus $1/f$ space into two regions in which either fatigue crack growth or pit growth predominates:

$$\Delta K_{tr} = \Delta K_{th} \quad (4.2)$$

$$\Delta K_{tr} = \left[\frac{\pi(1.12k_t\Delta\sigma)^4 C_P \beta_{tr}^2}{2 C_F \Phi_{tr}^4} \right]^{\frac{1}{n+4}} \left(\frac{1}{f} \right)^{\frac{1}{n+4}} \quad (4.3)$$

where k_t is the stress concentration factor of the hole; $\Delta\sigma$ is the applied cyclic stress range; C_P and C_F are the pit and fatigue crack growth rate coefficients, respectively; and β_{tr} and Φ_{tr} are the aspect ratio and shape factor (elliptical integral) for the equivalent semielliptical crack at transition. The first of these relationships simply reflects exceedance of the fatigue crack growth threshold (ΔK_{th}). The second, on the other hand, reflects a higher value of ΔK_{tr} required by rate competition. Data on pit-to-crack growth transition for the 2024-T3 alloy are shown in figure 4-2 to illustrate the efficacy of this representation.

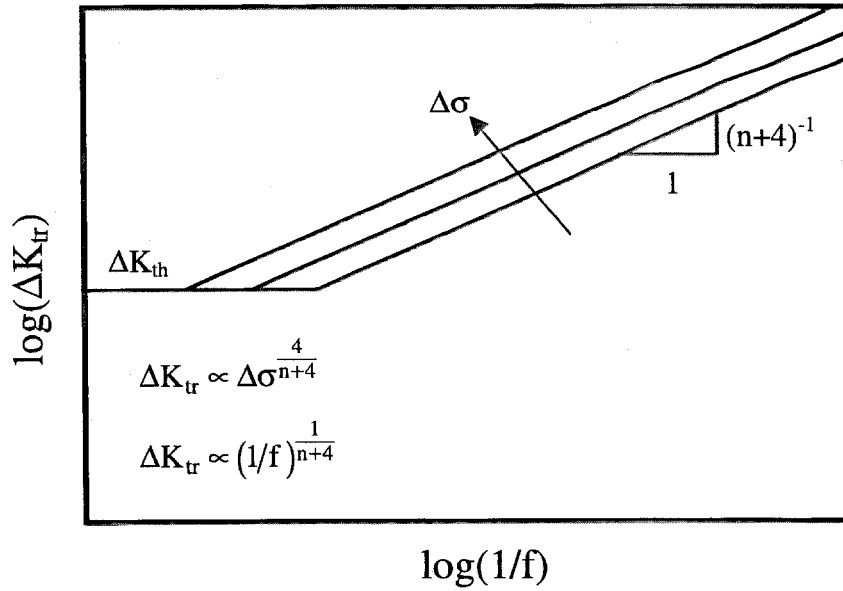


FIGURE 4-1. SCHEMATIC OF A PROPOSED CORROSION/FATIGUE MAP SHOWING THE RELATIONSHIP BETWEEN STRESS-INTENSITY FACTOR RANGE AND FREQUENCY WITH THE APPLIED CYCLIC STRESS RANGE AS A PARAMETER

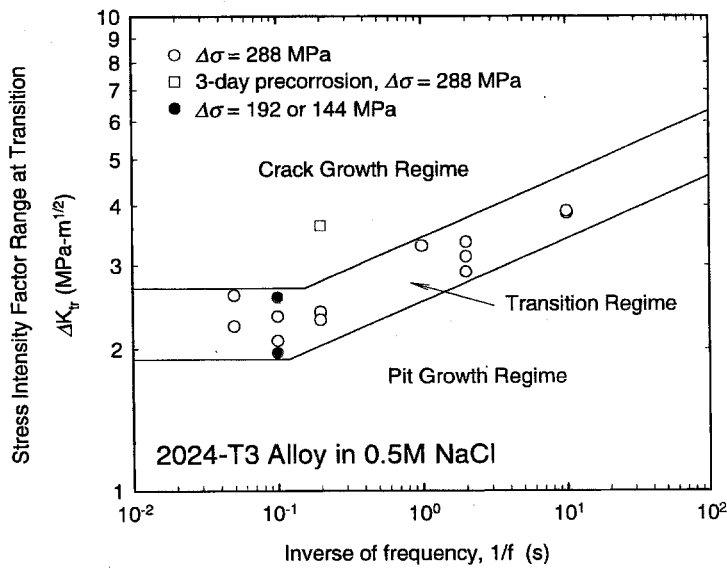


FIGURE 4-2. THE RELATIONSHIP BETWEEN THE STRESS-INTENSITY FACTOR RANGE OF EQUIVALENT CRACKS AT FATIGUE CRACK NUCLEATION AND THE FREQUENCY OF THE APPLIED CYCLIC STRESS

5. FATIGUE CRACK GROWTH.

In this section, the fatigue crack growth responses for the 2024-T3 and 7075-T651 aluminum alloys are considered, particularly in the “chemically short” crack growth regime. The influence of cyclic load frequency and the impact of chemically short-crack behavior on fatigue life are discussed. More detailed information may be found in references 9 through 11.

5.1 CHEMICALLY SHORT-CRACK BEHAVIOR.

The 2024-T3 and 7075-T651 aluminum alloys exhibited chemically short-crack behavior in an aerated 0.5M NaCl solution. The results are summarized in figures 5-1 through 5-5. Figures 5-1 through 5-3 show the chemically short-crack behavior for both alloys at a test frequency of 10 Hz. Figures 5-4 and 5-5 show the effect of frequency on the 7075-T651 chemically short-crack behavior. The fatigue crack growth (FCG) experiments were performed at room temperature under constant ΔK control on single-edge crack specimens with rectangular gage sections at a stress ratio (R) of 0.1. The pH value of the 0.5M NaCl solution was 6.2 ± 0.1 . The ΔK level and dissolved oxygen concentration ($[O_2]$) of the solution were systematically varied with ΔK ranging from 4 to 10 MPa m^{1/2} and $[O_2]$ from deaerated condition to about 30 ppm. FCG experiments in dehumidified air and oxygen showed growth rate similitude over the range of crack lengths (0.5 to 15 mm) examined in this study. The observance of growth rate similitude showed that the crack lengths were mechanically and microstructurally long.

5.1.1 2024-T3 Aluminum Alloy

The degree of the chemically short-crack behavior depended upon crack length, $[O_2]$, and ΔK level. The crack-growth rate response of the 2024-T3 aluminum alloy at several ΔK levels and a test frequency of 10 Hz is shown as a function of crack length in figure 5-1 in deaerated and aerated ($[O_2] = 7$ ppm) solutions. Growth rate similitude was observed over the range of crack lengths (0.5 to 15 mm) tested in the deaerated solution. The chemically short-crack behavior was observed when the experiments were performed in the aerated solution with $[O_2] = 7$ ppm. Crack growth rate similitude broke down at crack lengths shorter than 4 mm. The growth rates at a crack length of 0.5 mm, for ΔK of 4 and 5 MPa m^{1/2}, were approximately 1.5 times greater than those at crack lengths greater than 4 mm. The chemically short-crack behavior was not observed at ΔK levels above 5 MPa m^{1/2} in the aerated solution with $[O_2] = 7$ ppm. The behavior was seen, however, up to a ΔK level of 8 MPa m^{1/2} when the solution was saturated with dissolved oxygen ($[O_2] = 30$ ppm) as shown in figure 5-2. The chemically short-crack behavior does not exist at ΔK levels of 10 MPa m^{1/2} or higher regardless of the dissolved oxygen concentration.

5.1.2 7075-T651 Aluminum Alloy

The 7075-T651 aluminum alloy also exhibited chemically short-crack behavior at a test frequency of 10 Hz as shown in figure 5-3. Similar to the 2024-T3 alloy, the chemically short-crack behavior does not exist in the deaerated aqueous environment. The effect was observed in this alloy at all ΔK levels between 5 and 10 MPa m^{1/2} with $[O_2] = 7$ ppm. Increasing the

dissolved oxygen concentration to 30 ppm did not produce further increases in growth rates above those at 7 ppm. The growth rates at a crack length of 0.5 mm were two times greater than those at crack lengths longer than 8 mm up to a ΔK of $9 \text{ MPa m}^{1/2}$. The ratio of chemically short- to long-crack rates was reduced to 1.3 at a ΔK of $10 \text{ MPa m}^{1/2}$. The length of the chemically short-crack regime increases with increasing ΔK up to $\Delta K = 9 \text{ MPa m}^{1/2}$. The chemically short-crack behavior was also frequency dependent.

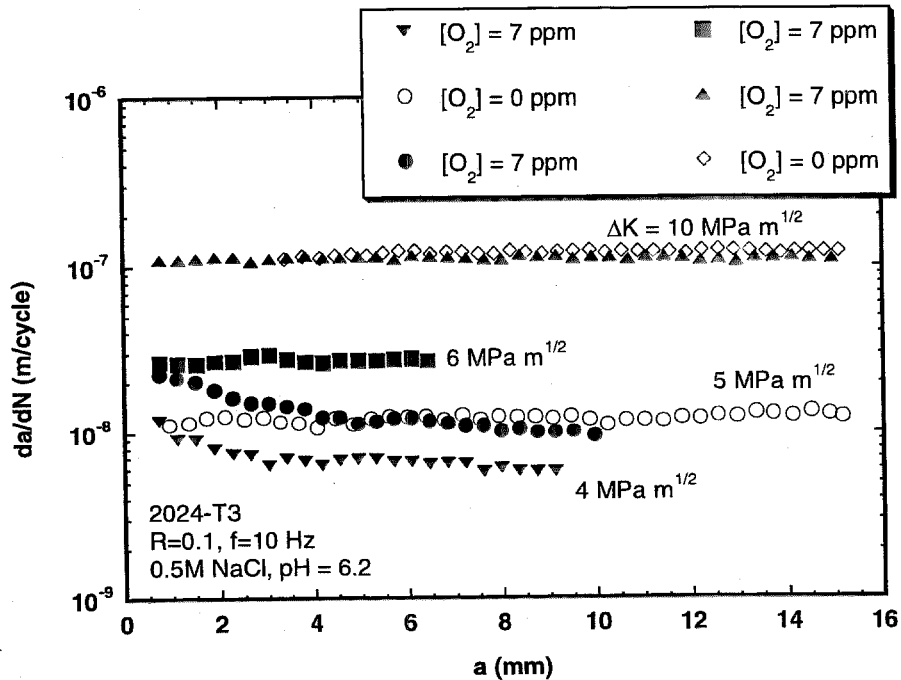


FIGURE 5-1. CHEMICALLY SHORT-CRACK BEHAVIOR IN THE 2024-T3 ALUMINUM ALLOY IN A DEAERATED AND AERATED SOLUTION WITH $[O_2] = 7 \text{ PPM}$

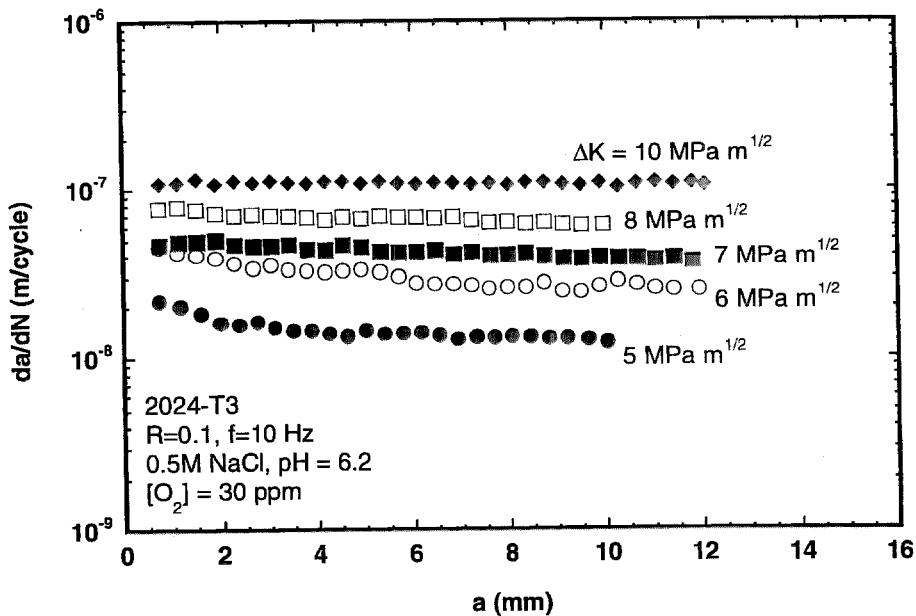


FIGURE 5-2. CHEMICALLY SHORT-CRACK BEHAVIOR IN THE 2024-T3 ALUMINUM ALLOY IN THE AERATED SOLUTION WITH $[O_2] = 30 \text{ PPM}$

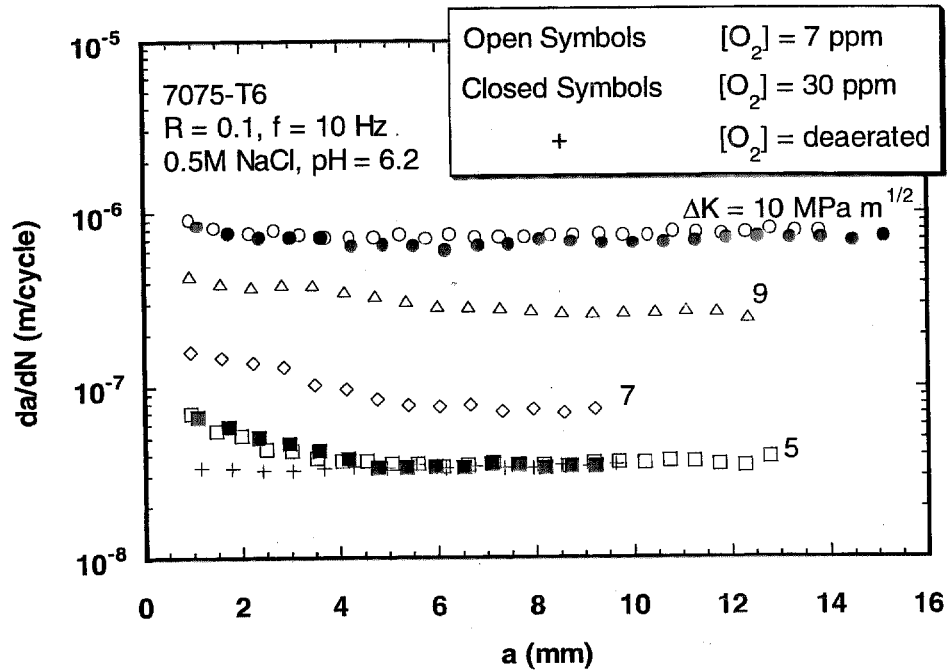


FIGURE 5-3. CHEMICALLY SHORT-CRACK BEHAVIOR IN THE 7075-T6 ALUMINUM ALLOY

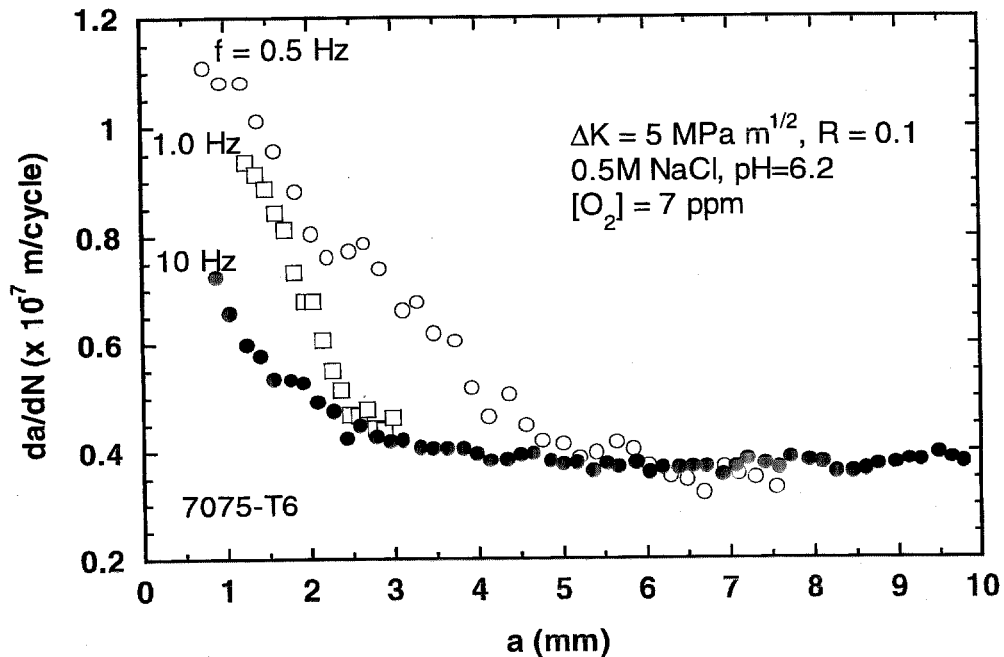


FIGURE 5-4. EFFECT OF FREQUENCY ON THE CHEMICALLY SHORT-CRACK BEHAVIOR IN A 7075-T6 ALUMINUM ALLOY AT A ΔK OF $5 \text{ MPa m}^{1/2}$

Chemically short-crack behavior in the 7075-T651 aluminum alloy was frequency dependent such that a decrease in frequency produced an increase in the ratio of chemically short-crack growth rates over those in the chemically long-crack regime as shown in figures 5-4 and 5-5. The influence of frequency on the chemically short-crack growth rates depended on the ΔK level.

Figure 5-4 shows that at a ΔK of $5 \text{ MPa m}^{1/2}$ the ratios of chemically short- to long-crack growth rates at a crack length of 0.5 mm were 3, 2.5, and 2 at frequencies of 0.5, 1, and 10 Hz, respectively. The frequency dependence at a ΔK of $10 \text{ MPa m}^{1/2}$ is shown in figure 5-5. The ratios of chemically short- to long-crack growth rates at a crack length of 0.5 mm were 2, 1.7, and 1.3 at the same frequencies, respectively.

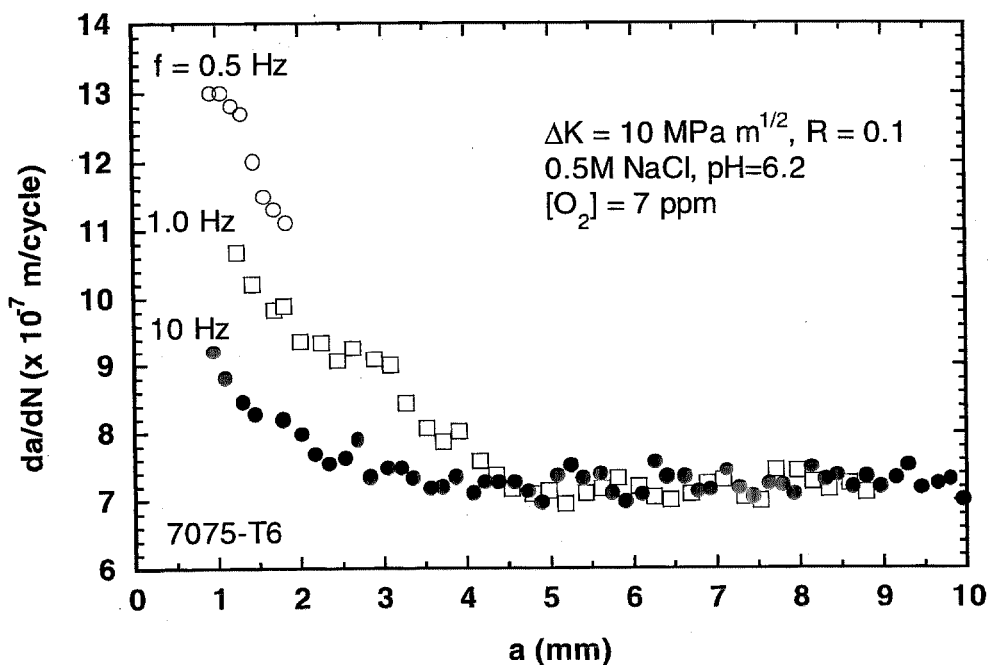


FIGURE 5-5. EFFECT OF FREQUENCY ON THE CHEMICALLY SHORT-CRACK BEHAVIOR IN A 7075-T6 ALUMINUM ALLOY AT A ΔK OF $10 \text{ MPa m}^{1/2}$

5.2 IMPACT OF CHEMICALLY SHORT-CRACK BEHAVIOR ON FATIGUE LIFE.

5.2.1 7075-T651 Aluminum Alloy

To assess the impact of the chemically short-crack behavior, fatigue life was estimated for growing a crack from a corrosion pit in a 1-mm-thick sheet of 7075-T651 aluminum alloy at frequencies of 0.5 and 10 Hz. For simplicity, the fatigue life was estimated by attributing the chemically short-crack behavior to the crack length interval from $30 \mu\text{m}$ to 1 mm and the chemically long-crack behavior from 1 to 6 mm. Since the crack was assumed to nucleate from a corrosion pit, the chemically short-crack life ($30 \mu\text{m}$ to 1 mm) was determined by using the ΔK solution for a semicircular surface crack in an infinite plate. Transition to long-crack growth was assumed to occur when the semicircular crack penetrated the sheet. The crack was then modeled as a through-thickness crack, with a starting length of 1 mm. The chemically long-crack life (1 to 6 mm) was determined by using the ΔK solution for a through-thickness crack in an infinite plate. The fatigue life was then estimated by establishing a relationship of the FCG rates (da/dN) to ΔK and integrating over the given crack length intervals. The da/dN - ΔK relationship followed a power-law relationship such that

$$\frac{da}{dN} = C \cdot \Delta K^n \quad (5.1)$$

where

$$\Delta K = \beta \cdot \Delta \sigma \cdot \sqrt{\pi a} \quad (5.2)$$

and $\beta = 2.2/\pi$ for the semicircular surface flaw (β_1), $\beta = 1$ for the through crack (β_2), $\Delta \sigma$ was the applied stress range at the pit, and a was the crack length. The chemically short-crack growth rates were taken to be 3.0 and 2.0 times greater than the chemically long growth rates on average at frequencies of 0.5 and 10 Hz, respectively. The crack-growth rate coefficients (C) and exponents (n) are shown in table 5-1 as estimated from the FCG data in figure 5-6. The power-law exponent (n) was assumed to be the same for the long- and short-crack regimes. The growth rate coefficients were different for the long- and short-crack regimes and are designated C_{LC} and C_{SC} , respectively.

TABLE 5-1. CRACK GROWTH RATE COEFFICIENTS AND EXPONENTS FOR THE 7075-T6 ALLOY AT 10 AND 0.5 HZ. THE UNITS FOR THE COEFFICIENTS (C) ARE (m cyc⁻¹)(MPa√m)⁻ⁿ

Frequency	C_{SC}	C_{LC}	n
10 Hz	3.48×10^{-11}	7.00×10^{-11}	4.24
0.5 Hz	1.04×10^{-10}	7.00×10^{-11}	4.24

The fatigue life, considering the long- and short-crack behavior, was determined by substituting Equation 5.2 into Equation 5.1 and rearranging such that

$$N_f = \int_{a_{iSC}}^{a_{fSC}} \left[C_{SC}^{-1} \cdot \beta^{-n} \cdot \Delta \sigma^{-n} \cdot \pi^{\frac{n}{2}} \cdot a^{-\frac{n}{2}} \right] da + \int_{a_{iLC}}^{a_{fLC}} \left[C_{LC}^{-1} \cdot \beta^{-n} \cdot \Delta \sigma^{-n} \cdot \pi^{\frac{n}{2}} \cdot a^{-\frac{n}{2}} \right] da. \quad (5.3)$$

Integrating over the chemically short- and long-crack growth regimes produces

$$N_f = C_{SC}^{-1} \cdot \beta_1^{-n} \cdot \Delta \sigma^{-n} \cdot \pi^{\frac{n}{2}} \cdot \left(\frac{n}{2} - 1 \right) \cdot \left[a_{iSC}^{\left(\frac{1-n}{2} \right)} - a_{fSC}^{\left(\frac{1-n}{2} \right)} \right] + C_{LC}^{-1} \cdot \beta_2^{-n} \cdot \Delta \sigma^{-n} \cdot \pi^{\frac{n}{2}} \cdot \left(\frac{n}{2} - 1 \right) \cdot \left[a_{iLC}^{\left(\frac{1-n}{2} \right)} - a_{fLC}^{\left(\frac{1-n}{2} \right)} \right]. \quad (5.4)$$

Equation 5.4 was then used to estimate fatigue life over the prescribed crack length intervals using two different stress ranges ($\Delta \sigma = 100$ and 60 MPa) at a frequency of 10 Hz. The estimated fatigue lives in table 5-2 show that the chemically long fatigue life is approximately 4 percent of the total life. The chemically long-crack regime (1 to 6 mm) was, therefore, neglected in subsequent estimations of fatigue life.

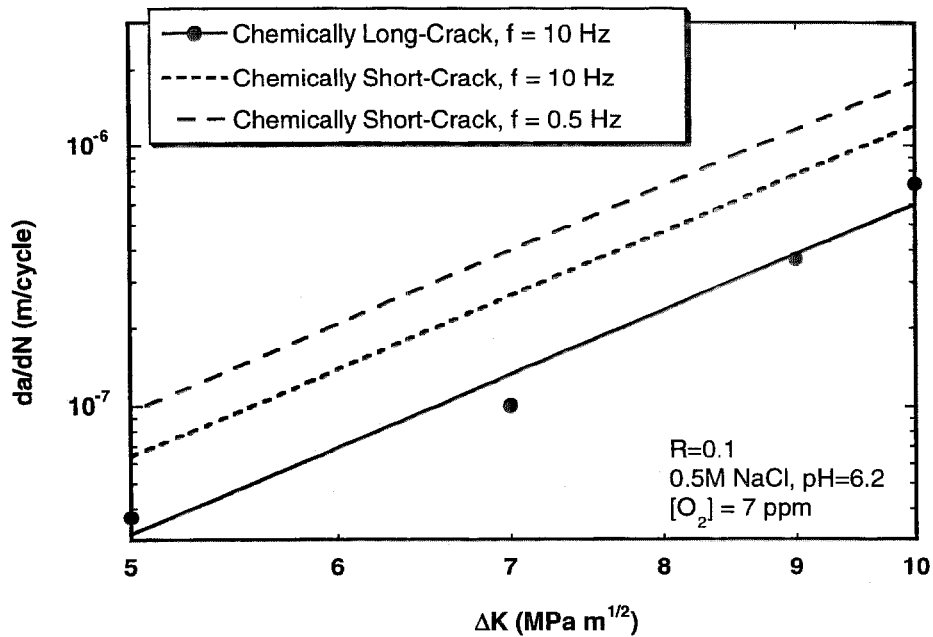


FIGURE 5-6. POWER-LAW RELATIONSHIP FOR THE CHEMICALLY LONG- AND SHORT-CRACK REGIMES FOR A 7075-T6 ALUMINUM ALLOY IN A 0.5M NaCl SOLUTION

To further demonstrate the impact of the chemically short-crack behavior and frequency, fatigue lives were estimated by considering the chemically short-crack growth behavior from a crack length of 30 μm to 1 mm at frequencies of 0.5 and 10 Hz. The applied stress was systematically varied to produce resulting fatigue lives using the first term in Equation 5.4. The fatigue lives were then compared against lives estimated using only the chemically long-crack growth rates. The impact of the chemically short-crack behavior is shown in figure 5.7 as a reduction in estimated fatigue life by approximately one-half at a frequency of 10 Hz and two-thirds at a frequency of 0.5 Hz. The cut off for the short-crack effect is due to the reduction of the chemically short-crack effect at that ΔK level. The decrease in fatigue life, when considering the chemically short-crack behavior, is commensurate with the increase in the chemically short-crack growth rates over those in the chemically long-crack regime.

TABLE 5-2. ESTIMATED FATIGUE LIFE FOR THE 7075-T6 CHEMICALLY SHORT- AND LONG-CRACK REGIMES AT 10 HZ. FATIGUE LIVES ARE GIVEN AS CYCLES

Stress (MPa)	Chemically Short ($a = 0.03\text{-}1\text{ mm}$)	Chemically Long ($a = 1\text{-}6\text{ mm}$)	Total Life
100	1.94×10^6	1.5×10^4	1.96×10^6
60	1.69×10^7	1.31×10^5	1.70×10^7

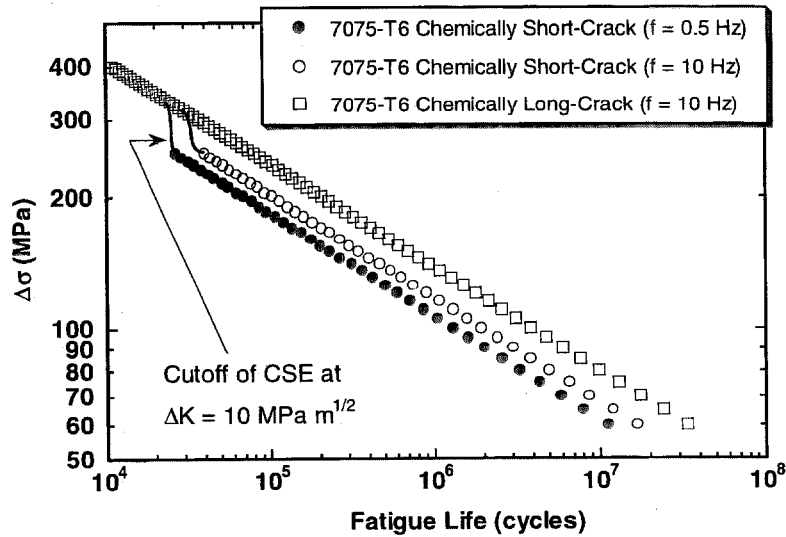


FIGURE 5-7. REDUCTION IN FATIGUE LIFE FROM A CRACK LENGTH OF 0.03 TO 1 MM CAUSED BY CHEMICALLY SHORT-CRACK BEHAVIOR IN THE 7075-T6 ALUMINUM ALLOY

5.2.2 2024-T3 Aluminum Alloy

The same analysis was performed for the 2024-T3 aluminum alloy given that the chemically short-crack growth rates were one and one-half times higher than the chemically long rates at a test frequency of 10 Hz. This alloy experienced a one-third reduction in fatigue life as shown in figure 5-8. The reduction in fatigue life was commensurate with the ratio of chemically short- to long-crack growth rates. The cutoff for the short crack effect occurs at a lower stress than for the 7075-T6 alloy since it corresponds to a lower ΔK level. Chemically short-crack behavior was not observed at a ΔK level greater than $5 \text{ MPa m}^{1/2}$ for the 2024-T3 alloy with $[\text{O}_2] = 7 \text{ ppm}$ in the solution.

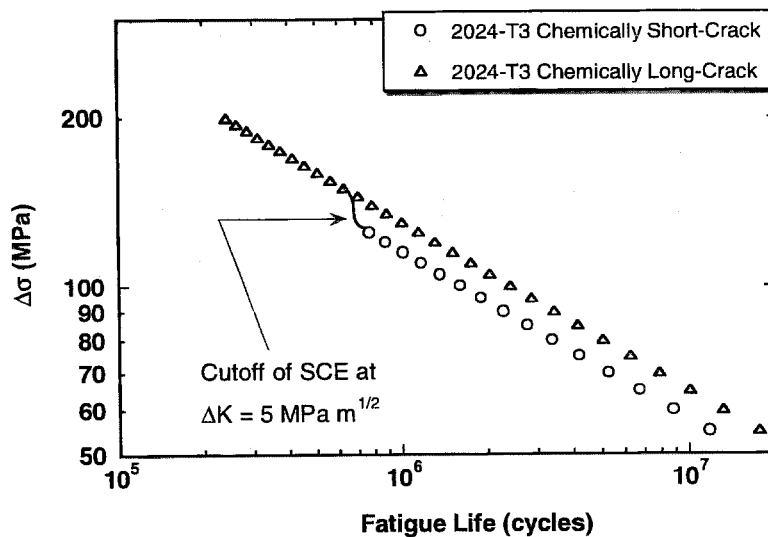


FIGURE 5-8. THE REDUCTION IN THE 2024-T3 FATIGUE LIFE FROM A CRACK LENGTH OF 0.03 TO 1 MM WHEN CONSIDERING CHEMICALLY SHORT-CRACK BEHAVIOR AT A FREQUENCY OF 10 HZ

6. MODELING AND INSIGHT.

Based on the foregoing mechanistic understanding, simplified modeling of corrosion and corrosion fatigue crack growth, based on first principles, was considered. The understanding was first applied to a possible clarification of the dichotomy between the conventional stress-life (S-N) and fracture mechanics approaches to corrosion fatigue [12-14]. The modeling was enhanced by the addition of probability and statistics considerations in order to predict damage accumulation and service life. The mechanistically based probability modeling allowed for a comparison of the probability of occurrence (PoO) of damage and the probability of its detection (PoD) by current nondestructive inspection (NDI) techniques [13].

6.1 EFFECT OF PITTING CORROSION ON FATIGUE LIFE.

An apparent dichotomy between the conventional stress-life (S-N) and fracture mechanics approaches to corrosion fatigue has been in existence since the 1960s. It is manifested in the fact that fatigue lives obtained conventionally through tests of smooth and notched specimens are sensitive to changes in external electrochemical variables (including applied potential, solution pH, and specific ions and their concentration). On the other hand, fatigue crack growth, based on precracked specimens, is essentially insensitive to changes in the same variables. Clarification of this dichotomy may be addressed through an estimation of the effect of corrosion pits on fatigue (or crack growth) life. In other words, the observed fatigue life may be governed essentially by the size of the initiating damage (particle or pit) and the rate of subsequent crack growth, and crack nucleation time, if present at all, could be reasonably neglected.

6.1.1 Modeling and Initial Comparison

For this estimate, the initiating corrosion pit was assumed to be hemispherical in shape and to be equivalent to a semicircular surface crack with the same radius. Fatigue crack growth was assumed to follow a power-law of the form

$$\frac{da}{dN} = C_F (\Delta K - \Delta K_{th})^{n_c}; \quad \Delta K = \beta \Delta \sigma \sqrt{a} \quad (6.1)$$

where C_F is crack growth rate coefficient; ΔK_{th} is the fatigue threshold ΔK ; $\beta = 2.2\pi^{1/2}$ is a geometric parameter; and n_c is the power-law exponent. The parameters C_F , n_c , and ΔK_{th} are functions of environment, temperature, and other factors. Based on data for 2024-T3 alloy in 0.5M NaCl solution, they are estimated to be $C_F = 3.95 \times 10^{-11} \text{ (m cyc}^{-1}\text{)(MPa}\sqrt{\text{m}}\text{)}^{-3.55}$, $n_c = 3.55$ and $\Delta K_{th} = 0.5 \text{ MPa}\sqrt{\text{m}}$. The choice of ΔK_{th} is somewhat arbitrary and recognizes that the level associated with a corrosion pit may be substantially lower than that observed from long-crack experiments. Because the initiating pits are much smaller than the final crack at fracture, the fatigue life is given simply from integrating Equation 6.1 by Equation 6.2. The influence of initial pit size is reflected through the initial value ΔK_i .

$$N_F \approx \frac{2}{(n_c - 2)C_F \beta^2 \Delta \sigma^2 (\Delta K_i - \Delta K_{th})^{(n_c - 2)}} \left[1 + \frac{(n_c - 2)\Delta K_{th}}{(n_c - 1)(\Delta K_i - \Delta K_{th})} \right] \quad (6.2)$$

The predicted fatigue lives at different stress levels from 100 to 400 MPa, for an initial pit radius of 10 to 200 μm , are shown in figure 6-1. The predictions are consistent and in agreement with the very early conventional stress-life (S-N) data for corrosion fatigue, with a reduction in life and a lowering of the endurance limit, figure 6-1 [12]. The reductions in fatigue lives are clearly identified with increases in the size of a corrosion pit (e.g., a 200 μm deep pit at 300 MPa reduced life from 10^6 cycles to less than 2×10^4 cycles). The response may be viewed also as a reflection of the influence of loading frequency; producing larger pits at the lower frequencies and, hence, shorter lives (see figure 6-1). They are also consistent with earlier estimates based on data obtained by Harmsworth on pre-pitted rotating bending specimens of a 2024-T4 alloy [14], figures 6-2 and 6-3. The compressive portion of the loading cycle was ignored in the analysis and aspect ratios were not taken into account because the information was not included in the original reference. Except for three points, the estimated lives are in good agreement with actual lives, figure 6-3. The scatter may be associated with variations in aspect ratio of the initiating pit or errors from optical measurements of the initial pit depth.

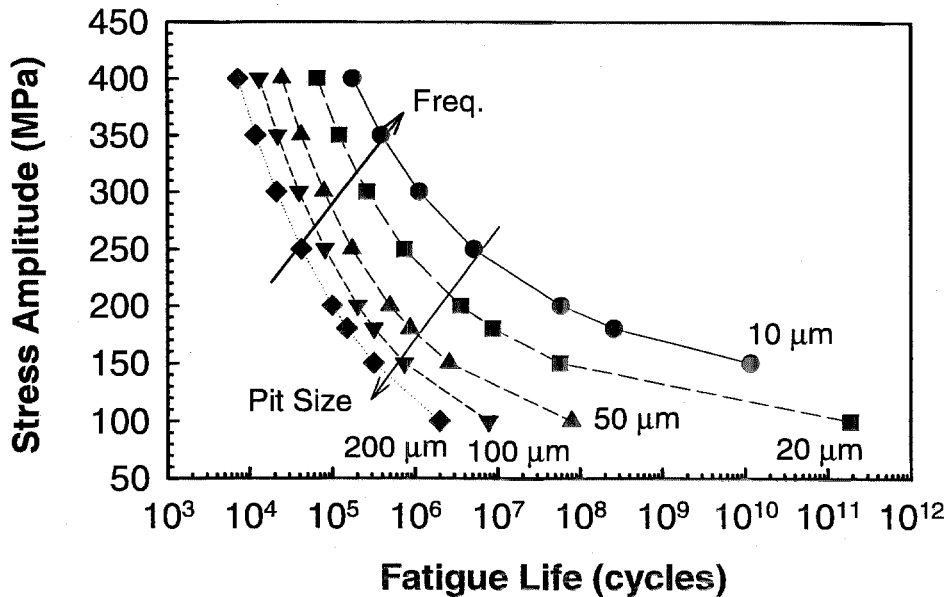


FIGURE 6-1. INFLUENCE OF STRESS, INITIAL PIT SIZE, AND FREQUENCY ON FATIGUE (CRACK GROWTH) LIFE

6.1.2 Further Verifications

To provide further verification of this hypothesis, notched specimens of 2024-T3 aluminum alloy were pre-corroded (i.e., prepitted) for up to 384 hours (16 days) and were tested in fatigue under uniaxial loading [14]. The specimens had either a central hole or a semi-circular edge notch. Fatigue lives of the pre-corroded specimens are shown as a function of pre-corrosion time in figure 6-4, and a typical crack-nucleating corrosion pit is shown in the micrograph of a fracture surface in figure 6-5. Figure 6-4 shows that the fatigue lives were reduced by more than one order of magnitude after pre-corrosion of up to 384 hours. The depth of the crack-nucleating corrosion pit for each specimen was determined from micrographs similar to that shown in figure 6-5. The fatigue life as a function of this nucleating pit size is shown in figure 6-6, and the trend is

consistent with those shown in figure 6-2. Figure 6-6 shows that fatigue lives correlated better with pit depth as opposed to corrosion time (figure 6-4). The greater scatter seen in figure 6-4 is attributed to the variations in pit depths at a given pre-corrosion time. Figure 6-6 shows that more than one order of magnitude reduction in fatigue life had resulted from pit depth of 30 to 50 μm .

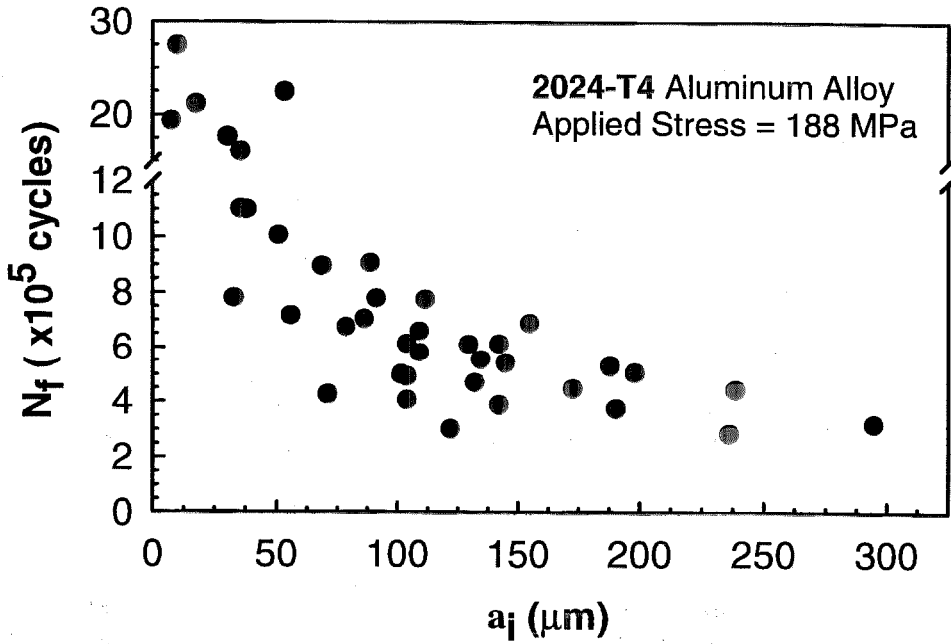


FIGURE 6-2. OBSERVED REDUCTION IN FATIGUE LIFE FOR THE 2024-T4 ALUMINUM ALLOY AS A FUNCTION OF THE INITIAL PIT SIZE

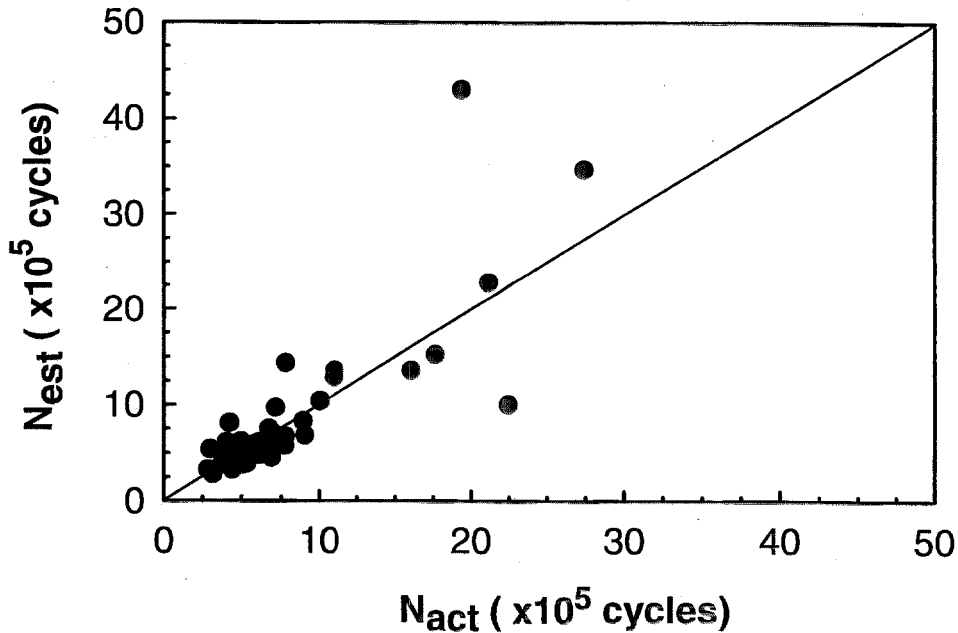


FIGURE 6-3. ESTIMATED FATIGUE LIFE IS IN GOOD AGREEMENT WITH THE ACTUAL FATIGUE LIFE FOR THE 2024-T4 ALUMINUM ALLOY

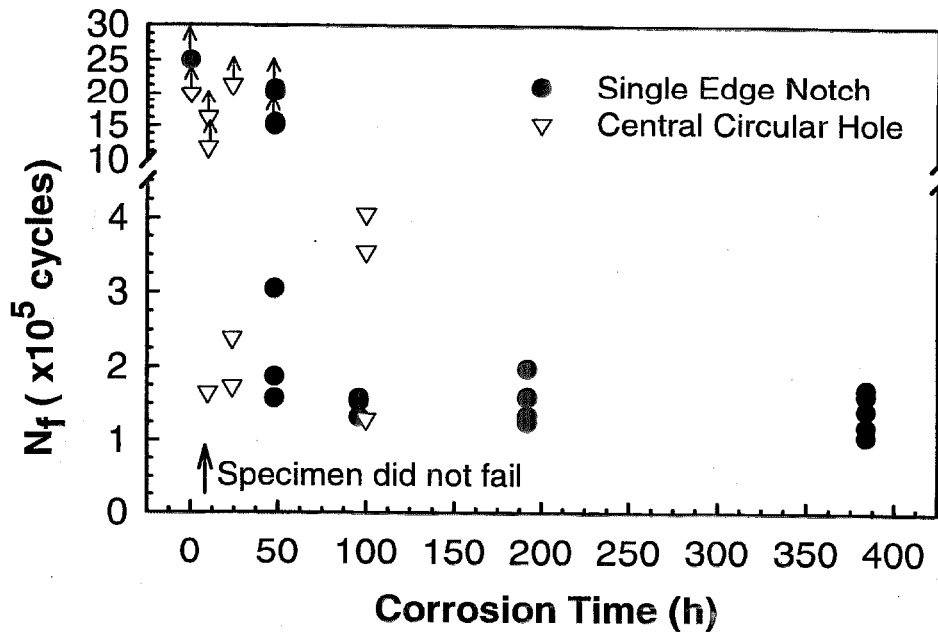


FIGURE 6-4. OBSERVED REDUCTION IN FATIGUE LIFE FOR THE 2024-T3 ALUMINUM ALLOY AS A FUNCTION OF PRECORROSION TIME IN A 0.5M NaCl SOLUTION

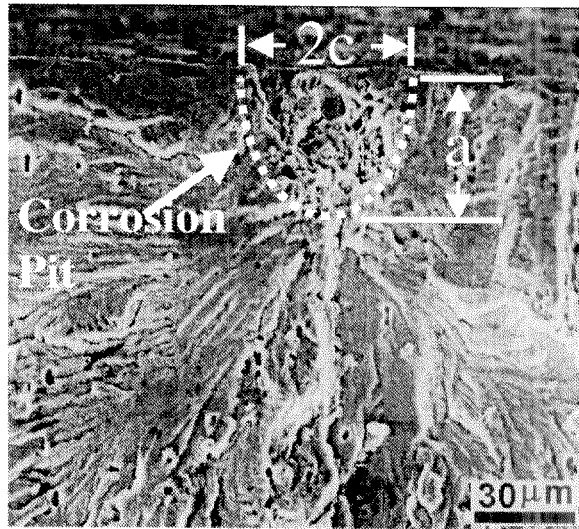


FIGURE 6-5. FRACTOGRAPH SHOWING A CORROSION PIT THAT NUCLEATED THE DOMINANT CRACK IN THE 2024-T3 ALUMINUM ALLOY AFTER 384 HOURS OF PRECORROSION

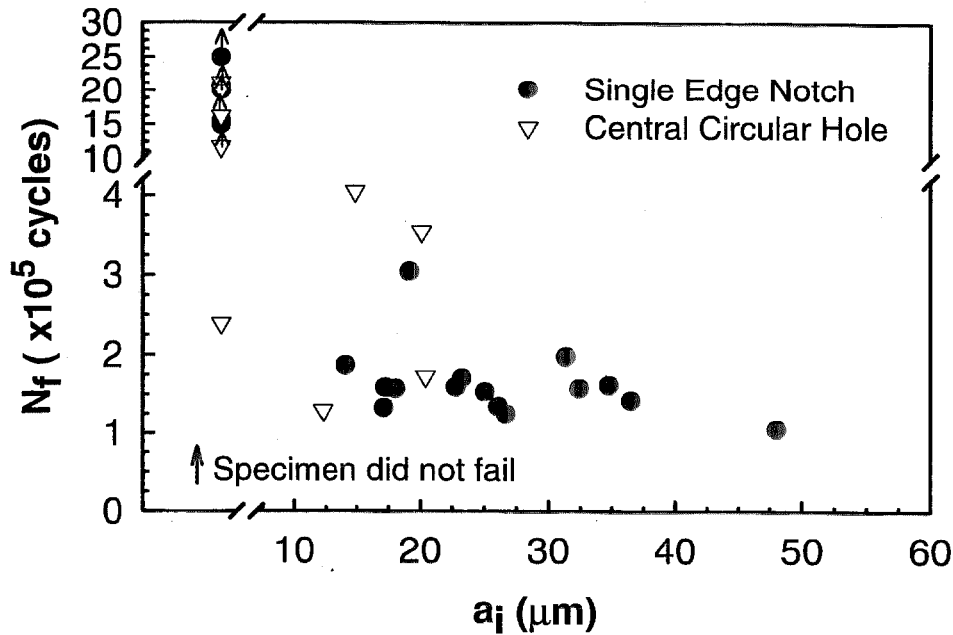


FIGURE 6-6. OBSERVED REDUCTION IN FATIGUE LIFE FOR THE 2024-T3 ALUMINUM ALLOY AS A FUNCTION OF INITIAL PIT SIZE

AFGROW, a life prediction software, was used to estimate the fatigue lives for these notched specimens to account for crack nucleation from the hole or edge notch in the specimens. It accounted for the influences of the stress concentrating effect of the hole and notch and variations in the aspect ratio of the nucleating pit on the stress-intensity factor, as well as for the transition from a surface to a through-thickness crack. Estimates were made using Equation 6.1 and the crack growth parameters given previously except that the influence of ΔK_{th} was neglected. The crack size just prior to fast fracture was measured from the fracture surface of each specimen and was used as the final crack size. A comparison of the estimated and observed fatigue lives is shown in figure 6-7 and shows good agreement with the actual fatigue life as for the 2024-T4 alloy.

These results suggest that the numbers of cycles required to nucleate a crack from a corrosion pit are relatively small and may be neglected. As such, the fatigue lives represent essentially the crack growth lives from nucleating pits and can be estimated if the nucleating pit sizes are known. Based on this comparison, it is clear that corrosion pits act as pre-existing cracks (or crack nuclei) in the structure that could propagate if the crack driving force were high enough. The influence of pre-existing corrosion pits (like other forms of mechanical damage), therefore, needs to be incorporated into damage-tolerance life management and design methodologies. In of precorroded specimens based on crack growth analysis alone and to examine the probabilistic implications of pitting corrosion.

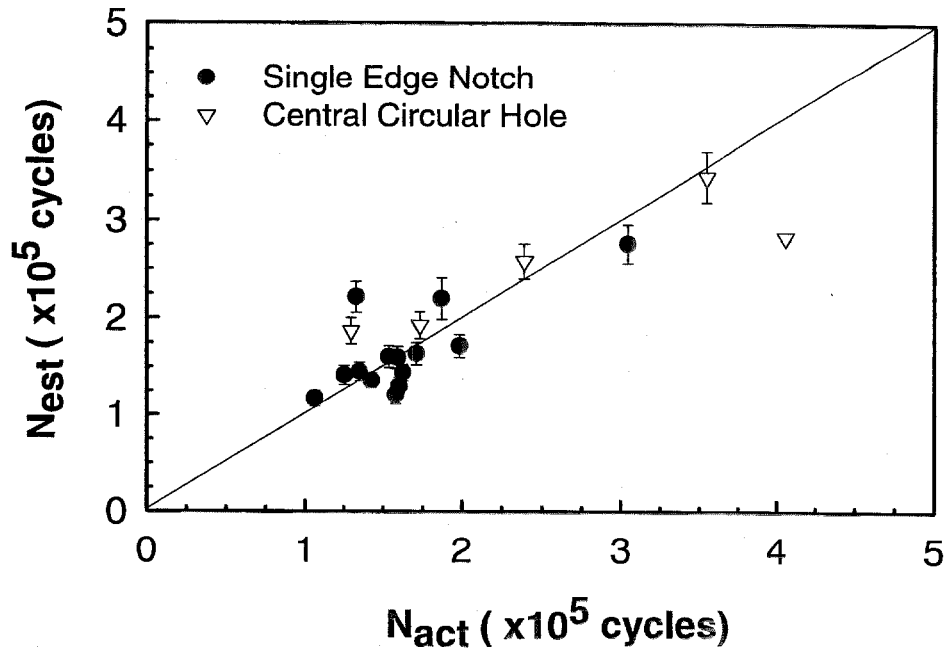


FIGURE 6-7. ESTIMATED FATIGUE LIFE IS IN GOOD AGREEMENT WITH THE ACTUAL FATIGUE LIFE FOR THE 2024-T3 ALUMINUM ALLOY

6.1.2 Probabilistic Analysis

To assess the probabilistic contribution of pit size to fatigue lives, the fracture surface of the four specimens that were pre-corroded for 384 hours were examined. The depths of all of the pits seen on the fracture surfaces were measured, including the pit that nucleated the fatigue failures. The cumulative distribution function (cdf) of the pit depth representing the probability of having a pit deeper than a given value is shown in figure 6-8. The numbers 1-4 on the plot represent the pits that nucleated failure in each of the four specimens. The solid line represents the fit to a simplified mechanistic model for pitting. Based on this distribution, one hundred random pit sizes were generated by Monte Carlo simulation. Pit sizes determined from this distribution were used as the starting sizes for estimating crack growth lives by AFGROW, with the life taken as the number of cycles required to grow from the starting pit, to a crack length of 3 mm. The line in figure 6-9 in Weibull probability coordinates shows the estimated distribution in fatigue life. The closed data points in the plot represent the distribution of the observed fatigue lives, with the numbers 1-4 corresponding to those shown in figure 6-8. The shorter fatigue lives such as #4 correspond to the larger pits in general. The actual data correlate well with the simulated data. The probabilistic analysis showed that the distribution of corrosion pits had a substantial effect on the distribution of fatigue life. The fatigue life was estimated knowing the distribution of initial crack sizes, local stress, and the FCG properties of the material.

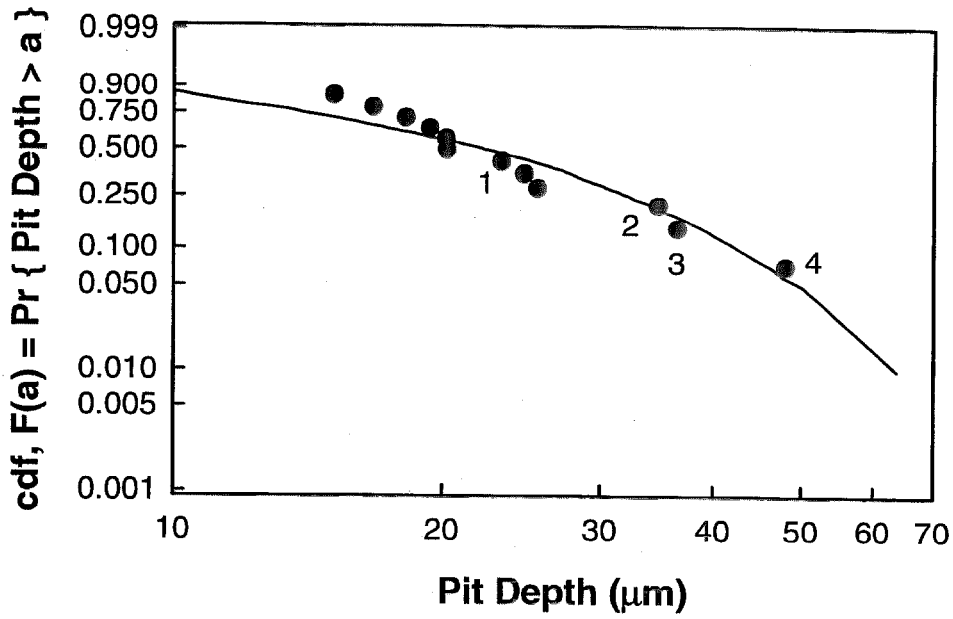


FIGURE 6-8. PIT DEPTH DISTRIBUTION FOLLOWING 384 HOURS OF CORROSION IN AN AQUEOUS 0.5M NaCl SOLUTION ON THE 2024-T3 ALUMINUM ALLOY

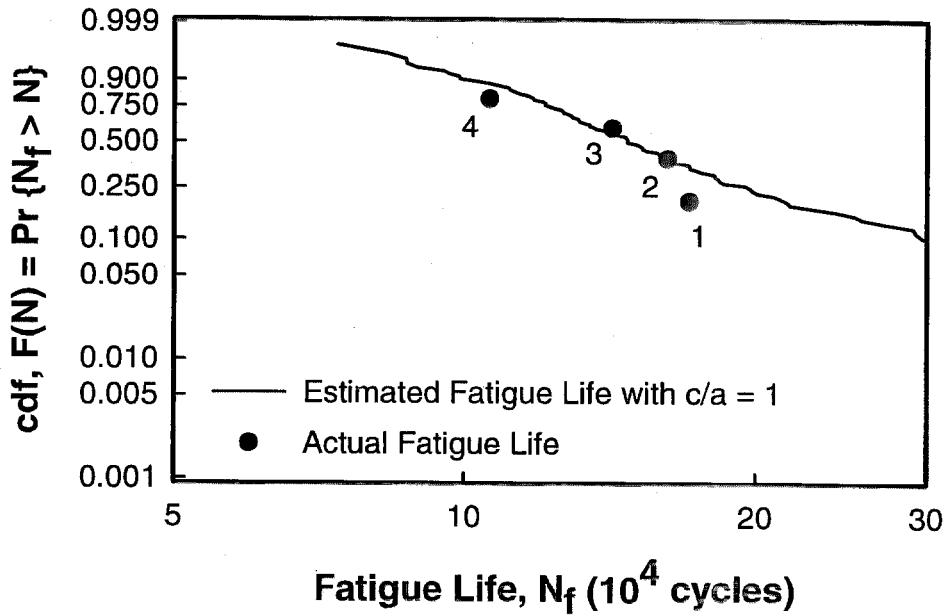


FIGURE 6-9. ESTIMATED AND ACTUAL DISTRIBUTIONS OF FATIGUE LIFE SHOWING THAT THE DISTRIBUTION OF PIT DEPTH DICTATES THE DISTRIBUTION OF FATIGUE LIFE FOR THE 2024-T3 ALUMINUM ALLOY

6.2 A MECHANISTICALLY BASED PROBABILITY APPROACH: PROBABILITIES OF OCCURRENCE AND DETECTION.

To demonstrate the integration of the damage processes into a mechanistically based probability framework, a simplified probability model for pitting and corrosion fatigue was formulated [13,15,16]. This model assumed pitting corrosion to predominate initially and to be at a constant volumetric rate, and the subsequent fatigue crack growth to follow a simple power-law model given by Equation 6.1, except that the explicit contribution of ΔK_{th} is excluded. The transition from pitting to fatigue crack growth occurs when the ΔK for the equivalent crack exceeds ΔK_{th} and when the time-based rate of crack growth exceeds the pit growth rate; i.e.:

$$\Delta K \geq \Delta K_{th} \quad \text{and} \quad \left(\frac{da}{dt} \right)_{crack} \geq \left(\frac{da}{dt} \right)_{pit} \quad (6.3)$$

The shape of the pit is again assumed to be hemispherical and semi-circular for the crack. The details of the model are given in reference 15.

Specifically, the pit depth a at a given time t , up to the transition size a_{tr} , is given by Equation 6.4:

$$a = \left\{ \left[\frac{3MI_p}{2\pi n F \rho} \right] t + a_o^3 \right\}^{1/3} = \left\{ \left[\frac{3MI_{p_o}}{2\pi n F \rho} \exp\left(-\frac{\Delta H}{RT}\right) \right] t + a_o^3 \right\}^{1/3}; \quad a \leq a_{tr} \quad (6.4)$$

In Equation 6.4, I_p and I_{p_o} are, respectively, the effective pitting current and pitting current coefficient; ρ is the density, M is the molecular weight, and n is the valence of the aluminum; ΔH is the activation energy to reflect the temperature dependence for pitting, F is Faraday's constant; and R is the universal gas constant. The crack depth a at time t following transition, where $t = N/f$ (or number of cycles over frequency), is given by Equation 6.5:

$$a = \left\{ a_{tr}^{(2-n_c)/2} - \frac{C_F(n_c-2)}{2} \left[\frac{2.2\Delta\sigma}{\sqrt{\pi}} \right]^{n_c} f(t-t_{tr}) \right\}^{2/(2-n_c)} \quad \text{if } n_c \neq 2 \text{ and } t \geq t_{tr} \quad (6.5)$$

The first critical point (a_{th}, t_{th}) , at which the pit size is sufficiently large for fatigue crack growth to begin, is obtained from the first of two transition criteria in Equation 6.3 by setting $\Delta K = \Delta K_{th}$ and solving for a_{th} and t_{th} from Equations 6.1 and 6.4, respectively.

$$a_{th} = \pi \left(\frac{\Delta K_{th}}{2.2\Delta\sigma} \right)^2 \quad \text{and} \quad t_{th} = \frac{2\pi n F \rho}{3MI_p} (a_{th}^3 - a_o^3) \quad (6.6)$$

The second critical point (a_{tr}, t_{tr}) , at which the fatigue crack can outpace pit growth, is given by the second transition criterion in Equation 6.3 and is the solution of the following equation.

$$\left\{ \left[\frac{3MI_P}{2\pi nF\rho} \right] t + a_o^3 \right\}^{1/3} = \left\{ a_{th}^{(2-n_c)/2} - \frac{C_F(n_c-2)}{2} \left[\frac{2.2\Delta\sigma}{\sqrt{\pi}} \right]^{n_c} f(t-t_{th}) \right\}^{2/(2-n_c)} \quad (6.7)$$

The parameters I_{Po} , a_o , C_F , and ΔK_{th} are chosen as random variables that are mechanistically and statistically independent of time. The pitting current coefficient I_{Po} reflects the scatter associated with the rate of electrochemical reaction for pit growth. Scatter in material properties, environmental sensitivity, and resistance to fatigue crack growth are reflected in C_F . Finally, material and manufacturing quality is reflected through a_o and ΔK_{th} . Equations 6.4 to 6.7 may be used to estimate the evolution of damage with time or to estimate the distribution of damage at a given time. Values for these parameters and their variability are given in reference 15.

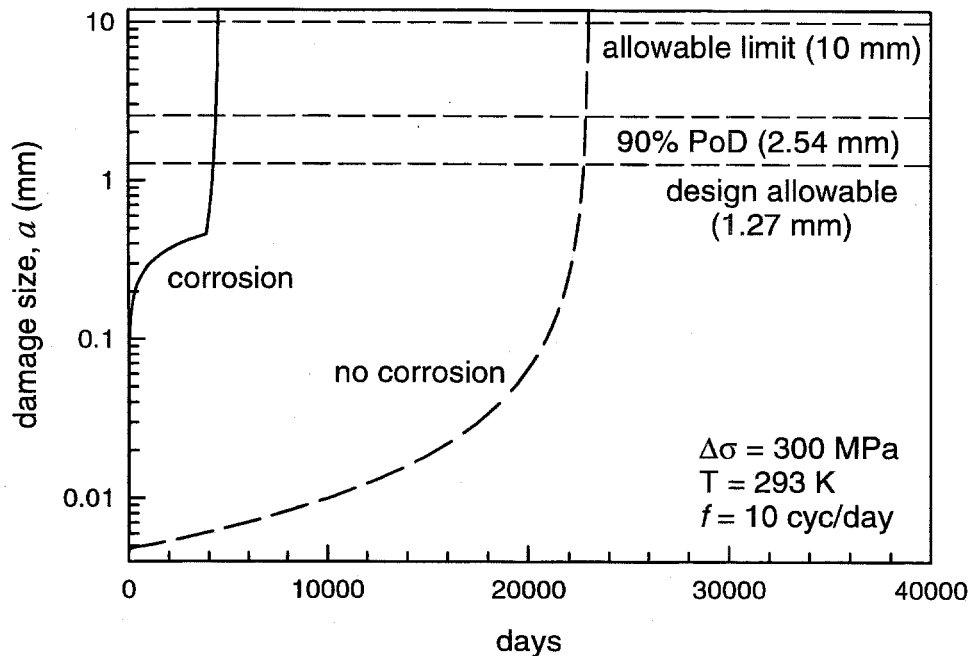


FIGURE 6-10. EVOLUTION OF AVERAGE DAMAGE SIZE WITH AND WITHOUT CORROSION

The effect of corrosion is clearly seen in figure 6-10 which shows a comparison of the evolution of average damage size with time at 300 MPa (based on mean values of the random variables) with and without corrosion. Corrosion effectively reduces the fatigue life to less than 20% of that without corrosion. Most of the reduction is associated with the time required to reach the transition point $a_{tr} = 460 \mu\text{m}$ by fatigue. The probability that the damage exceeds size a at time t , or its probability of occurrence (PoO), was estimated through Monte Carlo simulation, and the results are shown in figure 6-11. The time, from 500 to 4500 days, encompasses typical behavior. For 500 to 2500 days, pitting predominates. At longer times, however, cracking becomes significant and is reflected by the abrupt change in the shape of the probability curves. This type of information may be used to assess the sensitivity requirements for nondestructive inspection (NDI) and to estimate the probability for structural failure. By comparing with a typical NDI probability of detection (PoD) curve, for example, at $t = 4500$ days, it is seen that the PoO of a damage of size greater than 1.27 mm is about 50%, but the PoD for that damage size is

only 50%. In other words, about half of the damage would go undetected. Clearly, from figures 6-10 and 6-11, the impact of corrosion must be incorporated into programs for ensuring structural integrity and reliability, and nondestructive inspection procedures must be sufficiently sensitive to detect early corrosion damage.

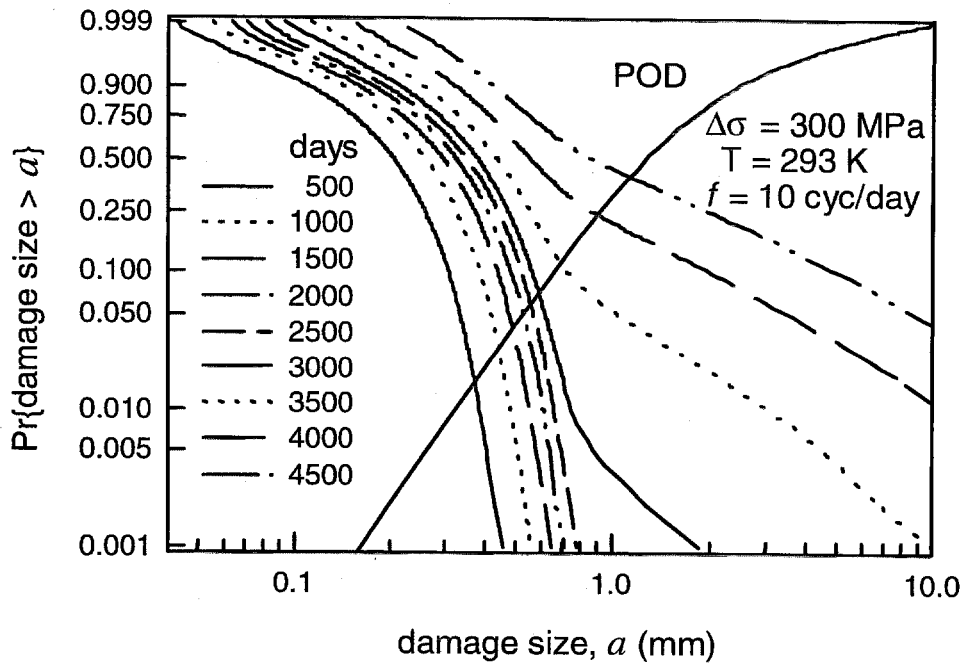


FIGURE 6-11. PROBABILITY DISTRIBUTION OF DAMAGE AT A GIVEN TIME AT 293 K AND 10 CYC/DAY

7. PROBABILITY MODELING AND ANALYSIS OF J-STARS TEAR-DOWN DATA FROM TWO B707 AIRCRAFT.

Airworthiness, in a structural context, requires the assurance of continued structural integrity and safety of an aircraft throughout its planned period of operation from its current state to the next scheduled inspection and maintenance. Its accurate assessment depends critically on the development of a quantitative methodology that integrates information from state-of-the-art nondestructive inspection (NDI) with validated methods for prediction of damage accumulation and structural integrity assessments. The overall problem in aging-aircraft life extension and management (i.e., in ensuring airworthiness) may be understood with the aid of figure 7-1. Airworthiness is typically assessed in relation to the current or initial state of the structure (i.e., at the time of scheduled inspection and maintenance). To manage the maintenance and life extension of aircraft structures, a broad range of quantitative tools and supporting data are needed to assess their current state (i.e., their integrity or safety) and to make probabilistic predictions regarding their future state (i.e., their continued operational safety). These tools and databases are used to assess the airworthiness of the as-inspected structure and how it might be altered by damage accrued during subsequent service. For these assessments, a set of structural analysis and life prediction tools based on the pristine initial state and validated by experimentation and service experience is typically used in conjunction with NDI information on the current state of the aircraft. These tools, along with the NDI information, then serve as a basis for certification, maintenance planning, and overall fleet management.

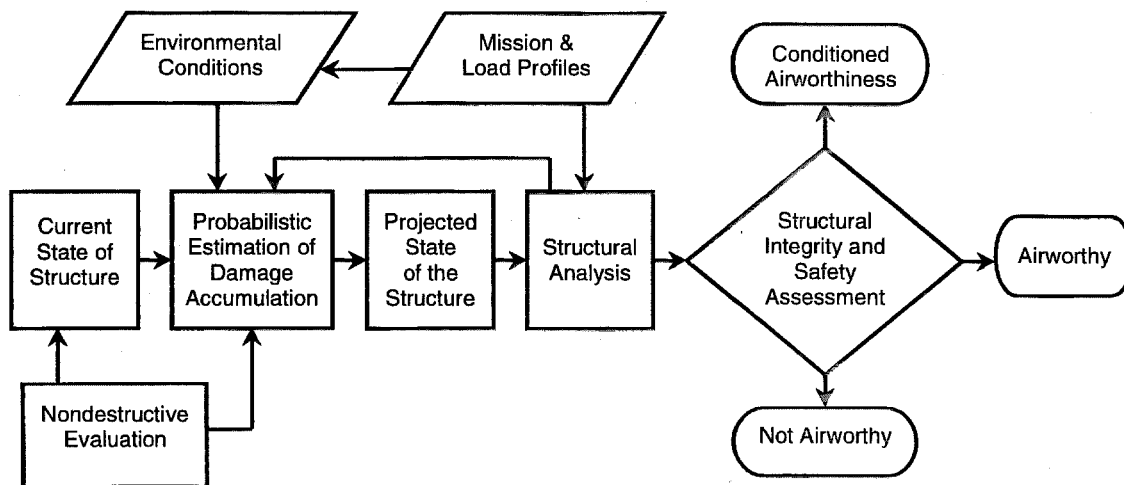


FIGURE 7-1. SCHEMATIC DIAGRAM OF THE PROCESSES FOR AIRWORTHINESS, STRUCTURAL INTEGRITY, AND DURABILITY ASSESSMENTS

In this section, the simplified, mechanistically based probability model for damage accumulation, described in section 6.2, is modified to incorporate the stress concentration effect of a fastener hole and to account for through-thickness crack growth. The model is considered and evaluated in the context of a statistical evaluation of the teardown inspection data on the lower wing panels and stiffeners from two transport aircraft that had been in commercial service for about 24 and 30 years. Preliminary results from metallographic examinations of the panels from one of these

aircraft are used to lend further insight into the damage processes. Implications of these findings on modeling and structural integrity are discussed. Additionally, the use of the model in estimating the distribution of damage for use in assessing multiple site damage (MSD) is illustrated. The information is summarized in reference 17.

7.1 MODIFICATION OF THE MECHANISTICALLY BASED PROBABILITY MODEL.

The simplified mechanistically based probability model was summarized in section 6.2. The transition criteria are given in Equation 6.3, and the distribution in damage (pit) size as a function of time is given by Equation 6.4. Because interest is focused here on damage evolution from a fastener hole, the driving force ΔK for fatigue crack growth is considered to be different according to whether the crack is a surface crack or a through-the-thickness crack. For a surface crack ΔK is given, as a modified form of Equation 6.1, by Equation 7.1:

$$\Delta K_{sc} = \frac{2.2}{\pi} K_t \Delta \sigma \sqrt{\pi a} \quad (7.1)$$

In Equation 7.1, $\Delta \sigma$ is the far field stress range, $2.2/\pi$ is a geometric factor for a semicircular crack in an infinite plate, and $K_t = 2.8$ is the stress concentration factor for a circular hole. When the crack is a through-the-thickness crack, ΔK is assumed to be equal to the following:

$$\Delta K_{tc} = F_{tc}(a/r_o) \Delta \sigma \sqrt{\pi a} \quad (7.2)$$

In Equation 7.2, r_o is the radius of the hole. Numerical values for $F_{tc}(a/r_o)$ for an infinite plate under uniaxial tension containing a circular hole with a single through-crack emanating from the hole perpendicular to the loading axis can be fit empirically, to within graphical resolution, by the following function:

$$F_{tc}(a/r_o) = \frac{0.865}{(a/r_o) + 0.324} + 0.681 \quad (7.3)$$

Let t_{tr} be the time at which a pit transitions into a surface crack and similarly let t_{tc} be the time at which the surface crack transitions into a through-the-thickness crack. When $t_{tr} \leq t < t_{tc}$, the driving force is ΔK_{sc} , and a is given by Equation 7.4.

$$a = \left[a_{tr}^b - b f C_c \left(\frac{2.2 K_t \Delta \sigma}{\sqrt{\pi}} \right)^{n_c} (t - t_{tr}) \right]^{1/b}; \quad b = \frac{2 - n_c}{2}; \quad n_c \neq 2 \quad (7.4)$$

When $t \geq t_{tc}$, a is obtained implicitly by using ΔK_{tc} from Equation 7.5.

$$t = t_{tc} + \frac{1}{f C_c (\Delta \sigma \sqrt{\pi})^{n_c}} \int_{a_{tc}}^a \frac{da}{[F_{tc}(a/r_o) \sqrt{a}]^{n_c}} \quad (7.5)$$

In Equation 7.5, a_{tc} is the size of the damage at t_{tc} . The integral in Equation 7.5 typically must be evaluated numerically.

The parameters I_{Po} , a_o , C_c , and ΔK_{th} are taken to be the random variables (*rvs*). The statistical variability is assumed to be captured through them. The parameters are assumed to be mechanistically and statistically independent of time. Scatter in material properties, environmental sensitivity, and resistance to fatigue crack growth is reflected in C_c . Material and manufacturing quality is depicted by a_o and ΔK_{th} . Finally, I_{Po} reflects the scatter associated with the electrochemical reaction for pit growth. The three-parameter Weibull cumulative distribution function (cdf), given by Equation 7.6, has been found to characterize each *rv* adequately.

$$F(x) = 1 - \exp\left\{-\left[\frac{(x-\gamma)}{\beta}\right]^\alpha\right\}, \quad x \geq \gamma \quad (7.6)$$

7.2 PoO AND STATISTICAL ANALYSIS OF J-STARS TEARDOWN DATA.

The efficacy of the above simplified mechanistically based probability model is assessed in relation to the PoO of damage in service. Based on the foregoing model, the PoO of damage was calculated for conditions that are typical for lower wing structures for two transport aircraft that had been in commercial service for 24 and 30 years.

The inspections were a part of the United States Air Force Joint Surveillance, Target, and Attack Radar System (J-STARS) program to convert retired Boeing 707 aircraft for use by the Air Force. The Boeing 707-123 (s/n #17635, line #15) aircraft had been in commercial service for about 30 years and had accumulated 78,416 flight hours and 36,359 flight cycles. This aircraft had the highest time of service of those in the inventory. Similarly, the Boeing 707-321B (s/n #19266, line #531), with about 24 years of commercial service, had 57,383 flight hours and 22,533 flight cycles. Likewise, this aircraft had the highest time for the 300 series aircraft in the inventory. The USAF designated airframe identification numbers for the aircraft are CZ-180 and CZ-184, respectively. The CZ-184 aircraft was reported to have evidence of greater corrosion damage. Some of the lower wing panels and associated stiffeners and frames from the left side were examined visually for evidence of cracking. Here, only damage that occurred on the walls of fastener holes in the wing panels and in the stiffeners is considered. The fasteners were removed from sections of the lower wing panels, and the surfaces were cleaned, including a light acid etch to remove corrosion products. Damage, i.e., cracks, was measured optically, with the aid of dye penetrants, using a 20× magnifying lens. Multiple hole-wall cracks (MHWCs) were observed in the fastener holes of both the skin and stiffeners; some involved cracking on both sides in the highly stressed regions of the holes. In each case, however, only the longest estimated crack from each group was reported. Fatigue cracks were identified at 2,631 fastener hole locations of the 1,675 stiffener holes and 869 wing skin holes that were inspected. More cracked holes were found on the CZ-184 aircraft; however, a larger area of the wing and more holes were inspected. For the inspected sections, a total of 350 and 494 MHWCs were reported for the CZ-180 and CZ-184 aircraft skins, respectively. Similarly, the total MHWCs reported for the stiffeners were 583 and 1,617 for CZ-180 and CZ-184, respectively. Since the MHWCs were reported in increments of 0.127 mm (0.005 in), the data were grouped appropriately. The

damage sizes are surface lengths, and they were assumed to be equal to the diameter of the damage for modeling purposes. The filled circles in figures 7-2 to 7-5 show the empirical distribution of the damage in the skins and stiffeners for each aircraft on Weibull probability paper. For consistency with the modeling, the damage shown is taken to be one-half the reported values which implicitly assumed an aspect ratio of one for the damage. (This assumption is used throughout this section.) Because many of the damages were estimated to have the same size, the number of data points in each of the figures appears limited.

Based on reasonable values of localized corrosion and corrosion fatigue crack growth rates and by considering the primary loading from ground-air-ground (adjusted for average gust loading) cycles, the PoO of damage is estimated for each aircraft and is shown as a solid line in each of the figures. For the skins, the agreement is very encouraging. It suggests that it is feasible to estimate service performance quite well on the basis of laboratory data provided that the predictive methodology is based upon reasonable mechanistic models. On the other hand, the agreement for the stiffeners is not as good. There are a variety of reasons for the discrepancy. The aluminum alloy for the stiffeners is 7075-T651, for which the experimental data needed to estimate the model parameters accurately is more limited than that for the 2024-T3 alloy used for the skins. The stiffeners are typically thicker than the skin, and the model may need to be adjusted accordingly. Stresses may be sufficiently different in the stiffeners so that improvements in the crack growth portion of the model may be required. The assumption of hemispherical growth of the corrosion pits may be inappropriate. It also should be noted that the model is based upon a single (dominant) damage and the measurements reflected a single value for each location; whereas, multiple cracks were observed for the fastener holes in the skins and the stiffeners. This aspect will be discussed further in relation to the metallographic examination. Consequently, further experimental testing and modeling is warranted for this application. Nevertheless, the maximum deviation from the empirical data and the estimated PoO is less than 9% for CZ-180, which may be reasonable for predictions. The maximum deviation for CZ-184, however, is at best about 21%. On the other hand, there is some error incurred from the J-STARS observation method.

The uncertainty in measurement for the stiffeners may be estimated from available data on the skins. For 42 selected fastener holes from the CZ-184 skin, the crack lengths were estimated by employing higher resolution optical microscopy, described below, and the average relative difference exceeds 75%. Figure 7-6 duplicates figure 7-5 with the addition of error bars for the reported crack lengths, assuming that the measurement error was 50%. This leads to a relatively broad error band for the data. For this scenario the predicted PoO falls within all of the error bounds. Even so, the prediction does not appear to be satisfactory. Again, further analyses are warranted. Thus, the viability of the model for estimating the PoO has been established in terms of the reported teardown data for the wing skins, but caution must be exercised for the stiffeners.

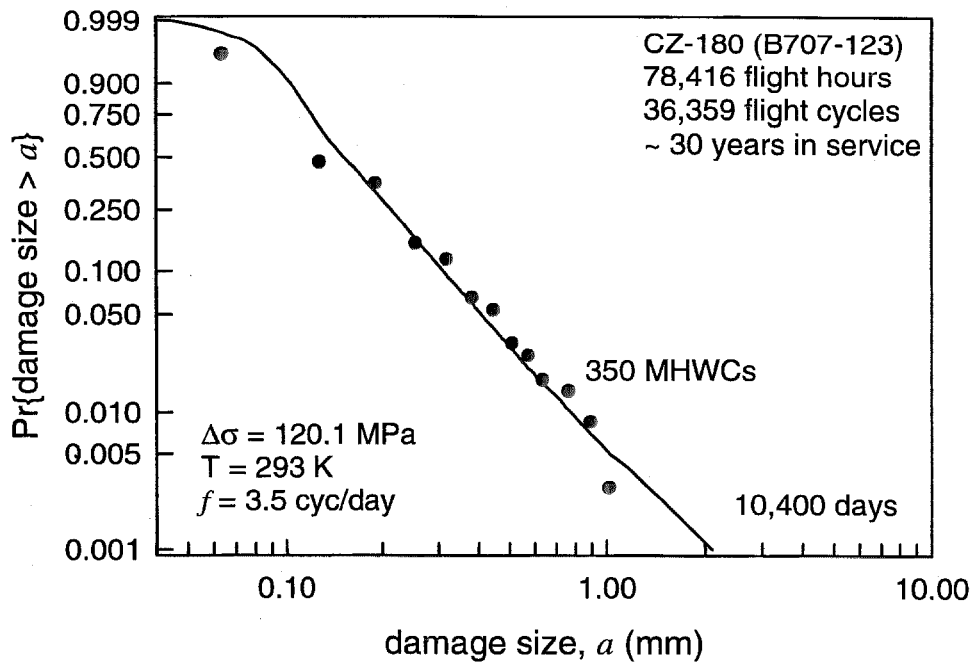


FIGURE 7-2. A COMPARISON BETWEEN THE PREDICTED AND OBSERVED PoO FOR HOLE-WALL DAMAGE IN THE LEFT-HAND LOWER WING SKINS (2024-T3 ALUMINUM ALLOY) OF THE CZ-180 AIRCRAFT

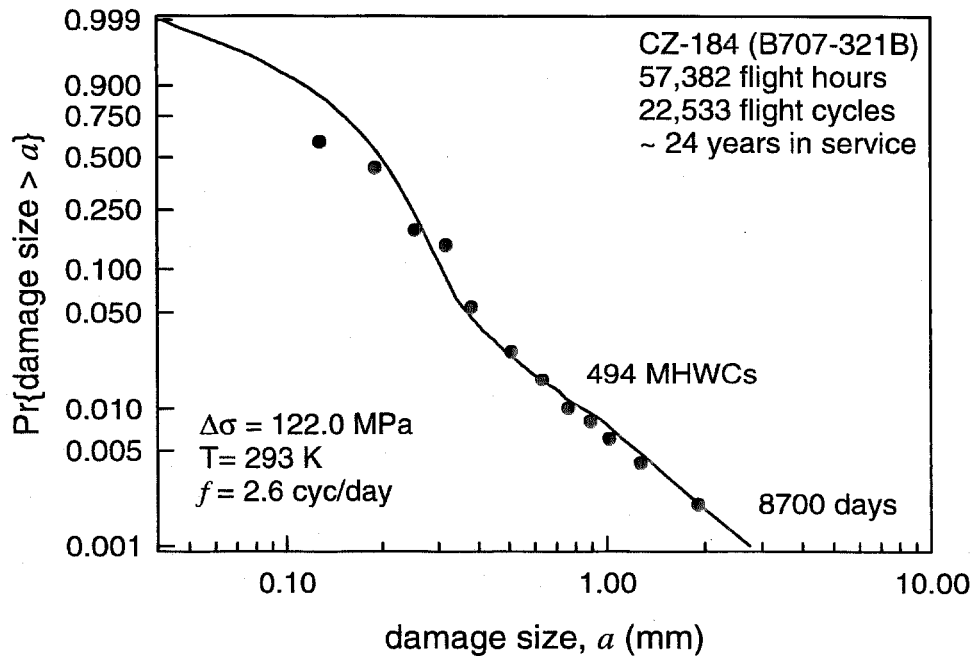


FIGURE 7-3. A COMPARISON BETWEEN THE PREDICTED AND OBSERVED PoO FOR HOLE-WALL DAMAGE IN THE LEFT-HAND LOWER WING SKINS (2024-T3 ALUMINUM ALLOY) OF THE CZ-184 AIRCRAFT

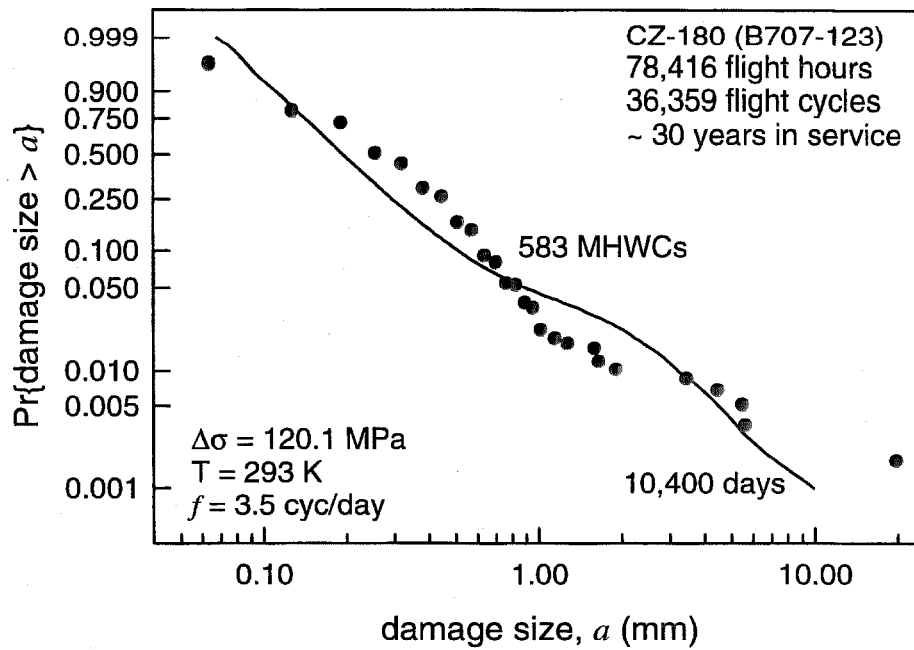


FIGURE 7-4. A COMPARISON BETWEEN THE PREDICTED AND OBSERVED POO FOR HOLE-WALL DAMAGE IN THE LEFT-HAND LOWER WING STIFFENERS (7075-T6 ALUMINUM ALLOY) OF THE CZ-180 AIRCRAFT

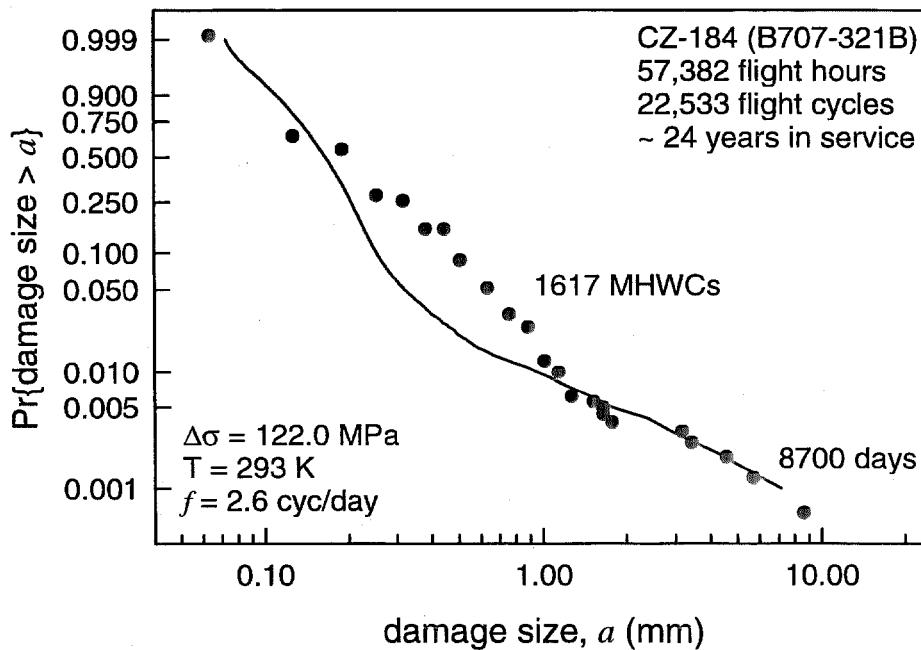


FIGURE 7-5. A COMPARISON BETWEEN THE PREDICTED AND OBSERVED PoO FOR HOLE-WALL DAMAGE IN THE LEFT-HAND LOWER WING STIFFENERS (7075-T6 ALUMINUM ALLOY) OF THE CZ-184 AIRCRAFT

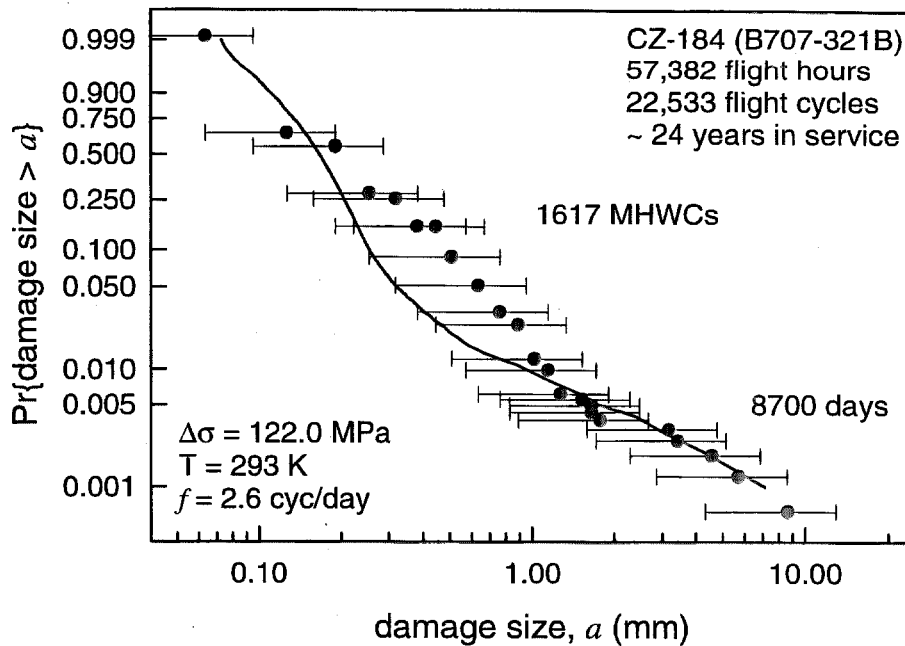


FIGURE 7-6. A COMPARISON BETWEEN THE PREDICTED AND OBSERVED PoO WITH ESTIMATED ERROR BARS FOR THE DATA FOR HOLE-WALL DAMAGE IN THE LEFT-HAND LOWER WING STIFFENERS OF THE CZ-184 AIRCRAFT

7.3 ESTIMATION OF MULTISITE DAMAGE (MSD).

The availability of a validated predictive model for PoO provides a rational method for estimating the distribution of damage for use in MSD analyses. The approach and methodology is illustrated by using the predicted PoO distribution for the CZ-184 aircraft, figure 7-3. Using Monte Carlo simulation for the largest crack length in each fastener hole, the damage distribution for a collection of fastener holes may be estimated. Damage from hole to hole, as well as at the two highly stressed sides of each hole, is considered to be statistically independent. Two such distributions, each representing one simulation, are shown in figure 7-7 for 100 fastener holes arranged in four rows along a spliced joint. Each simulation may represent different locations in a single aircraft or the same location for different aircraft under comparable service conditions. From these figures, it is seen that different levels of damage are possible, and critical locations may be identified through the size and clustering of damage at a given stage in service. To illustrate the effect of considering larger populations of holes, a simulation for 1,000 holes is shown in figure 7-8. Note that the extreme values, i.e., larger size damage, in the distribution are considerably more prominent, and a number of critical areas can be identified readily. These illustrations demonstrate the value of this approach in airworthiness assurance and management of civil and military aircraft.

7.4 METALLOGRAPHIC EXAMINATIONS OF DAMAGE AND IMPLICATIONS.

Much of the wing panel sections (mostly from the CZ-180 aircraft) have been distributed to various organizations for further investigation. The fastener regions of the remaining sections

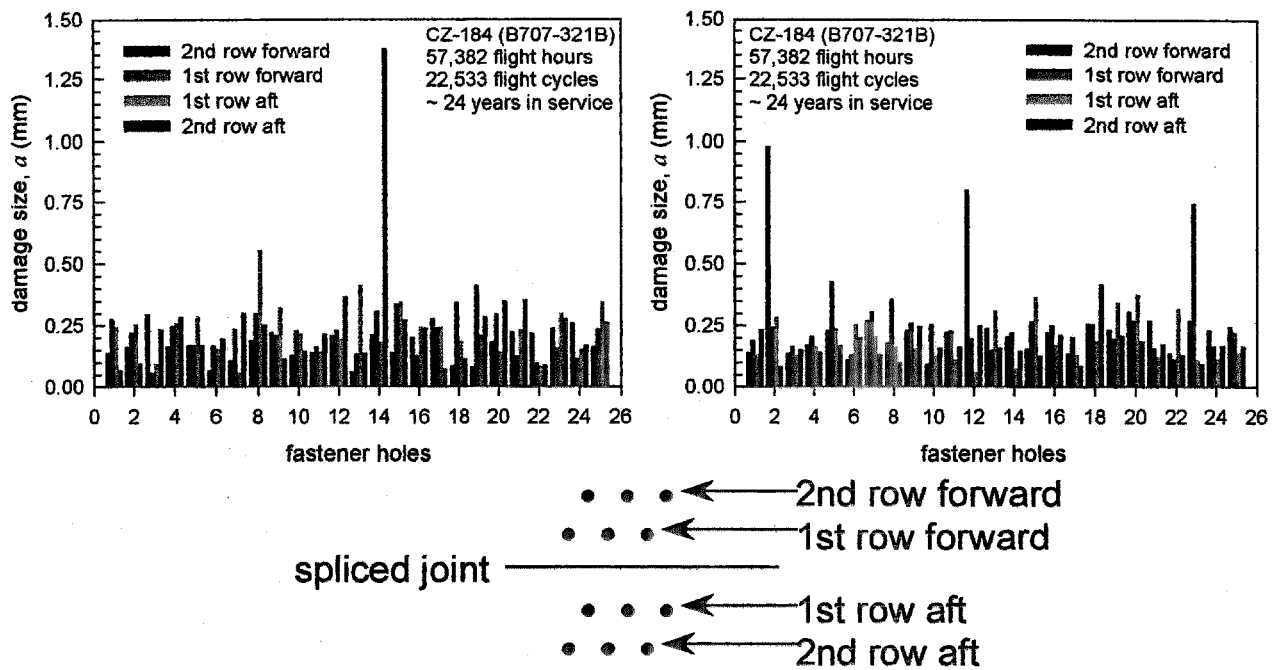


FIGURE 7-7. VARIATIONS IN THE SIMULATED DAMAGE DISTRIBUTIONS FOR 100 FASTENER HOLES BASED ON THE PoO FOR THE SKIN OF THE CZ-184 AIRCRAFT

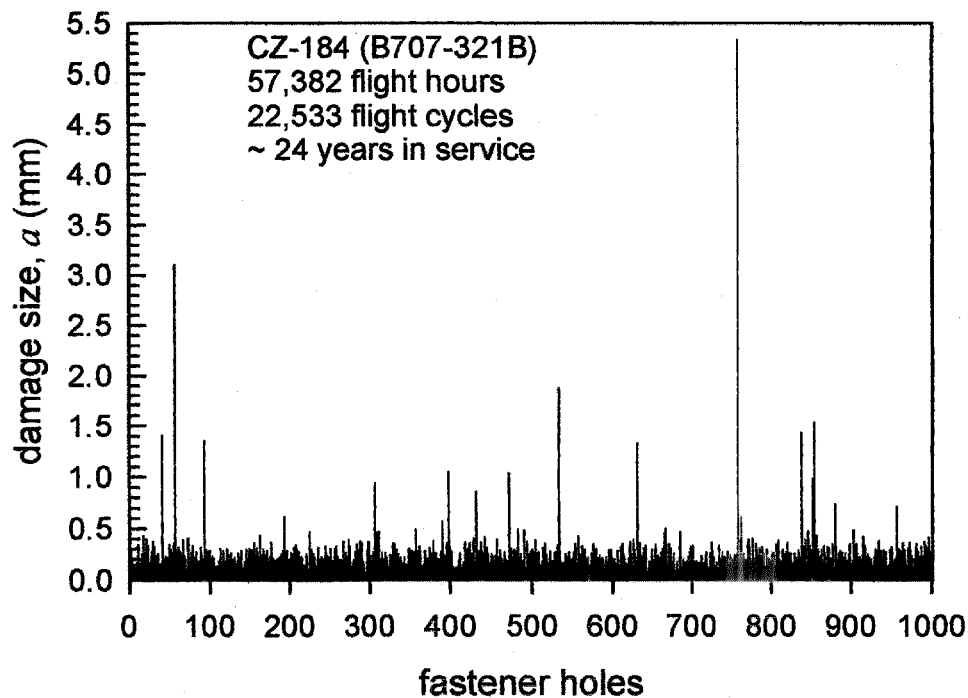


FIGURE 7-8. SIMULATED DAMAGE DISTRIBUTION FOR 1,000 FASTENER HOLES BASED ON THE PoO FOR THE SKIN OF THE CZ-184 AIRCRAFT

from the CZ-184 aircraft were salvaged and were made available to Lehigh University by the Air Vehicles Directorate of the Air Force Research Laboratory for further investigation and for archival purposes. To date, examinations by optical microscopy (at 50 to 300×) have been carried out with a Hi-Scope¹ video imaging system. Selected fastener holes have been sectioned and examined by SEM to better understand the processes for damage evolution. The findings from these investigations are summarized below along with their implications for airworthiness assessment.

Initially, the examinations focused upon those fastener holes in which damage had been reported by the teardown inspections². The thrust of this activity has been restricted to MHWCs in the wing panels. They revealed a multiplicity of damage at the highly stressed regions of the hole surface. The shapes of this damage, as indicated by the remaining dye penetrant could not be readily identified as cracks. More detailed examinations of four of the fastener hole-walls were carried out by SEM, after removing the dye penetrant.

Figure 7-9 shows multiple damage as evidence of extensive corrosion in the high stress region on the wall of hole 54 in panel B2-2-2 [18]. This hole was observed in the as-received condition. The figure clearly shows evidence of general and localized corrosion damage, and elongated damage transverse to the direction of the wing-bending stresses. Many of the elongated damage appear to have linked up. The shorter damage appears shallow and has a rounded bottom. The longer damage, on the other hand, appears deep and to be associated with cracking. The shapes of the elongated damage, however, could not be identified readily with fatigue cracking.

Hole #77 in panel B3-2-5 was sectioned to better understand the processes of damage evolution. The surface was acid cleaned to remove the residual corrosion products. In figures 7-10 and 7-11, the sectioned specimen was tilted 40° to show both the fastener hole-wall and the sectioned surface. Figure 7-10 shows that the larger elongated type of damage seen in figure 7-9 are cracks that have been corroded near the surface. Figure 7-11 suggests that the shallow features are small cracks that have been corroded away entirely. Thus, the figure indicates that multiple damage forms in the highly stressed regions of a hole. This damage is in the form of corrosion pits or cracks, some of which may link up to form even larger cracks.

In order to evaluate the extent of damage in fastener holes, several were scrutinized carefully by optical microscopy. Two holes, #107 and #103 from B32-2-2 along stiffener 7, are displayed partially in figures 7-12 and 7-13, respectively. Hole #107 was selected to highlight the magnitude of MHWCs. The longest crack is 4.78 mm (0.188 in) in a skin section of thickness 9.65 mm (0.38 in) or about 50%. Clearly, it is approximately 75% of the bore thickness; however, the largest reported crack length for the hole is 1.27mm (0.05 in). Furthermore, it can be seen that the dominant crack resulted from the coalescence of several others. Also, there is a reasonably extensive region covered with damage. In fact, this is a common occurrence; hence the adjective multiple in MHWC. Figure 7-13 shows a large cluster of MHWCs. Assuming that

¹ Hi-Scope is a trade-mark of HiRox Co., Ltd., Tokyo, Japan; distributed in the United States by Hi-Scope Systems Co., Closter, NJ.

² Hole and panel designations are keyed to reference 18. The panel numbers refer to those holes in which cracks were observed. The extensions to these designations (*e.g.*, -2) are assigned at Lehigh University to denote individual sections from the panel.

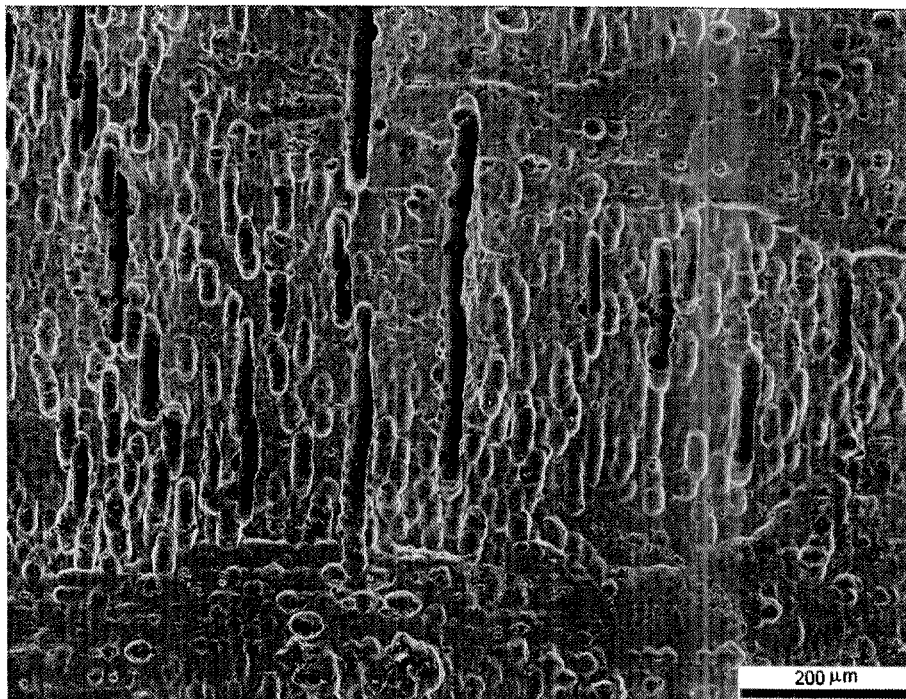


FIGURE 7-9. SEM MICROGRAPH OF CORROSION-RELATED DISTRIBUTED DAMAGE AT HOLE #54 IN PANEL B2-2-2 OF THE CZ-184 AIRCRAFT

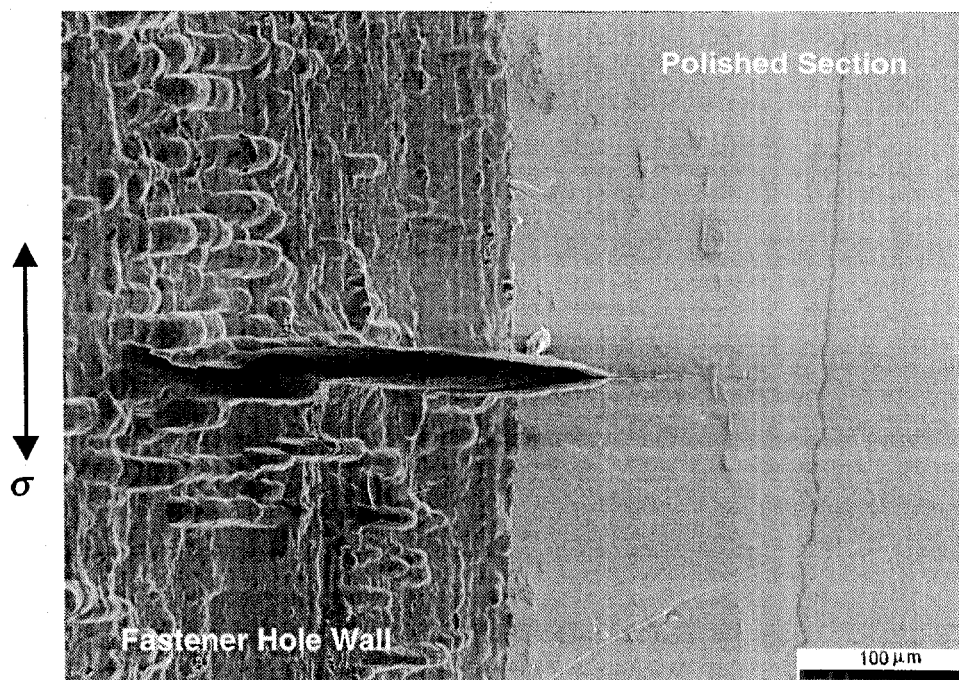


FIGURE 7-10. SEM MICROGRAPH OF A SECTION THROUGH AN ELONGATED DAMAGE AT HOLE #77 IN WING PANEL B3-2-5 OF THE CZ-184 AIRCRAFT SHOWING CORROSION ATTACK OF THE FATIGUE CRACK

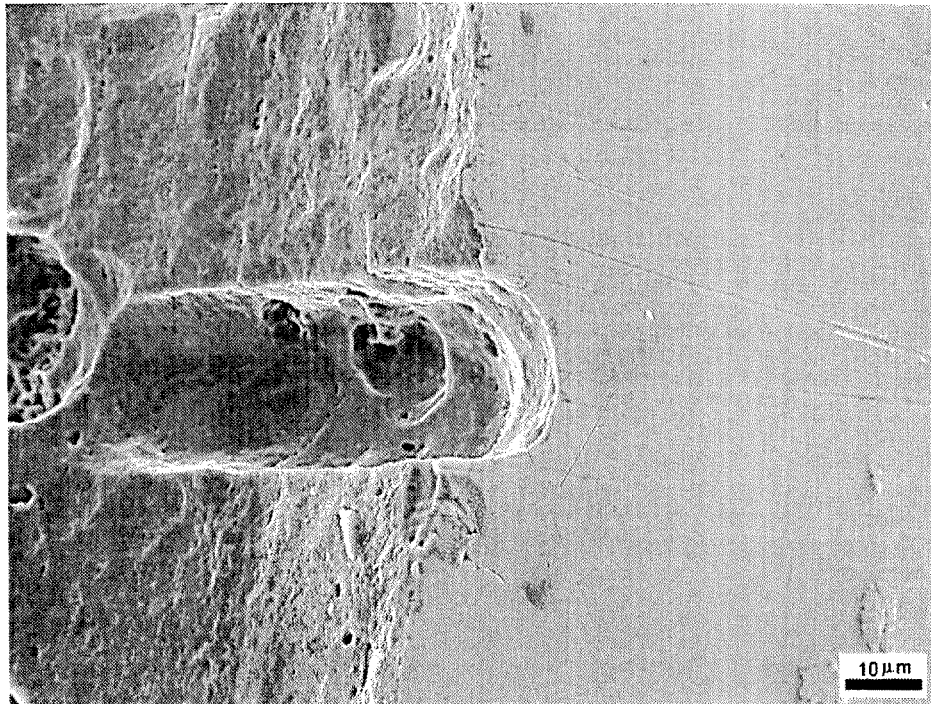


FIGURE 7-11. SEM MICROGRAPH OF A THROUGH SECTION OF A SHALLOW DAMAGE AT HOLE #77 IN WING PANEL B3-2-5 OF THE CZ-184 AIRCRAFT SUGGESTING THAT THE CRACK WAS DISSOLVED BY CORROSION

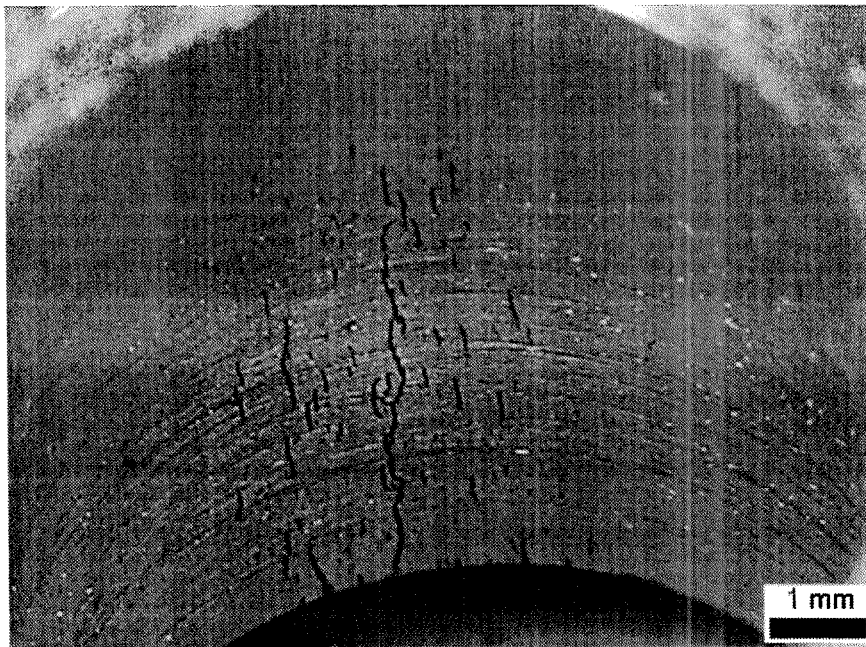


FIGURE 7-12. OPTICAL MICROGRAPH OF A HIGHLY STRESSED REGION OF HOLE #107 IN WING PANEL B3-2-2 OF THE CZ-184 AIRCRAFT SHOWING EXTENSIVE CORROSION FATIGUE CRACKING

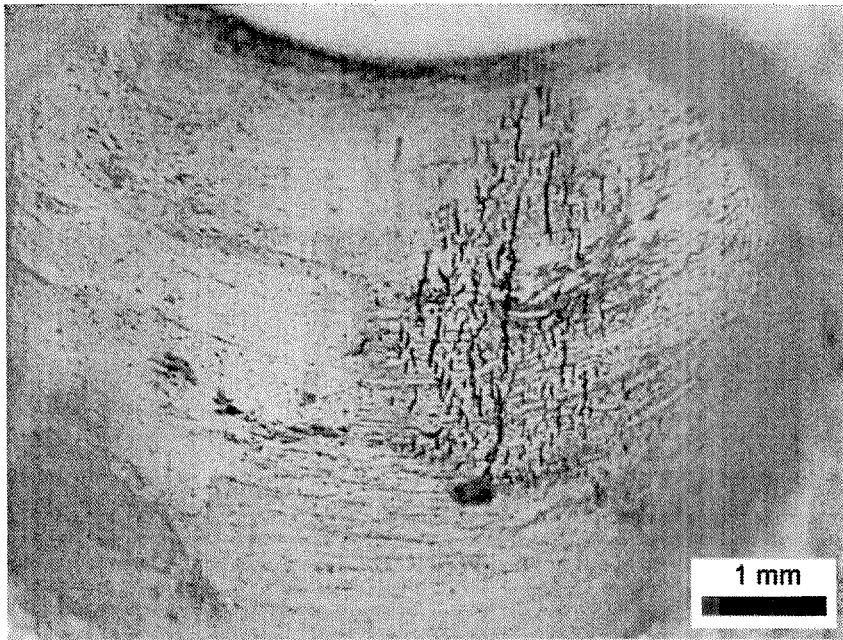


FIGURE 7-13. OPTICAL MICROGRAPH OF A HIGHLY STRESSED REGION OF HOLE #103 IN WING PANEL B3-2-2 OF THE CZ-184 AIRCRAFT SHOWING EXTENSIVE CORROSION FATIGUE CRACKING

the damage area may be approximated by an ellipse, the area of the damage is approximately 10.0 mm^2 (0.016 in^2) which is about 8% of the entire hole-wall surface area or over 90% of the high-stress region on that side of the hole.

Not only do these metallographic findings support the postulated processes for corrosion enhanced damage evolution, but they also imply that further statistical analyses are required. Detailed analyses will lend additional insight into the actual damage processes and improve the modeling of the processes.

7.5 STATISTICAL ANALYSES OF THE LOWER LEFT WING SKIN OF CZ-184.

The first issue to consider is the accuracy of the values in the J-STARS report. As mentioned above, a large number of holes were inspected, but with only a $20\times$ magnifying lens. This activity is very tedious and probably not especially accurate based on the magnification and the difficult angles required to view the cracks. Figure 7-14 shows the damage sizes for 42 holes that were selected because the J-STARS report indicated MHWCs of significant length. The graph also includes the sizes measured with the aid of the Hi-Scope video imaging system at a magnification of 50 to $150\times$ described above and estimated effective crack lengths to capture the entirety of the damage region. Clearly, there are significant differences between the three data sets. In fact, the average value for each of the three sets is 0.36 mm (0.014 in), 0.61 mm (0.024 in), and 1.43 mm (0.056 in), respectively. The range of the data, from left to right, increases indicating greater scatter. This may be an artifact of the methodologies in that the data from the J-STARS report are grouped, and the estimation of effective lengths was somewhat subjective (see, for example, figure 7-13). Nevertheless, the overriding conclusion is that, if possible and feasible, higher-resolution microscopy is needed to accurately characterize the damage in fastener holes.

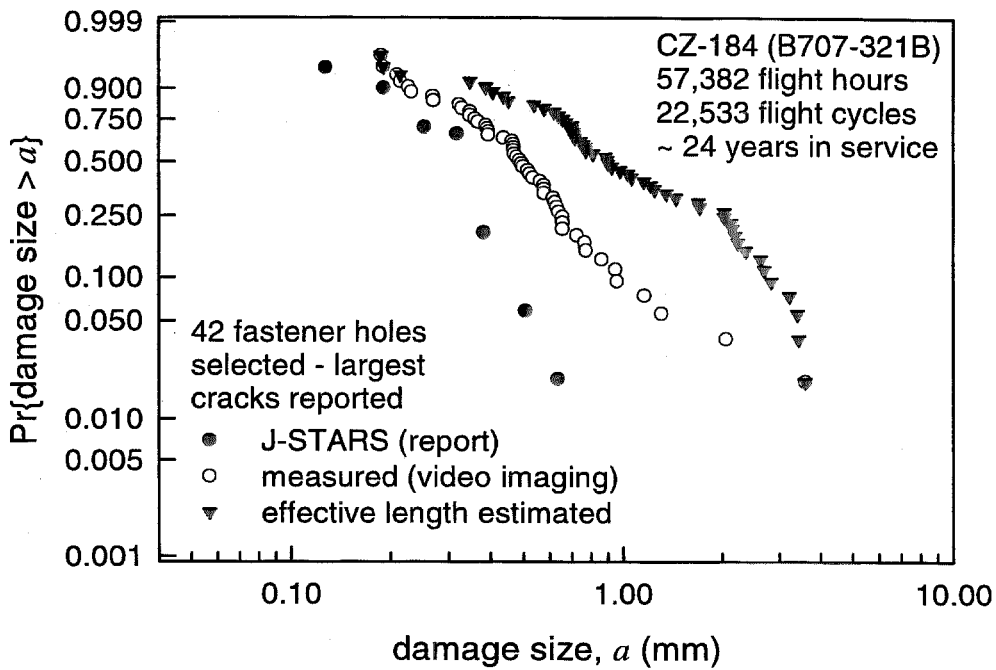


FIGURE 7-14. COMPARISON OF THE P₀O FOR THE MAXIMUM MHC LENGTHS REPORTED BY J-STARS MEASURED USING VIDEO IMAGING MICROSCOPY AND EFFECTIVE LENGTH ESTIMATED FROM THE OVERALL EXTENT OF THE FIELD OF DAMAGE FOR SELECTED HOLES FROM THE CZ-184 AIRCRAFT

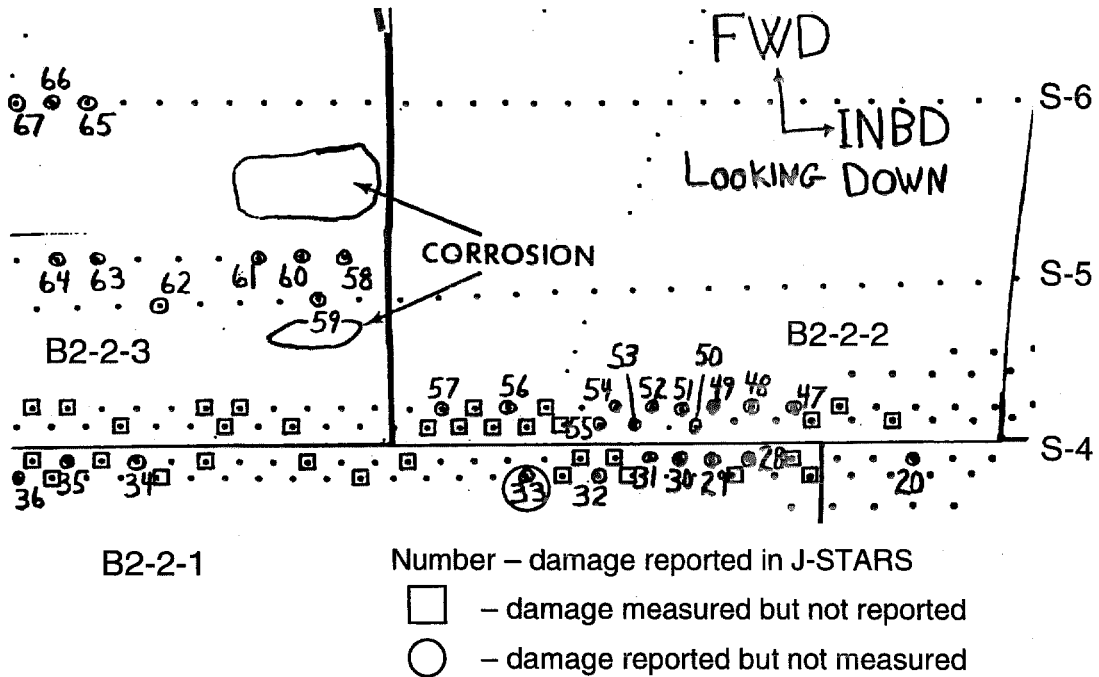


FIGURE 7-15. A PORTION OF SECTION 2 ALONG STIFFENER 4 FROM THE CZ-184 AIRCRAFT FOR WHICH MICROSCOPY AND STATISTICAL ANALYSES ARE MADE

In an attempt to complete a carefully formulated statistical analysis for a significant number of fastener holes, 110 holes from B2-2 along S-4 were observed with the Hi-Scope system. Figure 7-15 is taken from figure B2-2 in [18]. The holes considered are those in the two rows forward and aft of the spliced joint in panels B2-2-1 to B2-2-3. The holes that have been circled and numbered are those in which damage was observed by the J-STARS analyses. Thirty-two additional holes with damage, circumscribed by a square, were found to have damage using the Hi-Scope, but were not included in the J-STARS report. Hole #33 was reported to have damage, but none was found in the Hi-Scope examination. Clearly, the fraction of holes with damage in this section along this stiffener is quite high, with 51 out of the 110 holes (not including #33) having experienced damage. A contributing factor to this observation is that steel fasteners were used with 2024-T3 aluminum alloy skin along S-4. Galvanic coupling between the fasteners and the skin, in the presence of a deleterious environment, would enhance the nucleation and growth of corrosion. In passing, notice that J-STARS inspectors highlighted two patches of corrosion observed on the surface of the skin.

Figure 7-16 shows the empirical PoO from the J-STARS report, the predicted PoO for that data, and the empirical PoO for the MHWCs from the 110 holes shown in figure 7-15. Since the new data lie to the left of the other, the position of the solid line suggests that it overestimated distribution and severity of damage, although the actual extent of damage was greater in terms of the number of fastener holes affected. The discrepancy reflects principally the difference in measurement resolution and secondarily measurement procedure. In the J-STARS examinations, the smallest value reported was $a = 0.127$ mm for all of the panels, whereas the new measurements were as small as $a = 0.015$ mm. Also, the J-STARS report included only the "largest" crack found on each side of a hole. The new measurements, on the other hand, considered every resolvable crack in each hole along S-4 in panel B2-2. Consequently, care should be exercised in the application of the proposed model.

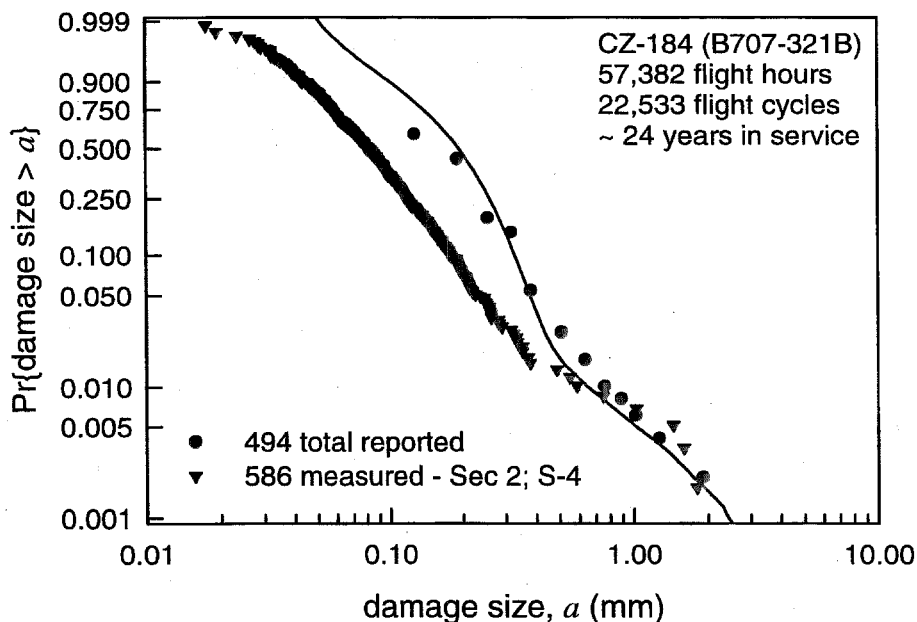


FIGURE 7-16. COMPARISON OF THE PoO FOR ALL MHW LENGTHS REPORTED BY J-STARS AND ALL OF THOSE MEASURED USING VIDEO IMAGING MICROSCOPY FOR 110 HOLES FROM SECTION 2 ALONG STIFFENER 4 FROM THE CZ-184 AIRCRAFT

Figure 7-17 shows the density of the MWHCs for the 110 holes along S-4 shown in figure 7-15 obtained using video imaging microscopy. The holes are numbered right to left, similar to the J-STARS enumeration; however, each of the four rows are numbered separately. The holes with the most severe damage are also labeled for easy reference. There are three holes with at least 60 cracks and another three with at least 40. Furthermore, all six of these holes are rather close, as indicated on figure 7-15. Figure 7-18 shows a plot of the largest measured cracks along S-4. The pattern is similar to the estimated distributions shown in figures 7-7 and 7-8 and attests to the efficacy of the approach for estimating MSD. It is also closely related to the numbers of cracks per fastener hole shown in figure 7-17 and suggests the potential link-up of the MWHCs leading to MSD.

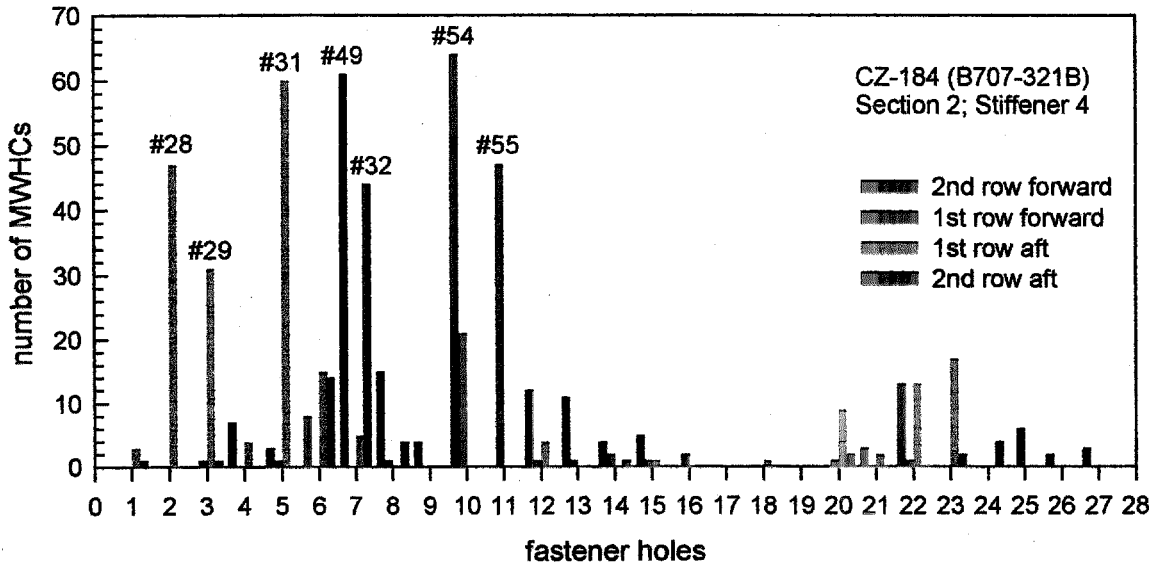


FIGURE 7-17. DENSITY OF MEASURED CRACKS PER FASTENER HOLE FOR SECTION 2; STIFFENER 4 FROM THE CZ-184 AIRCRAFT

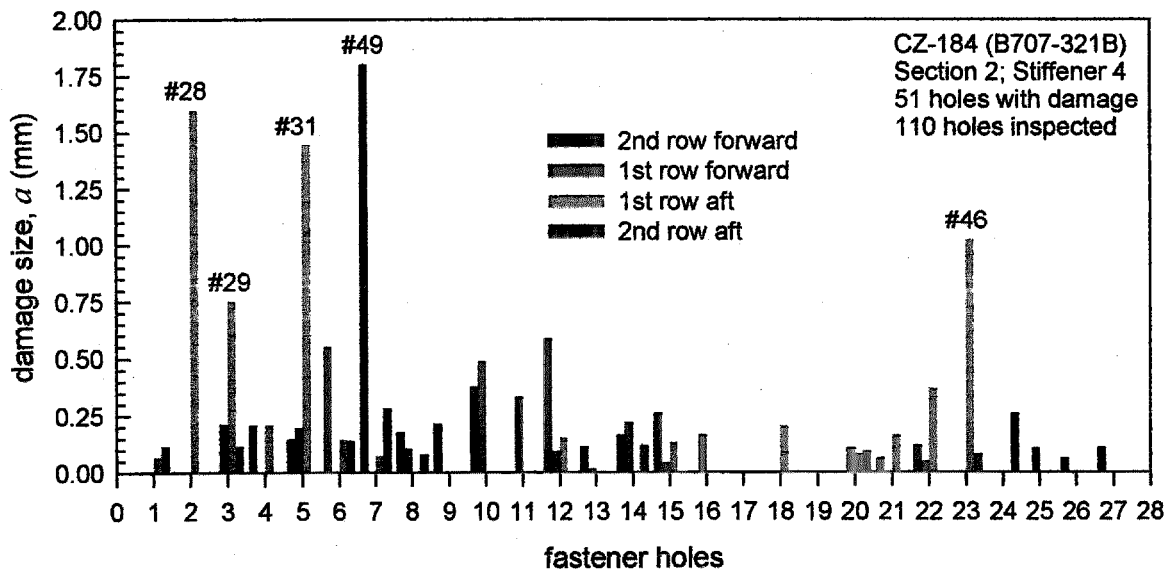


FIGURE 7-18. DAMAGE DISTRIBUTION OF MAXIMUM CRACK LENGTHS FOR 110 FASTENER HOLES FROM SECTION 2 ALONG STIFFENER 4 FROM THE CZ-184 AIRCRAFT

8. SUMMARY.

This report summarizes research performed under the Phase II program from 15 June 1995 to 30 September 1999 and includes results from companion programs sponsored by AFOSR.

Research under these programs has demonstrated the efficacy and value of using a multidisciplinary, mechanistically based probability approach to address the issues of aging of civil and military aircraft. Localized corrosion and corrosion fatigue (acting in competition) has been shown to be a principal material aging mechanism in structural aluminum alloys used in aircraft construction. The operation of this mechanism in service is confirmed by teardown inspection data from the lower wing panels and stiffeners from two transport aircraft that had been in commercial service for about 24 and 30 years. It is supported by preliminary metallographic information from the lower wing panels of one of the aircraft. Localized corrosion nucleated at constituent particles in highly stressed areas of aluminum alloys through particle induced galvanic attack of the matrix and grew from particle to particle in a cluster or contiguous clusters of particles to form severe corrosion pits. These severe pits (on the order of 50 to 200 μm in depth) served as nuclei for fatigue cracking and can reduce the fatigue (crack growth) life by a factor of 10. Localized corrosion, therefore, is deemed to be the principal contributor to the early onset of multi-site (fatigue) damage (MSD), and its impact on structural integrity and flight safety needs to be assessed.

Based on these findings, it is clear that corrosion pits act as pre-existing cracks (or crack nuclei) in the structure, cracks that could propagate if the crack driving force were high enough. Because electrochemical variables strongly influence pit growth, they would also affect the conventional S-N data. Crack growth, on the other hand, occurs by hydrogen embrittlement and would depend on the cracktip environment, which is, by and large, shielded from changes in external electrochemical variables. As such, it would be essentially independent of these variables. From this perspective, therefore, the perceived dichotomy (i.e., the inconsistency in electrochemical response) between the conventional and fracture mechanics approaches to corrosion fatigue (and stress corrosion cracking) is resolved.

The results also indicate that the influence of pre-existing corrosion pits (like other forms of mechanical damage) needs to be incorporated into damage tolerance life management and design methodologies. The reduction in fatigue life depends upon the precorrosion time and in turn the initial pit size. The total fatigue life could be estimated if the initial crack size, local stress, and FCG properties were known. A probabilistic analysis showed that the distribution in fatigue lives is directly related to the distribution in the size of crack nuclei but is also expected to reflect variations in crack growth properties. This finding provides a direct connection between the conventional and fracture mechanics based approaches to corrosion fatigue in that it suggests that the S-N response might be directly predicted from linear fracture mechanics considerations of crack growth.

A 67 percent reduction in fatigue life is substantial in terms of long-term design lives of approximately 20 years. A damage tolerance design and life management philosophy requires an accurate estimate of the fatigue crack-growth rates in a structure. As seen with the 7075-T651 aluminum alloy, the FCG rates were different given changes in the environment, crack length,

and crack driving force. The finding could be different if the fatigue crack had nucleated at an open hole in the sheet material. The stress concentration effect of the hole may produce a sufficiently high ΔK where the chemically short-crack behavior is not manifested. This is especially true for the 2024-T3 aluminum alloy where the effect is not seen at ΔK levels above 5 Mpa m^{1/2}. Care must be exercised in characterizing the stresses and environments during aircraft operations so that accurate predictions of fatigue lives can be made.

Based on understanding developed under these programs, a simplified, mechanistically based probability model was developed and used for estimating the PoO of damage in aircraft aluminum alloys subjected to localized (pitting) corrosion and corrosion fatigue crack growth. The model was used to estimate the PoO of damage in the skin and stiffeners of the left lower wing structures of two aircraft that had experienced long-term commercial service, 24 and 30 years. The predicted PoO, based on reasonable values of damage rates and loading, agreed well with the teardown inspection data from these two aircraft. The method underlying the approach and methodology would facilitate the prediction of the evolution and distribution of damage, and the associated PoO, in terms of their size, geometry, and location. Its utility as a basis for quantitative estimations of the distribution of damage for use in MSD analyses, vis-à-vis, the more ad hoc approaches used heretofore, was illustrated.

The evidence confirms the basic tenets of the proposed mechanistically based probability model for corrosion and corrosion fatigue crack growth. Fatigue cracks are most likely nucleated at sites of localized corrosion (pits) and grow in competition with (crevice) corrosion; albeit, in sequence with corrosion while the aircraft is on the ground and fatigue during flight. From the airworthiness assurance and MSD perspective, the influence of damage evolution must be properly taken into account. The methodology outlined heretofore serves as a useful beginning for the formulation of improved methods. Because of multiple-crack nucleation sites within a given fastener hole, the concept of a dominant crack especially needs to be reexamined along with other details of the modeling. Additional and more thorough statistical analyses are warranted for the J-STARS teardown data, especially in relationship to the PoO modeling efforts. The metallographic examinations and statistical analyses of the wing panels from the J-STARS CZ-184 aircraft indicate that the character and distribution of damage are much more complex. As such, both modeling and detection of damage need to be substantially improved in the development of effective tools for airworthiness assessment and fleet management.

9. REFERENCES.

1. R. P. Wei and D. G. Harlow, "Corrosion and Corrosion Fatigue of Airframe Materials," U.S. Department of Transportation, Federal Aviation Administration, DOT/FAA/AR-95/76, February 1996, Final Report, National Technical Information Service, Springfield, VA 22161.
2. G. S. Chen, M. Gao, and R. P. Wei, "Microconstituent-Induced Pitting Corrosion in a 2024-T3 Aluminum Alloy," *CORROSION*, 52, No. 1, pp. 8-15, January 1996.
3. Ming Gao, C. R. Feng, and Robert P. Wei, "An AEM Study of Constituent Particles in Commercial 7075-T6 and 2024-T3 Alloys," *Metall. and Materials Trans.*, 29A, pp. 1145-1151, April 1998.
4. Robert P. Wei, Chi-Min Liao, and Ming Gao, "A TEM Study of Micro-Constituent Induced Corrosion in 2024-T3 and 7075-T6 Aluminum Alloys," *Metall. and Materials Trans.*, 29A, pp. 1153-1160, April 1998.
5. Chi-Min Liao, "Particle-Induced Pitting Corrosion of Aluminum Alloys," Ph.D. Dissertation, Lehigh University, 1997.
6. Chi-Min Liao and Robert P. Wei, "A Technique for Studying the 3-Dimensional Shape of Pits," *Scripta Mater.*, 35, No. 11, pp. 1341-1346, 1996.
7. Chi-Min Liao and Robert P. Wei, "Galvanic Coupling of Model Alloys to Aluminum – A Foundation for Understanding Particle-Induced Pitting in Aluminum Alloys," *Electrochimica Acta*, 45, pp. 881-888, 1999.
8. Gim S. Chen, Chi-Min Liao, Kuang-Chung Wan, Ming Gao, and Robert P. Wei, "Pitting Corrosion and Fatigue Crack Nucleation," in *Effects of the Environment on the Initiation of Crack Growth*, ASTM STP 1298, W. A. Van Der Sluys, Robert S. Piascik, and Robert Zawierucha, Eds., American Society for Testing and Materials, pp. 18-33, 1997.
9. Kuang-Chung Wan, "Mechanical and Chemical Aspects of Corrosion Fatigue of a 2024-T3 Aluminum Alloy in the Short Crack Regime," Ph.D. Dissertation, Lehigh University, 1996.
10. K.-C. Wan, G.S. Chen, M. Gao, and R.P. Wei, "Interactions between Mechanical and Environmental Variables for Short Fatigue Cracks in a 2024-T3 Aluminum Alloy in 0.5M NaCl Solutions," *Metall. Mater. Trans.* (to appear).
11. Evan J. Dolley, Jr., "Chemically Short-Crack Behavior of the 7075-T6 Aluminum Alloy," Ph.D. Dissertation, Lehigh University, 1999.
12. Robert P. Wei, "Corrosion Fatigue: Science and Engineering," *Recent Advances in Corrosion Fatigue*, Sheffield, UK 16-17 April 1997.

13. Robert P. Wei, Chitang Li, D. Gary Harlow, and Thomas H. Flourney, "Probability Modeling of Corrosion Fatigue Crack Growth and Pitting Corrosion," ICAF 97, *Fatigue in New and Ageing Aircraft*, Edinburgh, Scotland, Vol. I, R. Cook and P. Poole, eds., EMAS, 1997, pp. 197-214.
14. E. J. Dolley, B. Lee, and R. P. Wei, "The Effect of Pitting Corrosion on Fatigue Life," *Fat. & Fract. of Engr. Mat. & Structures* (to appear).
15. D. Gary Harlow and Robert P. Wei, "Probability Approach for Corrosion and Corrosion Fatigue Life," *J. of the Am. Inst. of Aeronautics and Astronautics*, 32, No. 10, October, pp. 2073-2079, 1994.
16. D.G. Harlow and R. P. Wei, "Probabilistic Aspects of Aging Airframe Materials: Damage versus Detection," *Proceedings of the Third Pacific Rim International Conference on Advanced Materials and Processes (PRICM 3)*, M. A. Imam, R. DeNale, S. Hanada, Z. Zhong, and D.N. Lee, eds., The Minerals, Metals & Materials Society, July 12-16, 1998, Honolulu, Hawaii, pp. 2657-2666.
17. D. Gary Harlow, Lisa D. Domanowski, Evan J. Dolley, and Robert P. Wei, "Probability Modeling and Analysis of J-STARS Tear-Down Data from Two B707 Aircraft," *Proceedings of Third Joint FAA/DoD/NASA Conference on Aging Aircraft*, Albuquerque, NM, September 20-23, 1999.
18. A.J. Hug, et al., "Laboratory Inspection of Wing Lower Surface Structure From 707 Aircraft for the J-STARS Program," Boeing FSCM No. 81205, Document No. D500-12947-1, April 4, 1996.

APPENDIX A -- PRESENTATIONS AND PUBLICATIONS FROM THE PROGRAM

Presentations and publications based on results from the FAA and AFOSR sponsored programs are given in the following subsections.

A-1. Presentations

"A Probabilistic Approach to Life Prediction for Corrosion Fatigue Crack Growth," **Robert P. Wei**, Boeing Commercial Airplane Group Seminar, Seattle, WA, October 17, 1991.

"A Mechanistically Based Probability Approach to Life Prediction for Corrosion and Corrosion Fatigue of Airframe Materials," **R. P. Wei**, FAA/NASA Workshop on Corrosion, ALCOA, PA, November 22, 1991.

"A Mechanistically Based Probability Approach to Life Prediction for Corrosion and Corrosion Fatigue of Airframe Materials," **Robert P. Wei** and D. Gary Harlow, International Workshop on Structural Integrity of Aging Airplanes, Atlanta, GA, April 1, 1992.

"A Mechanistically Based Probability Approach to Life Prediction for Corrosion and Corrosion Fatigue of Airframe Materials," **Robert P. Wei** and D. Gary Harlow, Seminar at Exxon, NJ, August 4, 1992.

"Mechanistic Understanding of Corrosion and Corrosion Fatigue and Prediction of Service Life," **R. P. Wei**, ALCOA Seminar, Alcoa Center, PA, December 7, 1992.

"Corrosion and Corrosion Fatigue of Airframe Materials," **R. P. Wei**, NASA Research Center, VA, April 27, 1993.

"Corrosion and Fatigue of Aluminum Alloys: Chemistry, Micromechanics and Reliability," **R. P. Wei** and **D. Gary Harlow**, Workshop on Aging Aircraft Research, Georgia Institute of Technology, Atlanta, GA, April 27, 1993.

"A Probability Model for Predicting Corrosion and Corrosion Fatigue Life of Aluminum Alloys," **D. Gary Harlow** and **R. P. Wei**, NIST and Temple University Conference, Gaithersburg, MD, May 4, 1993.

"A Mechanistically Based Probability Approach for Predicting Corrosion and Corrosion Fatigue Life," **R. P. Wei** and D. Gary Harlow, 17th Symposium of the International Committee on Aeronautical Fatigue, Stockholm, Sweden, June 9, 1993.

"A Dominant Flaw Probability Model for Corrosion and Corrosion Fatigue," D. Gary Harlow and **Robert P. Wei**, 12th International Corrosion Congress, Houston, TX, September, 1993.

"Corrosion and Corrosion Fatigue of Aircraft Aluminum Alloys," **Robert P. Wei**, FAA/NASA Corrosion Working Group Meeting, Lehigh University, Bethlehem, PA, November 2, 1993.

"Corrosion and Corrosion Fatigue of Aircraft Aluminum Alloys," **R. P. Wei**, Materials Degradation Panel of USAF Scientific Advisory Board, Arlington, VA, January 19, 1994.

"Corrosion and Corrosion Fatigue of Airframe Materials," **R. P. Wei**, FAA Meeting, Salt Lake City, UT, March 24, 1994.

"Corrosion and Corrosion Fatigue of Airframe Aluminum Alloys," G. S. Chen, M. Gao, D. G. Harlow, and **R. P. Wei**, FAA/NASA International Symposium on Advanced Structural Integrity Methods for Airframe Durability and Damage Tolerance, Hampton, VA, May 4-6, 1994.

"Corrosion and Fatigue of Aluminum Alloys: Chemistry, Micromechanics, and Reliability," **Robert P. Wei**, Second Air Force Aging Aircraft Conference, Oklahoma City, OK, May 17-19, 1994.

"Overview of Lehigh Research in Corrosion/Fatigue," **R. P. Wei**, Air Force Corrosion/Fatigue Research Meeting, Wright Laboratory, WPAFB, OH, June 3, 1994.

"A Probability Model for Pitting Corrosion in Aluminum Alloys," **D. G. Harlow**, G. Chen, and Robert P. Wei, Proceedings of U.S. National Congress for Applied Mechanics, Seattle, WA, June 26-July 1, 1994.

"Corrosion and Corrosion Fatigue in Airframe Materials," **R. P. Wei**, CAA/FAA Workshop on Corrosion Fatigue Interactions, Cranfield University, Cranfield, England, July 1994.

"Corrosion and Corrosion Fatigue in 2024-T3 and 7075-T6 Aluminum Alloys," **Robert P. Wei**, AFOSR URI meeting on Corrosion, Tribology, Lubrication, and Materials Fatigue Under Extreme Conditions, University of Illinois, Urbana, IL, August 17-18, 1994.

"Pitting Corrosion and Short-Crack Growth," **R. P. Wei**, FAA/NASA Corrosion Working Group meeting, SRI, Menlo Park, CA, November 2-3, 1994.

"Corrosion and Fatigue of Aluminum Alloys: Chemistry, Micromechanics, and Reliability," **R. P. Wei**, Corrosion/Fatigue Program Planning Meeting, U. S. Air Force, Wright Laboratory/Flight Dynamics Directorate, WPAFB, OH, February 8-9, 1995.

"A Mechanistically Based Probability Approach for Life Prediction," **Robert P. Wei** and D. Gary Harlow, International Symposium on Plant Aging and Life Prediction of Corrodible Structures, Sapporo, Japan, May 15-18, 1995.

"Spatial Statistics of Particles and Corrosion Pits in 2024-T3 Aluminum Alloy," **D. G. Harlow**, N. R. Cawley, and R. P. Wei, Proceedings of Canadian Congress of Applied Mechanics, Victoria, British Columbia, May 28-June 2, 1995.

"Pitting Corrosion in Aluminum Alloys," FAA/NASA Corrosion Working Group, **Robert P. Wei**, U.S. DOT/Volpe National Transportation Systems Center (Volpe Center), Cambridge, MA, June 15-16, 1995.

"Environmentally Enhanced Crack Growth in Nickel-Based Alloys at Elevated Temperatures," **M. Gao**, S. F. Chen, G. S. Chen, and R. P. Wei, ASTM 27th National Symposium on *Fatigue and Fracture Mechanics*, Williamsburg, VA, June 26-29, 1995.

"Life Prediction: A Case for Multi-Disciplinary Research," **Robert P. Wei**, ASTM 27th National Symposium on *Fatigue and Fracture Mechanics*, Williamsburg, VA, June 26-29, 1995.

"Pitting Corrosion in Aluminum Alloys: Experimentation and Modelling," **R. P. Wei**, Ming Gao, and D. Gary Harlow, Air Force 3rd Aging Aircraft Conference, Dayton, OH, September 26-28, 1995.

"Transition From Pitting Corrosion to Fatigue Crack Growth in a 2024-T3 Aluminum Alloy," **G. S. Chen**, K.-C. Wan, M. Gao, and R. P. Wei, TMS Materials Week '95, Cleveland, OH, October 29-November 2, 1995.

"In Situ Monitoring of Pitting Corrosion in Aluminum Alloys," **Chi-Min Liao**, Ming Gao, and Robert P. Wei, TMS Materials Week '95, Cleveland, OH, October 29-November 2, 1995.

"Mechanical and Environmental Effect on Growth of Short-Fatigue Cracks in a 2024-T3 Aluminum Alloy," **K.-C. Wan**, G. S. Chen, M. Gao, and R. P. Wei, TMS Materials Week '95, Cleveland, OH, October 29-November 2, 1995.

"Evolution of Pitting Corrosion in a 2024-T3 Aluminum Alloy," Raymond M. Burynski, Jr., Gim-Syang Chen, and **Robert P. Wei**, ASME Winter Annual Meeting, *Structural Integrity in Aging Aircraft*, San Francisco, CA, November 12-17, 1995.

"A Probability Model for the Nucleation and Coalescence of Corrosion Pits in Aluminum Alloys," **D. Gary Harlow** and Robert P. Wei, ASME Winter Annual Meeting, *Structural Integrity in Aging Aircraft*, San Francisco, CA, November 12-17, 1995.

"Mechanical and Environmental Effects on Growth of Short Fatigue Cracks in a 2024-T3 Aluminum Alloy," **K.-C. Wan**, G. S. Chen, M. Gao, and R. P. Wei, ASTM November Meeting, Task Group E08.06.04 on Small Cracks, Norfolk, VA, November 14, 1995.

"Modelling Corrosion and Corrosion Fatigue for Aging Aircraft," **D. Gary Harlow**, Seminar, Dept. of Theoretical and Applied Mechanics, Cornell University, Ithaca, NY, January 31, 1996.

"A Mechanistically Based Probability Approach for Service Life Prediction," **Robert P. Wei**, Seminar at Rutgers University, Piscataway, NJ, February 21, 1996.

"Pitting Corrosion and Fatigue Crack Nucleation," G. S. Chen, C.-M. Liao, M. Gao, and **R. P. Wei**, ASTM Symposium on *Effects of the Environment on the Initiation of Crack Growth*, Orlando, FL, May 20-21, 1996.

"Pitting Corrosion Study of Aluminum Alloys by an InSitu Monitoring Method," **Chi-Min Liao**, Jean-Marc Olive, Ming Gao, and Robert P. Wei, ASTM Symposium on *Effects of the Environment on the Initiation of Crack Growth*, Orlando, FL, May 20-21, 1996.

"A Mechanistically Based Probability Approach for Service Life Prediction," **Robert P. Wei**, ASME Symposium on *Materials and Mechanics Issues in Structural Life Prediction*, Johns Hopkins University, Baltimore, MD, June 13-14, 1996.

"Corrosion and Corrosion Fatigue Aspects of Aging Aircraft," **Robert P. Wei**, Ming Gao, and D. Gary Harlow, Proceedings of Air Force 4th Aging Aircraft Conference, United States Air Force Academy, CO, July 9-11, 1996.

"Probability and Statistics Modeling of Constituent Particles and Corrosion Pits as a Basis for MSD Analysis," N. R. Cawley, D. G. Harlow, and **R. P. Wei**, FAA-NASA Symposium on *Continued Airworthiness of Aircraft Structures*, Atlanta, GA, August 28-29, 1996.

"Mechanistically Based Probabilistic Considerations of Creep Crack Growth," **Robert P. Wei** and D. Gary Harlow, FAA/Air Force Workshop on *Application of Probabilistic Methods to Gas Turbine Engines*, Dayton, OH, 8-9 October 1996.

"TEM Studies of Particle-Induced Corrosion in 2024-T3 and 7076-T6 Aluminum Alloys," **Robert P. Wei** and Ming Gao, 1997 TMS Annual Meeting, Orlando, FL, February 9-13, 1997.

"Identification of Constituent Particles in 2024-T3 and 7075-T6 Aluminum Alloys," **Ming Gao**, Robert P. Wei, and Jerry Feng, 1997 TMS Annual Meeting, Orlando, FL, February 9-13, 1997.

"Corrosion Fatigue - Science and Engineering," **R. P. Wei**, Keynote speaker for The Institute of Materials Symposium on Recent Advances in Corrosion Fatigue, Sheffield, UK, 16-17 April, 1997.

"Effect of Statistical Variability in Material Properties on Springback Predictability," **D. G. Harlow**, ASM: Aeromat '97, Williamsburg, VA, May 14, 1997.

"Probability Modeling of Fatigue Crack Growth and Pitting Corrosion," **Robert P. Wei**, Chitang Li, D. Gary Harlow, and Thomas H. Flournoy, 19th ICAF Symposium, Edinburgh, UK, June 16-20, 1997.

"Aging of Airframe Materials: From Pitting to Cracking," **Robert P. Wei** and D. Gary Harlow, First Joint DoD/FAA/NASA Conference on Aging Aircraft, Ogden, Utah, July 8-10, 1997.

"Corrosion Modeling," **Robert P. Wei**, Corrosion Modeling Technical Interchange Meeting, Robbins Air Force Base, GA, August 14, 1997.

"Life Prediction and Fleet Management: A Case for Multidisciplinary Research," **Robert P. Wei**, Keynote presentation for Workshop on *Fatigue, Fracture, and Failure (F^3)*, Naval Research Laboratory, Washington, DC, September 9-10, 1997.

"Aging of Airframe Aluminum Alloys: From Pitting to Cracking," **Robert P. Wei**, Workshop on *Intelligent NDE Sciences for Aging and Futuristic Aircraft*, El Paso, TX, September 30-October 2, 1997.

"Corrosion Fatigue – Science and Engineering," **Robert P. Wei**, Departmental Colloquim, Dept. of Materials Science and Mineral Engineering, University of California-Berkeley, Berkeley, CA, January 29, 1998.

"Corrosion Fatigue – Science and Engineering," **Robert P. Wei**, Departmental Seminar, Department of Aerospace and Mechanical Engineering, University of Notre Dame, Notre Dame, IN, March 31, 1998.

"Aging of Airframe Aluminum Alloys: From Pitting to Cracking," **Robert P. Wei**, Interdepartmental Seminar, Cornell University, Ithaca, NY, April 24, 1998.

"Life-Time and Reliability of Materials in Engineering Environments," **Robert P. Wei**, Principal lecturer for Post-graduate course coordinated by faculty of Mechanical Engineering and Materials Science and Engineering, University of Twente, Arnhem, The Netherlands, May 11-15, 1998.

"Aging of Airframe Materials: From Pitting to Cracking," D. G. Harlow and R. P. Wei, Proceedings of symposium on *Problems in Mechanics and Applied Mathematics*, honoring Professor Fazil Erdogan, Lehigh University, Bethlehem, PA, June 28-30, 1998.

"Aging of Airframe Materials: Probability of Occurrence Versus Probability of Detection," **D. Gary Harlow** and Robert P. Wei, Second Joint NASA/FAA/DoD Conference on *Aging Aircraft*, Williamsburg, VA, September 2, 1998.

"Importance of Chemically Short-Crack Growth on Fatigue Life," **Evan J. Dolley** and Robert P. Wei, Second Joint NASA/FAA/DoD Conference on *Aging Aircraft*, Williamsburg, VA, September 2, 1998 (Poster session).

"Constituent-Particle Induced Pitting Corrosion in 2024-T3 Aluminum Alloy," **Robert P. Wei**, DOE Contractors' Meeting, Albuquerque, NM, September 18-19, 1998.

"Importance of Chemically Short-Crack Growth on Fatigue Life," **Evan Jarrett Dolley** and Robert P. Wei, TMS Fall Meeting, Rosemont, IL, October 12, 1998.

"Influence of Pre-existing Corrosion Pits on Fatigue Life in a 2024-T3 Aluminum Alloy," **Baekho Lee**, Evan Jarrett Dolley, and Robert P. Wei, TMS Fall Meeting, Rosemont, IL, October 12, 1998.

"Aging Airframe Materials: A Multi-Disciplinary Issue From Pitting to Cracking," **Robert P. Wei** and D. Gary Harlow, Symposium on *Aging of Engineered Systems with Focus on Aircraft*, Materials Research Society 1998 Fall Meeting, Boston, MA, November 30-December 4, 1998.

"Corrosion and Corrosion Fatigue in Airframe Materials: Probability of Occurrence Versus Probability of Detection," **D. Gary Harlow** and Robert P. Wei, Symposium on *Aging of*

Engineered Systems with Focus on Aircraft, Materials Research Society 1998 Fall Meeting, Boston, MA, November 30-December 4, 1998.

“Life Prediction: A Case for Multidisciplinary Research,” **Robert P. Wei**, Department of Mechanical Engineering and Mechanics Seminar, Lehigh University, April 16, 1999.

“Corrosion and Corrosion Fatigue of Aluminum Alloys – An Aging Aircraft Issue,” **Robert P. Wei** and D. Gary Harlow, FATIGUE '99, The Seventh International Fatigue Conference, Beijing, China, June 8-12, 1999.

“Probabilities of Occurrence and Detection and Airworthiness Assessment,” **Robert P. Wei** and D. Gary Harlow, ICAF'99, Proceedings of Symposium on *Structural Integrity for the Next Millennium*, Bellevue, WA, July 12-16, 1999.

“A Perspective on Environmentally Assisted Crack Growth in Steels,” **Robert P. Wei**, International Conference on *Environmental Degradation of Engineering Materials*, Gdansk-Jurata, Poland, September 19-23, 1999.

“Probability Modeling and Analysis of J-STARS Tear-Down Data from Two B707 Aircraft,” **D. Gary Harlow**, Lisa D. Domanowski, Evan J. Dolley, and Robert P. Wei, Third Joint FAA/DoD/NASA Conference on *Aging Aircraft*, Albuquerque, NM, September 20-23, 1999.

“The Effect of Frequency on Chemically Short-Crack Growth Behavior & Its Impact on Fatigue Life,” **Evan J. Dolley** and Robert P. Wei, Third Joint FAA/DoD/NASA Conference on *Aging Aircraft*, Albuquerque, NM, September 20-23, 1999.

A-2. Publications

D. G. Harlow and R. P. Wei, "A Mechanistically Based Approach to Probability Modeling for Corrosion Fatigue Crack Growth," *Engr. Frac. Mech.*, 45, No. 1, pp. 79-88, 1993.

Robert P. Wei and D. Gary Harlow, "A Mechanistically Based Probability Approach for Predicting Corrosion and Corrosion Fatigue Life," *ICAF Durability and Structural Integrity of Airframes*, Vol. I, A. F. Blom, ed., EMAS, Warley, United Kingdom, pp. 347-366, 1993.

D. Gary Harlow and Robert P. Wei, "A Dominant Flaw Probability Model for Corrosion and Corrosion Fatigue," *Corrosion Control For Low-Cost Reliability*, Proceedings of the 12th International Corrosion Congress, September 19-24, 1993, Houston, TX, pp. 3573-3586, 1993.

D. Gary Harlow and Robert P. Wei, "Probability Approach for Corrosion and Corrosion Fatigue Life," *J. of the Am. Inst. of Aeronautics and Astronautics*, 32, No.10, October, pp. 2073-2079, 1994.

G. S. Chen, M. Gao, D. G. Harlow, and R. P. Wei, "Corrosion and Corrosion Fatigue of Airframe Aluminum Alloys," FAA/NASA International Symposium on *Advanced Structural Integrity Methods for Airframe Durability and Damage Tolerance*, NASA Conference Publication 3274, Langley Research Center, Hampton, VA 23681, pp. 157-173, September 1994.

K.-C. Wan, G. S. Chen, M. Gao, and R. P. Wei, "Corrosion Fatigue of a 2024-T3 Aluminum Alloy in the Short Crack Domain," *Internat. J. of Fract.*, 69, 3, pp. R63-R67, 1995.

Raymond M. Burynski, Jr., "Corrosion Response of a 2024-T3 Alloy in 0.5M NaCl Solution," M.S. Thesis, Lehigh University, 1995.

Robert P. Wei and D. Gary Harlow, "A Mechanistically Based Probability Approach for Life Prediction," *Proceedings of International Symposium on Plant Aging and Life Prediction of Corrodible Structures*, Sapporo, Japan, , pp.47-58, May 15-18, 1995.

D. G. Harlow, N. R. Cawley, and R. P. Wei, "Spatial Statistics of Particles and Corrosion Pits in 2024-T3 Aluminum Alloy," *Proceedings of the 15th Canadian Congress of Applied Mechanics*, B. Tabarrok and S. Dost, Eds., May 28-June 2, 1995, Victoria, British Columbia, p. 116, 1995.

Raymond M. Burynski, Jr., Gim-Syang Chen, and Robert P. Wei "Evolution of Pitting Corrosion in a 2024-T3 Aluminum Alloy," 1995 ASME International Mechanical Engineering Congress and Exposition on *Structural Integrity in Aging Aircraft*, San Francisco, CA, 47, C. I. Chang and C. T. Sun, Eds., The American Society of Mechanical Engineers, New York, NY 10017, pp. 175-183, 1995.

D. Gary Harlow and Robert P. Wei, "Probability Modelling for the Growth of Corrosion Pits," 1995 ASME International Mechanical Engineering Congress and Exposition on *Structural Integrity in Aging Aircraft*, San Francisco, CA, 47, C. I. Chang and C. T. Sun, Eds., The American Society of Mechanical Engineers, New York, NY 10017, pp. 185-194, 1995.

G. S. Chen, M. Gao, and R. P. Wei, "Microconstituent-Induced Pitting Corrosion in a 2024-T3 Aluminum Alloy," *CORROSION*, 52, No. 1, pp. 8-15, January, 1996.

N. R. Cawley and D. G. Harlow, "Spatial Statistics of Particles and Corrosion Pits in 2024-T3 Aluminum Alloy," *J. of Materials Sci.*, 31, pp. 5127-5134, 1996.

K.-C. Wan, G. S. Chen, M. Gao, and R. P. Wei, "Technical Note on The Conventional K Calibration Equations for Single-Edge-Cracked Tension Specimens," *Engr. Fract. Mech.*, 54, No. 2, pp. 301-305, 1996.

G. S. Chen, K.-C. Wan, M. Gao, R. P. Wei, and T. H. Flournoy, "Transition From Pitting to Fatigue Crack Growth -- Modeling of Corrosion Fatigue Crack Nucleation in a 2024-T3 Aluminum Alloy," *Materials Sci. and Engr.*, A219, pp. 126-132, 1996.

Robert P. Wei, Ming Gao, and D. Gary Harlow, "Corrosion and Corrosion Fatigue Aspects of Aging Aircraft," *Proceedings of Air Force 4th Aging Aircraft Conference*, United States Air Force Academy, CO, July 9-11, 1996.

Chi-Min Liao and Robert P. Wei, "A Technique for Studying the 3-Dimensional Shape of Pits," *Scripta Mater.*, 35, No. 11, pp. 1341-1346, 1996.

Kuang-Chung Wan, "Mechanical and Chemical Aspects of Corrosion Fatigue of a 2024-T3 Aluminum Alloy in the Short Crack Regime," Ph.D. Dissertation, Lehigh University, 1996.

Robert P. Wei and D. Gary Harlow, "Corrosion and Corrosion Fatigue of Airframe Materials," U.S. Department of Transportation, Federal Aviation Administration, DOT/FAA/AR-95-76, February 1996, Final Report, National Technical Information Service, Springfield, VA 22161.

Robert P. Wei, "Corrosion Fatigue: Science and Engineering," *Recent Advances in Corrosion Fatigue*, Sheffield, UK April 16-17, 1997.

N. R. Cawley, D. G. Harlow, and R. P. Wei, "Probability and Statistics Modeling of Constituent Particles and Corrosion Pits as a Basis for Multiple-Site Damage Analysis," FAA-NASA Symposium on *Continued Airworthiness of Aircraft Structures*, DOT/FAA/AR-97/2, II, National Technical Information Service, Springfield, VA 22161, pp. 531-542, 1997.

Gim S. Chen, Chi-Min Liao, Kuang-Chung Wan, Ming Gao, and Robert P. Wei, "Pitting Corrosion and Fatigue Crack Nucleation," *Effects of the Environment on the Initiation of Crack Growth*, ASTM STP 1298, W. A. Van Der Sluys, Robert S. Piascik, and Robert Zawierucha, Eds., American Society for Testing and Materials, pp. 18-33, 1997.

Chi-Min Liao, "Particle Induced Pitting Corrosion of Aluminum Alloys," Ph.D. Dissertation, Lehigh University, 1997.

Robert P. Wei, "Life Prediction: A Case for Multi-Disciplinary Research," *Fatigue and Fracture Mechanics*, 27th Volume, ASTM STP 1296, R. S. Piascik, J. C. Newman, and N. E. Dowling, Eds., American Society for Testing & Materials, pp. 3-24, 1997.

Robert P. Wei, Chitang Li, D. Gary Harlow, and Thomas H. Flournoy, "Probability Modeling of Corrosion Fatigue Crack Growth and Pitting Corrosion," ICAF 97, *Fatigue in New and Ageing Aircraft*, Edinburgh, Scotland, Vol. I, R. Cook and P. Poole, Eds., EMAS, pp. 197-214, 1997.

Chi-Min Liao, Jean Marc Olive, Ming Gao, and Robert P. Wei, "In Situ Monitoring of Pitting Corrosion in a 2024 Aluminum Alloy," *CORROSION*, 54, No. 6, pp. 451-458, June 1998.

D. G. Harlow and R. P. Wei, "A Probability Model for the Growth of Corrosion Pits in Aluminum Alloys Induced by Constituent Particles," *Engr. Frac. Mech.*, 59, No. 3, pp. 305-325, 1998.

Robert P. Wei, Chi-Min Liao, and Ming Gao, "A TEM Study of Micro-Constituent Induced Corrosion in 2024-T3 and 7075-T6 Aluminum Alloys," *Metall. and Materials Trans.*, 29A, pp. 1153-1160, April 1998.

Ming Gao, C. R. Feng, and Robert P. Wei, "An AEM Study of Constituent Particles in Commercial 7075-T6 and 2024-T3 Alloys," *Metall. and Materials Trans.*, 29A, pp. 1145-1151, April 1998.

D.G. Harlow and R. P. Wei, "Probabilistic Aspects of Aging Airframe Materials: Damage versus Detection," Proceedings of the Third Pacific Rim International Conference on *Advanced Materials and Processes* (PRICM 3), M. A. Imam, R. DeNale, S. Hanada, Z. Zhong, and D.N. Lee, eds. The Minerals, Metals & Materials Society, July 12-16, 1998, Honolulu, Hawaii, pp. 2657-2666.

Chi-Min Liao and Robert P. Wei, "Pitting Corrosion Process and Mechanism of 2024-T3 Aluminum Alloys," China Steel Technical Report, No. 12, pp. 28-40, 1998.

D. Gary Harlow and Robert P. Wei, "Aging of Airframe Materials: Probability of Occurrence Versus Probability of Detection," 2nd Joint NASA/FAA/DoD Conference on *Aging Aircraft*, Williamsburg, VA, August 31-3 Sept. 3, 1998, NASA/CP-1999-208982/PART1, Charles E. Harris, ed., January 1999, pp. 275-283.

Evan J. Dolley and Robert P. Wei, "Importance of Chemically Short-Crack Growth on Fatigue Life," 2nd Joint NASA/FAA/DoD Conference on *Aging Aircraft*, Williamsburg, VA, August 31-Sept. 3, 1998, NASA/CP-1999-208982/PART2, Charles E. Harris, ed., January 1999, pp. 679-687.

Evan J. Dolley, Jr., "Chemically Short-Crack Behavior of the 7075-T6 Aluminum Alloy," Ph.D. Dissertation, Lehigh University, 1999.

Robert P. Wei and D. Gary Harlow, "Corrosion and Corrosion Fatigue of Aluminum Alloys – An Aging Aircraft Issue", FATIGUE '99, Vol. 4, Proceedings of the Seventh International Fatigue Conference, June 8-12, 1999, Beijing, China, X. R. Wu and Z. G. Wang, Eds., E.M.A.S., UK, 1999, pp. 2197-2204.

Robert P. Wei and D. Gary Harlow, "Probabilities of Occurrence and Detection and Airworthiness Assessment," Proceedings of ICAF'99 Symposium on *Structural Integrity for the Next Millennium*, Bellevue, WA, July 12-16, 1999.

Robert P. Wei, "A Perspective on Environmentally Assisted Crack Growth in Steels," Proceedings of International Conference on *Environmental Degradation of Engineering Materials – EDEM '99*, Gdansk-Jurata, Poland, September 19-23, 1999, Vol. I, A. Zielinski, D. Desjardins, J. Łabanowski, and J. Ćwiek, Eds., Gdansk Scientific Society, Grodzka St., 80-841 Gdansk, Poland, pp. 101-112, 1999.

Evan J. Dolley and Robert P. Wei, "The Effect of Frequency of Chemically Short-Crack-Growth Behavior & Its Impact on Fatigue Life," Proceedings of Third Joint FAA/DoD/NASA Conference on *Aging Aircraft*, Albuquerque, NM, September 20-23, 1999.

D. Gary Harlow, Lisa D. Domanowski, Evan J. Dolley, and Robert P. Wei, "Probability Modeling and Analysis of J-STARS Teardown Data from Two B707 Aircraft," Proceedings of Third Joint FAA/DoD/NASA Conference on *Aging Aircraft*, Albuquerque, NM, September 20-23, 1999.

Ki-Woo Nam, Robert P. Wei, and Ajit K. Mal, "Characteristics of Acoustic Emission Waveforms from Fatigue Crack Propagation at a Corrosion Pit in 2024-T3 Aluminum," Proceedings of Third Joint FAA/DoD/NASA Conference on *Aging Aircraft*, Albuquerque, NM, September 20-23, 1999.

D. Gary Harlow and Robert P. Wei, "Probabilities of Occurrence and Detection of Damage in Airframe Materials," *Fat. & Fract. of Engr. Matls & Structures*, 22, pp. 427-436, 1999.

Chi-Min Liao and Robert P. Wei, "Galvanic Coupling of Model Alloys to Aluminum – A Foundation for Understanding Particle-Induced Pitting in Aluminum Alloys," *Electrochimica Acta*, 45, pp. 881-888, 1999.

K.-C. Wan, G.S. Chen, M. Gao, and R.P. Wei, "Interactions between Mechanical and Environmental Variables for Short Fatigue Cracks in a 2024-T3 Aluminum Alloy in 0.5M NaCl Solutions," *Metall. Mater. Trans.* (to appear).

E. J. Dolley, B. Lee, and R. P. Wei, "The Effect of Pitting Corrosion on Fatigue Life," *Fat. & Fract. of Engr. Matls & Structures* (to appear).